

**INVESTIGATION OF DIAMAGNETISM IN LASER-  
PRODUCED PLASMA**

*By*  
**NARAYAN BEHERA**  
**PHYS06201204013**

**Institute for Plasma Research**  
**Gandhinagar - 382 428, India**

*A thesis submitted to the*  
*Board of Studies in Physical Sciences*  
*In partial fulfillment of requirements*  
*for the Degree of*  
**DOCTOR OF PHILOSOPHY**  
*of*  
**HOMI BHABHA NATIONAL INSTITUTE**



**June 2018**

# Homi Bhabha National Institute<sup>1</sup>

## Recommendations of the Viva Voce Committee

As members of the Viva Voce Committee, we certify that we have read the dissertation prepared by **Mr. Narayan Behera** entitled “**Investigation of Diamagnetism in Laser-Produced Plasma**” and recommend that it may be accepted as fulfilling the thesis requirement for the award of Degree of Doctor of Philosophy.

*Amita Das*

Chairman - Prof. Amita Das

Date: 27/11/2018

*Ajai Kumar*

Guide / Convener - Prof. Ajai Kumar

Date: 27/11/2018

*Reji Philip*

Examiner - Prof. Reji Philip

Date: 27/11/2018

*Vinay Kumar*

Member 1 - Dr. Vinay Kumar

Date: 27/11/2018

Member 2 - Dr. Hem Chandra Joshi

Date: 27/11/2018

*H.C. Joshi*

Member 3 - Dr. Ramasubramanian Narayanan

Date: 27/11/2018

*NRamnan*

Final approval and acceptance of this thesis is contingent upon the candidate's submission of the final copies of the thesis to HBNI.

I hereby certify that I have read this thesis prepared under my/our direction and recommend that it may be accepted as fulfilling the thesis requirement.

Date: 27/11/2018

Place: Gandhinagar

*Ajai Kumar*  
Prof. Ajai Kumar  
(Guide)

<sup>1</sup> This page is to be included only for final submission after successful completion of viva voce.

## STATEMENT BY AUTHOR

This dissertation has been submitted in partial fulfillment of requirements for an advanced degree at Homi Bhabha National Institute (HBNI) and is deposited in the Library to be made available to borrowers under rules of the HBNI.

Brief quotations from this dissertation are allowable without special permission, provided that accurate acknowledgement of source is made. Requests for permission for extended quotation from or reproduction of this manuscript in whole or in part may be granted by the Competent Authority of HBNI when in his or her judgment the proposed use of the material is in the interests of scholarship. In all other instances, however, permission must be obtained from the author.

*Narayan Behera*  
**Narayan Behera**

## DECLARATION

I, hereby declare that the investigation presented in the thesis has been carried out by me. The work is original and has not been submitted earlier as a whole or in part for a degree / diploma at this or any other Institution / University.

*Narayan Behera*

**Narayan Behera**

## List of Publications arising from the thesis

### Peer-reviewed journal papers:

1. Narayan Behera, R. K. Singh, V. Chaudhari and Ajai Kumar, “**Two directional fast imaging of plasma plume in variable magnetic field: Structure and dynamics of the plume in diamagnetic and non-diamagnetic limits**”, *Phys. Plasmas* **24**(3), 033511 (2017); <http://dx.doi.org/10.1063/1.4978792>.
2. Narayan Behera, R. K. Singh and Ajai Kumar, “**Confinement and re-expansion of laser induced plasma in transverse magnetic field: Dynamical behaviour and geometrical aspect of expanding plume**”, *Phys. Lett. A* **379**(37), 2215-2220 (2015); <http://doi.org/10.1016/j.physleta.2015.04.042>.

### Peer-reviewed conference papers:

1. Narayan Behera, R. K. Singh and Ajai Kumar, “**Diffusion of External Magnetic Field into Laser-produced Plasma Plume**”, in *Frontiers in Optics / Laser Science*, OSA Technical Digest (Optical Society of America, 2018), paper JW3A.37; <https://doi.org/10.1364/FIO.2018.JW3A.37>; ISBN: 978-1-943580-46-0.
2. Narayan Behera, R. K. Singh and Ajai Kumar, “**Singular Value Decomposition of Laser Produced Plasma in Transverse Magnetic field**”, *Proceedings of the DAE-BRNS National Laser Symposium* **25**, CP-7.20 (2016); ISBN: 978-81-903321-7-0.
3. Narayan Behera, R. K. Singh and Ajai Kumar, “**Dynamics and structural behaviour of laser induced plasma in transverse magnetic field**”, *Proceedings of the DAE-BRNS National Laser Symposium* **23**, CP-07-15 (2014); ISBN: 9788190332156.

### Manuscripts under preparation:

1. Narayan Behera, R. K. Singh, G. Veda Prakash and Ajai Kumar, “**Study of diamagnetism of laser-produced plasma using B-dot probe**”.
2. Narayan Behera, R. K. Singh and Ajai Kumar, “**Material dependence of diamagnetism in laser-produced plasma**”.
3. Narayan Behera, R. K. Singh, D. Sharma and Ajai Kumar, “**Two stream instability in laser-produced Barium plasma**”.

4. Narayan Behera, R. K. Singh, D. Sharma and Ajai Kumar, “**Y-shaped symmetrical bifurcation of laser-produced carbon plasma in transverse magnetic field**”.

### **Other publications:**

1. G. Veda Prakash, Kiran Patel, Narayan Behera and Ajai Kumar, “**Study of plume dynamics and plasma density during its expansion**”, preprint arXiv:1810.09191 [physics.plasm-ph]; <https://arxiv.org/abs/1810.09191>.
2. G. Veda Prakash, Kiran Patel, Narayan Behera and Ajai Kumar, “**Characterization of atmospheric pressure plasma plume**” (Manuscript to be submitted).

### **Conference presentations:**

#### **International:**

1. “**Measurement of time-varying induced magnetic field using B-dot probe in laser-produced plasma**”, Narayan Behera, R. K. Singh and Ajai Kumar, 2<sup>nd</sup> *Meghnad Saha Memorial International Symposium-cum-Workshop on Laser Induced Breakdown Spectroscopy (MMISLIBS-II 2018)*, University of Allahabad, Allahabad, Uttar Pradesh, India, Feb 19-21, 2018. [Oral presentation]
2. “**Temporal evolution of diamagnetic cavity in laser produced plasma**”, Narayan Behera, R. K. Singh and Ajai Kumar, 59<sup>th</sup> *Annual Meeting of the American Physical Society (APS) Division of Plasma Physics (DPP)*, Milwaukee, Wisconsin, USA, Oct 23-27, 2017. [Poster presentation]
3. “**Experimental demonstration of diamagnetism of laser produced plasma**”, Narayan Behera, R. K. Singh and Ajai Kumar, 44<sup>th</sup> *European Physical Society (EPS) Conference on Plasma Physics*, Queen's University, Belfast, Northern Ireland, UK, Jun 26-30, 2017. [Poster presentation]
4. “**Plume propagation in magnetic field: Field aligned Intensity Pattern**”, Narayan Behera, R. K. Singh and Ajai Kumar, *International Conference on Plasma Science, Technology & Application (ICPSTA-2016)*, Amity University, Lucknow Campus, Lucknow, Uttar Pradesh, India, Jan 20-21, 2016. [Oral presentation]
5. “**Two dimensional imaging of laser produced plasma in magnetic field**”, Narayan Behera, R. K. Singh and Ajai Kumar, 10<sup>th</sup> *Asia Plasma and Fusion*

*Association Conference (APFA-2015), Institute for Plasma Research, Gandhinagar, India, Dec 14-18, 2015. [Poster presentation]*

### **National:**

1. **“Plume dynamics in magnetic field”**, Narayan Behera, R. K. Singh and Ajai Kumar, 32<sup>nd</sup> National Symposium on Plasma Science & Technology (PLASMA-2017), Institute for Plasma Research, Gandhinagar, India, Nov 07-10, 2017. [Poster presentation]
2. **“Singular value decomposition of laser produced plasma in transverse magnetic field”**, Narayan Behera, R. K. Singh and Ajai Kumar, 25<sup>th</sup> DAE-BRNS National Laser Symposium (NLS-25), KIIT University, Bhubaneswar, India, Dec 20-23, 2016. [Poster presentation]
3. **“Dynamics of laser produced plasma in variable Magnetic field”**, Narayan Behera, R. K. Singh and Ajai Kumar, International Conference On Advances in Light Technologies and Spectroscopy of Materials (ICALTSM-2016), University of Lucknow, Lucknow, Uttar Pradesh, India, Jan 16-18, 2016. [Poster presentation]
4. **“External magnetic field induced instabilities in laser produced plasma”**, Narayan Behera, R. K. Singh and Ajai Kumar, 29<sup>th</sup> National Symposium on Plasma Science & Technology and the International Conference on Plasma & Nanotechnology (PLASMA- 2014), Mahatma Gandhi University, Kottayam, India, Dec 8-11, 2014. [Poster presentation]
5. **“Dynamics and structural behaviour of laser induced plasma in transverse magnetic field”**, Narayan Behera, R. K. Singh and Ajai Kumar, 23<sup>rd</sup> DAE-BRNS National Laser Symposium (NLS-23), Sri Venkateswara University, Tirupati, India, Dec 3-6, 2014. [Poster presentation]
6. **“Ion-ion two stream instability in laser produced Ba-plasma”**, Narayan Behera, R. K. Singh, Manoj Kumar Gupta, Devendra Sharma and Ajai Kumar, 28<sup>th</sup> National Symposium on Plasma Science & Technology (PLASMA-2013), KIIT University, Bhubaneswar, India, Dec 3-6, 2013. [Poster presentation]
7. **“Image analysis of expanding laser produced Al-plasma plume in transverse magnetic field”**, Narayan Behera, R. K. Singh and Ajai Kumar, Topical

*Conference on Atomic Processes in Plasmas (ISAMP-TC-2013), Institute for  
Plasma Research, Gandhinagar, India, Nov 18-20, 2013. [Poster presentation]*

*Narayan Behera*  
**Narayan Behera**

**Dedicated**  
**to**  
*My Parents*



## **Acknowledgements**

First of all, I would like to express my sincere gratitude to acknowledge my thesis supervisor Prof. Ajai Kumar for his continues guidance, immense support and motivating ideas for my PhD dissertation. I am also thankful for his many hours of help he provided me. His expertise in experiments always helped me in learning new techniques and experimental methods. It has been a wonderful experience for me while doing PhD under his guidance.

I would like to thank Dr. Rajesh Kumar Singh for his invaluable guidance in my PhD thesis work. He always stood with me whenever I required support in terms of scientific and technical matters. I am also grateful to him for his reviews and advice during the writing of thesis dissertation. His timely support and guidance helped me to complete the dissertation in time.

I would like to thank my lab members Dr. Hem Chandra Joshi, Mr. Jinto Thomas, Dr. V. Sivakumaran, Mr. Vishnu Chaudhari, Mr. Kiran Patel, Dr. Arvind Saxena, Dr. Kaushik Chaoudhury, Mr. Alamgir Mondal, Mr. Pabitra Kumar Mishra, Mrs. Neha Singh, Dr. M. Srinivasa Raju, Dr. Bhupesh Kumar, Dr. Raj Singh for providing an educational environment atmosphere to learn.

I would also like to thanks Dr. Devendra Sharma, Dr. D. Raju, Dr. G. Veda Prakash, Dr. Amulya Kumar Sanyasi, Mr. Pankaj K. Srivastava, Mr. Swadesh Kumar Patnaik, Dr. Bhavesh Patel for their help in my research work.

I would like to thank my doctoral committee members Prof. Amita Das, Dr. Vinay Kumar, Dr. Hem Chandra Joshi, Dr. Ramasubramanian Narayanan for their useful suggestions and guidance during my PhD.

I specially thank Prof. Subroto. Mukherjee (Dean, Academics & Student Affairs) and Dr. Mainak Bandyopadhyay (Chairman, Academic Committee) for their guidance in various matters and more importantly things related to HBNI.

I would like to thank Dr. G. Ravi, Dr. Ramasubramanian Narayanan, Prof. Subroto. Mukherjee, Dr. Shantanu Kumar Karkari, Prof. Prabal K. Chattopadhyay, Dr. Pintu Bandyopadhyay, Dr. Joydeep Ghosh, Dr. Devendra Sharma, Dr. Mrityunjay Kundu, Dr. Mainak Bandyopadhyay, Dr. Nirmal K. Bisai, Dr. Daniel Raju, Dr. V. P.

Anitha, Dr. Asim K. Chattopadhyay, Dr. V. Prahlad and others for their teaching to learn and understand the plasma physics and related subjects.

I want to thank my batch mates Amit, Ratan, Arghya, Anup, Umesh, Modhu, Sonu, Debraj, Rajnarayan, Ramkrishna, Bhumika, Surabhi for their support during my PhD.

I would like to thank my all juniors Sagar, Atul, Jervis, Alamgir, Sandeep, Prabhakar, Deepak, Meenakshee, Pallavi, Harshita, Chetan, Rupak, Shivam, Avnish, Trithendu, Subrata, Arun, Gaurav, Anirban, Dipshikha, Arnab, Priti, Garima, Neeraj, Srimanta, Mayank, Yogesh, Chinmoy, Girija Shankar, Piyush, Pranjal, Satadal, Soumen, Pradeep, Devshree, Nidhi, Sanjeev, Hariprasad, Ayushi, Pawandeep, Swapnali, Tanmay, Karim, Prince, Jagannath, Satya, Lavanya, Ram, Vivek and others and seniors Dr. Neeraj Chaubey, Dr. Bibhu Prasad Sahoo, Dr. Mangilal Choudhary, Dr. Vidhi Goyal, Dr. Akanksha Gupta, Dr. Deepa Verma, Dr. Chandrashekhar Shukla, Dr. Vara Prasad Kella, Dr. Samirsinh G. Chauhan, Dr. Harish Charan, Dr. Roopendra Singh Rajawat, Dr. Meghraj Sengupta, Dr. Vikram Singh Dharodi, Dr. Soumen Ghosh, Dr. Aditya Krishna swamy, Dr. Sayak Bose, Dr. Manjit Kaur, Dr. Rameshwar Singh, Dr. Pravesh Dhyani, Dr. Sushil Kumar Singh, Dr. Sanat Tiwari, Dr. Ujjwal Sinha, Dr. Gurudatt Gaur, Dr. Deepak Sangwan, Dr. Prabal Singh Verma, Dr. Vikram Sagar, Dr. Kshitish Kumar Barada, Dr. Sita Sundar, Dr. Ashwin Joy, Dr. Rana Yadav, Dr. Dushyant Kumar Sharma, Dr. Sandeep Rimza, Dr. G. Veda Prakash, Dr. Satyananda Kar, Dr. T. Shekar Goud, Dr. Sharad Kumar Yadav, Dr. P. N. Maya, Dr. Jugal Chowdhury, Dr. Jitendra Kumar, Dr. Amul Deshpande and others for providing friendly environment.

I would also like to thank Dr. Amulya Kumar Sanyasi, Mr. Pabitra Kumar Mishra, Mr. Swadesh Kumar Patnaik, Dr. Jyoti Shankar Mishra, Mr. Akshaya Kumar Shaw, Mr. Srikanta Sahu, Mr. Chandra Sekhar Sasmal, Mr. Dusmanta Mohanta, Mr. Subrat Kumar Das, Mr. Bikash Ranjan Dash, Dr. Subhanarayan Sahoo, Dr. Bibhu Prasad Sahoo, Mr. Sagar Sekhar Mahalik, Miss Rajashree Sahoo, Mr. Jagannath Mahapatra and others for their support in various occasions.

I am also grateful to people from the workshop, computer center, library, stores, purchase section, administration, transport section, accounts section, water plant,

canteen, security staff members and hostel mess cook Jeeva and his team for their cooperation during my PhD.

I would like to express my heartfelt gratitude to all my teachers. Mr. Bijay Panda, Mr. Biswamber Mohanty, Mr. Subas Kar, Mr. Sanjay Mohanty, Mr. Surendra Bal, Mr. Sukanta Chandra Panigrahi, Mr. Sriram Dash, Mr. Sushanta Kumar Pani, Mr. Rasmi Ranjan Guin are few of them.

I would also like to thank all friends for spending their valuable time in different part of my student life. I would like to express to Mr. Sanjay Kumar Nayak for his encouragement.

Lastly and very most importantly I would like to express sincere gratitude towards my father Mr. Gourang Behera, mother Mrs. Malati Behera, sisters Sulochona Behera and Subhadra Behera, brother Bijay Rout, sister-in-law Mrs. Laxmipriya Jati, nephew Satyajit Rout for their constant support and patience for the entire period. Their unconditional support helped me to make this possible.

I apologize if I missed mentioning anybody's name, I thank them for their support.



# Contents

Synopsis	v
List of figures	xvii
List of tables	xxi
<b>Chapter 1</b> Introduction	1
1.1 Plasma	3
1.1.1 Concept of temperature	3
1.1.2 Debye shielding	4
1.1.3 Quasi-neutrality in plasma	4
1.1.4 Criteria for ionised gas to be plasma	5
1.1.5 Plasma frequency	6
1.2 Laser-produced plasma	6
1.3 Physics of laser plasma formation	7
1.4 Plasma plume in vacuum	9
1.5 Plasma plume in background gas	10
1.5.1 Shock wave model	10
1.5.2 Drag force model	11
1.6 Plasma plume in transverse magnetic field	11
1.6.1 Plasma parameters in magnetic Field	11
1.6.1.1 Larmor radius (Gyroradius or cyclotron radius)	11
1.6.1.2 Plasma beta	12
1.6.1.3 Bubble radius (Confinement radius)	13
1.6.1.4 Magnetic diffusion time	13
1.6.1.5 Cyclotron frequency	14
1.6.1.6 Lower-hybrid frequency	14
1.6.2 Plasma plume in transverse magnetic field	14
1.6.2.1 Formation of diamagnetic cavity and confinement of the plume	15
1.6.2.2 Polarization of plume and $E \times B$ drift	16
1.7 Instabilities in plasma	17
1.7.1 Rayleigh-Taylor (RT) instability	17
1.7.2 Kelvin-Helmholtz (KH) instability	18
1.7.3 Electron-ion hybrid instability	18
1.8 Overview of earlier works	19
1.9 Motivation and objectives of the thesis	21
1.10 Organization of the thesis	23
<b>Chapter 2</b> Experimental scheme	25
2.1 Introduction	27
2.2 Components of experimental setup	28
2.2.1 Vacuum chamber and pumping system	28
2.2.2 Laser system	29
2.2.3 Magnet system	30
2.2.3.1 Magnetic trap	30
2.2.3.2 Helmholtz coil	30

	2.2.4	Targets and its handling system	31
2.3		Plasma diagnostic systems	31
	2.3.1	Time-resolved fast imaging using ICCD camera	31
	2.3.2	Optical emission spectroscopy (OES)	34
	2.3.3	B-dot Probe	35
2.4		Generation of variable uniform magnetic field using Helmholtz coil	36
	2.4.1	Pulse power system	37
	2.4.2	Coil structure	38
	2.4.3	RLC circuit analysis	40
	2.4.4	Uniformity of magnetic field	41
	2.4.5	Timing and Synchronization scheme	43
2.5		Summary and conclusion	44
<b>Chapter 3</b>		Dynamical behavior of plasma plume across the transverse magnetic field	47
	3.1	Introduction	49
	3.2	Experimental scheme	50
	3.3	Results and discussion	52
	3.3.1	Plume expansion across the magnetic field	52
		3.3.1.1 In vacuum	53
		3.3.1.2 In ambient gas	57
	3.3.3	SVD analysis of the plasma plume	59
	3.3.4	Plume dynamics in diamagnetic and non-diamagnetic limits	62
	3.4	Summary and conclusion	66
<b>Chapter 4</b>		Two directional fast imaging of plasma plume in variable magnetic field	69
	4.1	Introduction	71
	4.2	Experimental Scheme	72
	4.3	Results and Discussion	75
	4.3.1	Expansion in the absence of magnetic field	76
	4.3.2	Expansion in the presence of magnetic field	77
	4.3.3	Plasma parameters	82
	4.3.4	Plume dynamics in diamagnetic and non-diamagnetic limits	86
	4.3.5	Formation of striation-like structures	91
	4.4	Summary and conclusion	92
<b>Chapter 5</b>		Study of diamagnetism using B-dot probe	95
	5.1	Introduction	97
	5.2	Probe theory and calculation of magnetic field:	98
	5.3	Construction of probe	98
	5.4	Response of the probe	100
	5.4.1	Frequency response of the probe in Helmholtz coil	101
	5.4.2	Frequency response of probe in circular inductor	103

5.5	Calibration of the probe	107
5.6	Magnetic field measurement in expanding plasma plume	108
5.5.1	Theory of diamagnetic cavity	108
5.5.2	Experimental scheme	109
5.5.3	Results and analysis	109
5.7	Summary and conclusion	114
<b>Chapter 6</b>	Material dependent diamagnetic cavitization of laser-produced plasma	115
6.1	Introduction	117
6.2	Experimental scheme	118
6.3	Results and discussion	119
6.3.1	Time-resolved fast imaging of tungsten plasma	119
6.3.2	Time-resolved fast imaging of nickel plasma	121
6.3.3	Time-resolved fast imaging of aluminium plasma	123
6.3.4	Time-resolved fast imaging of carbon plasma	123
6.3.5	Comparative study of plasma plumes	126
6.4	Summary and conclusion	129
<b>Chapter 7</b>	Conclusion and future scope	131
7.1	Conclusion	133
7.2	Future scope	135
<b>References</b>		137



# Synopsis

This thesis investigates the diamagnetism in laser-produced plasma. The study of laser-produced plasmas in the presence of external magnetic field is useful to understand several important physical phenomena such as conversion of kinetic energy into plasma thermal energy, plume confinement, ion acceleration/deceleration, emission enhancement/decrease, and plasma instabilities. It is also important for many advanced research such as tokamak plasma, study of artificial comet, propulsion of space vehicles using laser ablation, investigation of acceleration of stellar winds, laboratory plasmas, increase in the detection sensitivity of laser-induced breakdown spectroscopy <sup>[1]</sup>, manipulation of plasma plume in pulse laser deposition <sup>[2-4]</sup>, debris mitigation <sup>[5]</sup> etc. Several researchers have tried to understand the plasma plume-magnetic field interactions in vacuum and presence of background gas pressure with uniform <sup>[6]</sup> and non-uniform magnetic field <sup>[7]</sup>. They have observed various phenomena like the formation of diamagnetic cavity and flute-like structures <sup>[8, 9]</sup>, plasma oscillations <sup>[10]</sup>, edge instability and dramatic structuring <sup>[11, 12]</sup> and sub-Alfvénic plasma expansion <sup>[13]</sup>.

Apart from the above, the dynamics of plasma plume is influenced significantly in the presence of external magnetic field and therefore it is useful to control the dynamic properties of highly transient plasma plume. The manipulation of geometrical shape, size and dynamics of plasma plume by the introduction of the external magnetic field has great importance in applied research and also in fundamental studies. Due to initial conversion of thermal energy into directed energy, the sum of directed pressure and thermal pressure of plasma plume is much larger than the magnetic pressure (that is plasma beta > 1). As the time evolves, electron

temperature and density of the plasma plume decrease rapidly resulting in a decrease in plasma beta with time. Therefore, two different approaches have been taken to explain the dynamics of laser-produced plasma across the transverse magnetic field. In the first approach expansion of the plasma plume is treated as expansion in the diamagnetic limit where the applied magnetic field is displaced by the induced magnetic field due to the diamagnetic current in plasma, and the plasma plume experiences the decelerating force. In the second approach, it is considered that external magnetic field is diffused in the plasma plume and produces polarized electric field (due to the deflection of electrons and ions in opposite direction), perpendicular to both the expansion direction and the magnetic field. In this case plasma plume experiences the  $E \times B$  field and drifts in the axial direction. However, in most of the previous experiments with nanosecond laser and moderate laser energy (up to few hundred mJ) <sup>[14]</sup>, the dynamics of the plasma plume across the magnetic field is explained in terms of  $J \times B$  interaction induced by the diamagnetic behaviour of plasma plume. The  $E \times B$  drift of the laser plasma and the field aligned instability (striation-like structure) is largely ignored in the reported work in the case of a moderate magnetic field ( $< 1$  T) and the ablating laser energy of the order of few hundred mJ. Also, the systematic experimental observation of the formation of diamagnetism of the plasma plume and its transition into the non-diamagnetic limit (diffused magnetic field) is scarce in the literature. Here it should be noted that most of the previous experiments have been performed with permanent bar magnets where plume imaging along the magnetic field lines is not possible because of experimental constraints. The plume structure in a magnetic field is highly asymmetrical, and therefore, complete geometrical information of the plume, especially the structure of the induced

diamagnetic cavity cannot be extracted from plume images projected across the magnetic field direction.

In view of the above, in the thesis work we have systematically investigated the expansion of transient plasma plume in diamagnetic limit followed by the drift across the polarized electric field. Emphasis is given on the experimental demonstration of the formation, evolution and three dimensional structure of the diamagnetic cavity in different experimental conditions. A new model for the three dimensional structure of diamagnetic cavity has been proposed based on the projections of plume images in two perpendicular planes. The validity of the different theoretical models, which are responsible for observed results, has also been discussed.

In this work, we have used fast imaging method, optical emission spectroscopy and B-dot probe for characterization of the laser-produced plasma plume in the presence of magnetic field. An Nd:YAG laser ( $\lambda = 1064$  nm, 8 ns pulse width) of 1.6 J maximum pulse energy has been used to ablate the metallic targets. By varying the laser energy of focused beam of diameter 1.0 mm, we had set the laser fluence in the range of 19.1 - 38.2 J/cm<sup>2</sup> on the target surface. Experiments have been performed with the both fixed magnetic field (using NdFeB permanent bar magnets) and variable magnetic fields (using Helmholtz coil). Also a three-axis, high-frequency, B-dot probe has been designed to study the diamagnetism of laser-produced plasma. A wide range of target materials having low and high atomic number e.g. carbon, aluminium, nickel and tungsten have been used for this study.

The thesis is organized into seven chapters as outlined below.

## **Organization of the thesis**

### **Chapter 1: Introduction**

This chapter presents a brief introduction of basic physics of laser-produced plasma and its interaction with the external magnetic field. A detailed literature survey related to this field has also been incorporated in this chapter. This review is followed by motivation and the objective of the thesis research work.

### **Chapter 2: Experimental scheme**

The laser-produced plasma is created in a multi-port cylindrical non-magnetic stainless steel chamber, which is evacuated by rotary pump and turbomolecular pump to a base pressure less than  $10^{-6}$  Torr. An Nd:YAG laser ( $\lambda = 1064$  nm, 8 ns pulse width) of 1.6 J maximum pulse energy is used to ablate the metallic target. By varying the laser energy of focused beam of diameter 1.0 mm we set the laser fluence in the range of 19.1 - 38.2 J/cm<sup>2</sup> on the target surface. Two different schemes of uniform magnetic field generation have been employed for the present study. In the first scheme, a uniform magnetic trap was made by two rectangular NdFeB permanent magnets having dimensions 38 mm height, 76 mm length and 76 mm width. A non-magnetic stainless steel structure holds the magnets parallel to each other with 30 mm separation, which produces  $\sim 0.45$  T uniform magnetic field <sup>[15]</sup>. In the second scheme, a Helmholtz coil along with the capacitor bank based pulse power system <sup>[16,</sup> <sup>17]</sup> has been used to produce variable magnetic field varying from 0 to 0.57 T. The flat-top (uniformity) of the variable magnetic field was  $\sim 40$   $\mu$ s. The targets were in the form of plates of thickness 1-3 mm and were mounted on a movable target holder through a vacuum compatible feed-through and were placed in between the magnet bars/Helmholtz coils. A high speed gated intensified CCD camera has been used for time-resolved fast imaging of electronically excited plume species. Optical Emission

Spectroscopy (OES) is used to measure electron temperature and electron density. For that, the emitted light is viewed normal to the expansion direction through double-lens telescopic arrangement and fed at the entrance slit of the spectrometer (Acton SP2500A). A micro-controller based time control unit has been used to trigger the camera and spectrometer in synchronous with the laser pulse. An indigenously built three-axis, high-frequency B-dot probe is used to verify the diamagnetism of laser-produced plasma.

### **Chapter 3: Dynamical behavior of plasma plume across the transverse magnetic field**

The dynamical and geometrical behavior of laser produced aluminium plasma across the 0.45 T magnetic field produced by two NdFeB permanent magnet bars have been investigated using time-resolved fast imaging technique. In this experiment, the laser energy is set as 300 mJ. Several distinct features have been observed related to the axial and radial expansion of the plume, splitting pattern and geometrical formation which are significantly different from the reported results for similar kind of experiments. It has been observed that expanding plume experiences a resistive force and approaches the stagnation limit. Stagnation condition is maintained for some time and there-after plume begins to expand with uniform velocity. The above observations are explained on the basis of the temporal behavior of diamagnetism of laser plasma and  $E \times B$  drift of bulk plasma across the diffused field. The estimated field diffusion time and confinement radius well support the above interpretation. Well-separated intensity columns, which are probably due to the velocity shear driven instability, have been observed at the leading portion of the plume. Also, singular value decomposition (SVD) analysis of the image data matrix shows the structured profile of the bulk plasma along the applied field lines, which is not visible in the plume

images. Further, unique slab like splitting is observed in the presence of magnetic field and ambient gas. The leading component experienced the resistive force whereas trailing portion expanded freely. As a consequence, both components merged together and produced uniform density distribution in the transverse direction. Uniform intensity distribution in a large volume and almost flat expansion of the plume is an important observation which can be utilized in large area thin film deposition. In brief, the above study provides some additional information regarding the plasma dynamics in magnetic field. This work has been published in *N. Behera et al., Phys. Lett. A* **379** (37), 2215-2220 (2015) <sup>[15]</sup>, *N. Behera et al., Proceedings of the DAE-BRNS National Laser Symposium 23*, CP-07-15 (2014) and *N. Behera et al., Proceedings of the DAE-BRNS National Laser Symposium 25*, CP-7.20 (2016).

#### **Chapter 4: Two directional fast imaging of plasma plume in variable magnetic field**

A new experimental setup, which consists of a pulse magnetic field system, has been developed to capture the different phases of expanding plasma plume across the transverse magnetic field, varying from 0 to 0.57 T. In this experiment, the laser energy is set as 150 mJ. Two internally synchronized ICCD cameras mounted in the orthogonal direction have been used to record the two directional projections (across and along the magnetic field directions) of the plasma plume. The plume takes the conventional ellipsoidal shape in the absence of a magnetic field. Well-defined cavity-like structures have been observed in a plane perpendicular to the field direction, which is dominant at the early stage of the plasma and comparatively lower magnetic fields. As the time evolves, the cavity changes to jet/cone-like structures, which in turn change to slab-like structures with a further increase in time delay. On the other hand, well-separated intensity columns (striation-like structures) appeared in a plane

parallel to the magnetic field direction, which are more apparent at a higher magnetic field. Based on the projections of plume images in two perpendicular planes, the three dimensional structure of the plasma plume is modelled as an elliptical cylinder-like structure. The time dependence of dynamics and geometry of the plasma plume in the presence of a magnetic field are correlated with the expansion in diamagnetic and non-diamagnetic regimes. The striation-like structures are dominant at comparatively higher delay times and higher magnetic fields, which are related to electron-ion hybrid instability at higher magnetic fields <sup>[17]</sup>. These findings have been published in *N. Behera et al., Phys. Plasmas* **24** (3), 033511 (2017) <sup>[16]</sup> and *N. Behera et. al., in Frontiers in Optics / Laser Science, OSA Technical Digest (Optical Society of America, 2018), paper JW3A.37.*

#### **Chapter 5: Study of diamagnetism using B-dot probe**

When the plasma plume interacts with the external magnetic field, a current on its surface is produced which induces a time-varying magnetic field. The presence of diamagnetism in laser plasma can be verified by measuring this induced magnetic field. B-dot probe is commonly used to measure the time-varying magnetic field <sup>[18]</sup>. But major challenges involve in probe designing are probe should response to the desired frequency range, the size of the probe should be smaller than the Larmor radius and it should sensitive to the desired magnetic fields range. In the present case, the external magnetic field strength is 0 - 0.57 T and the electron temperature and density are 1.74 eV and  $2.6 \times 10^{22} \text{ m}^{-3}$  respectively. The estimated ion Larmor radii are 3.5-20 cm. We observed the duration of diamagnetic cavitization is in order of 200-1000 ns. Therefore, the probe should response for few MHz range. Based on the above considerations we have designed a three-axis, high-frequency magnetic probe. It is made of two twisted copper wires of Gauge 40 wound on a 3.2 mm G10 cube.

Each axis has two loops with 5 turns are connected in opposite direction to cancel capacitive pick-up, reduce the stray noise etc. Coil area, number of turns, self-inductance and shielding are carefully optimized to achieve the accurate measurement of the magnetic field with the reduced noise level. A separate differential amplifier having variable gain is indigenously designed for the present requirement. We have ensured the response of the probe up to 10 MHz. Further, the probe is calibrated at 1.27 MHz using a circular inductor of 22 mm radius, made by 10 turns of 0.8 mm thick copper wire. Here the magnetic field is produced by a pulsed power system using 2 nF capacitor discharge. The designed B-dot probe is placed at the expected diamagnetic cavity, which can measure the resultant magnetic field ( $\Delta B$ ) in this region. The measured  $\Delta B$  for different applied magnetic field and it was found to be  $\sim 10$  G, which indicates the diamagnetism of plasma plume. A manuscript is to be submitted for publication in *N. Behera et al., refereed journal*.

## **Chapter 6: Material dependent diamagnetic cavitation of laser-produced plasma**

Z-dependent plasma plumes and its interaction with magnetic field play an important role in various research such as laboratory astrophysics, tokamak diagnostics and laser-driven inertial fusion. In view of above, we have studied the dynamics and structural behaviour of plasma plume generated by low and high atomic number targets in presence of transverse magnetic field. Carbon ( $Z = 6$ ), aluminium ( $Z = 13$ ), nickel ( $Z = 28$ ) and tungsten ( $Z = 74$ ) have been taken for this study. By comparing the plume images of different Z-materials in identical experimental condition, it has been observed that plume geometrical shape, velocity, striation pattern, formation and shape of the diamagnetic cavity and its evolution is highly dependent on the target material. We have observed the expansion velocities of plasmas of metallic target

decrease with the increase of Z-number. The diamagnetic cavity exists for a longer time, and its width is smaller for high Z-materials (e.g. W) as compared to the low Z-materials (e.g. Al). As the time evolved, the cavity changed to jet/cone-like structure which in turn changes to the slab-like structure at an earlier time in case of low Z-material, this means magnetic diffusion time is less for low Z-materials as compared high Z-materials. Moreover, the number of magnetic striations is more and closely spaced in high Z-materials in comparison to low Z-materials where the striation is broader and well-separated. The validity of various plasma instabilities, which are responsible for observed density pattern (striation), has been also been discussed. On the other hand, carbon plasma is showing a dramatic behaviour in presence of magnetic field. Instead of well-defined cavity structure as in case of other metallic target, a Y-shaped symmetrical bifurcation is observed in the presence of magnetic field. Also we could not see any striation-like structure. Here it should be noted that electron temperature is weakly dependent on the metallic target-to-target ( $\sim 1.5-2$  eV) for laser-produced plasma. Therefore, for a fixed magnetic field and laser energy (with the general approximation that 50% of laser energy is utilized for plasma formation), classical cavity radius and magnetic diffusion time is independent of target materials, which contradict the present experimental observation. So detailed theoretical modeling with modified Z-dependent plasma motion and energy equation are required to explain the present observations. Above results are to be submitted for publication in *N. Behera et al., refereed journal*.

## **Chapter 7: Conclusion and future scope**

The major outcomes of the thesis research work have been summarized below:

Systematic experimental investigations have been performed to study the dynamical and geometrical behaviours of laser-produced plasmas across the transverse magnetic

field. Time-resolved emission spectroscopy, fast imaging and high frequency magnetic probe have been used to characterize the expanding plasma plume. Both permanent bar magnets and Helmholtz coils are utilized to produce uniform magnetic field.

In a presence of fix transverse magnetic field, plasma plume experience the resistive force due to magnetic pressure and tends to stagnation near magnetic diffusion time. Thereafter magnetic field diffuses into the plasma plume and hence the plasma plume re-expands linearly under the influence of polarized electric field ( $E \times B$  drift). Interestingly, in presence of both magnetic field and ambient gas, plume expands with uniform intensity distribution in large area (extended up to separation between the magnets) which can be utilized in film deposition technique.

Geometrical aspect of the evolving plasma plume along and across the magnetic field lines have been investigated by with indigenously designed setup based on Helmholtz coil and mutually synchronized two gated ICCD cameras. Time and field strength dependence of diamagnetism of laser produced plasma, that is formation and shape of diamagnetic cavity, cavity collapse and  $E \times B$  drift of bulk plasma is experimentally demonstrated. Observes plasma structure such as, elliptical cylinder, jet and finally slab-like structure in different phases of expansion is correlated with time varying plasma parameters and field diffusion into the plasma plume. Existence of plasma instability which is responsible for striation like structure is also discussed.

Diamagnetism of laser-produced plasma is also validated by indigenously designed three-axis, high-frequency B-dot probe. Further material dependence of plume expansion across the magnetic field, produced by low and high atomic number targets (C, Al, Ni and W) is thoroughly studied. It has been observed that formation and structure of diamagnetic cavity and its temporal evolution and dismissal is highly

dependent of the target material. Un-conventional behaviour of carbon plasma that is, instead of formation of diamagnetic cavity, a Y-shaped symmetrical bifurcation in presence of magnetic field is also discussed.

**Future scope:** This work can be extended for studying laser-produced plasma plume in presence of axial magnetic field and also plasma plume expansion in non-uniform magnetic field. It could be utilizing for the expansion of barium cloud in upper atmosphere, improve the sensitivity of laser-induced breakdown spectroscopy (LIBS), effect of external magnetic field in pulsed laser deposition, manipulation of shape and size of plasma plume etc.

## References

1. X. K. Shen, Y. F. Lu, T. Gebre, H. Ling and Y. X. Han, J. Appl. Phys. **100**, 053303 (2006).
2. J. D. Haverkamp, M. A. Bourham, S. Du and J. Narayan, J. Phys. D, Appl. Phys. **42**, 025201 (2008).
3. T. García, E. de Posada, M. Villagrán, J.L. Sánchez, P. Bartolo-Pérez and J.L. Pe'na, Appl. Surf. Sci. **255**, 2200 (2008).
4. M. Takichi and T. Kobayashi, Jpn. J. Appl. Phys. **38**, 3642 (1999).
5. S. S. Harilal, B. O'Shay and M. S. Tillack, J. Appl. Phys. **98**, 036102 (2005).
6. M. S. Raju, R. K. Singh, P. Gopinath and A. Kumar, J. Appl. Phys. **116**, 153301 (2014).
7. A. Neogi, R.K. Thareja, Phys. Plasmas **6**, 365 (1999).
8. S. Okada, K. Sato and T. Sekiguchi, Jpn. J. Appl. Phys. **20**, 157 (1981).
9. D. Winske, Phys. Fluids, B Plasma Phys. **1**, 1900 (1989).
10. D. K. Bhadra, Phys. Fluids **11**, 234 (1968).
11. G. Dimonte, L. Wiley, Phys. Rev. Lett. **67**, 1755 (1991).

12. A. Collette and W. Gekelman, *Phys. Plasmas* **18**, 055705 (2011).
13. B. H. Ripin, J. D. Huba, E. A. McLean, C. K. Manka, T. Peyser and H. R. Burris, J. Grun, *Phys. Fluids, B Plasma Phys.* **5**, 3491 (1993).
14. T. A. Peyser, C. K. Manka, B. H. Ripin, and G. Ganguli, *Phys. Fluids B: Plasma Physics* **4**, 2448 (1992).
15. N. Behera, R. K. Singh and Ajai Kumar, *Phys. Lett. A* **379 (37)**, 2215 (2015).
16. N. Behera, R. K. Singh, V. Chaudhari and Ajai Kumar, *Phys. Plasmas* **24 (3)**, 033511 (2017).
17. Kumar et al., *Rev. Sci. Instrum.* **80 (3)**, 033503 (2009).
18. E. T. Everson et al., *Rev. Sci. Instrum.* **80 (11)**, 113505 (2009).

# List of figures

1.1	The impact of intensity on the effect of the laser beam	9
1.2	Schematic of the constructing mechanism showing the outward motion of the ions, the radial electric field, the electron $E \times B$ drift, the resulting current (I), and the diamagnetic cavity	16
1.3	Drift motion of plasma plume in polarized electric field and external transverse magnetic field	17
2.1	Photograph of the vacuum chamber	28
2.2	Photograph of Nd:YAG laser (PRII 9030, Continuum Electro-Optic, Inc.) used for plasma production	29
2.3	(a) Schematic of the plasma plume in transverse magnetic trap, (b) magnetic field profile between the two magnets in the direction of plume expansion (z) and perpendicular to it (x) measured by Gauss meter	30
2.4	Photograph of Helmholtz coil installed inside the vacuum chamber	31
2.5	(a) An image of 5 mm $\times$ 5 mm grid used for calibration, (b) grey scale image of expanding plasma plume captured using ICCD camera, (c) pseudo-coloured image of plasma plume obtained using MATLAB colormaps (jet), (d) corresponding integrated intensity profile along the lateral direction	33
2.6	Photograph of designed B-dot probe	36
2.7	Schematic diagram of the capacitor bank pulsed power system	38
2.8	The measurement of magnetic field at 654 A input current, (a) Upper trace is the current transducer (CT) output, lower trace is Gauss meter output (b) Plot for magnetic field produced by Helmholtz Coil for different input current measured using gauss meter	39
2.9	Schematic of designed coil assemble structure integrated to SS vacuum chamber	40
2.10	Time response of RLC circuit	41
2.11	(a) Setup for mapping of magnetic field around plasma plume region, (b) magnetic field profile between the two poles of Helmholtz coil measured by Gauss meter at $x = 0$ mm and $x = 14$ mm for magnetic field 0.13 T.	42
2.12	Timing diagram for synchronization between laser and other auxiliary systems	44
3.1	Schematic of the experimental set-up	51
3.2	The sequence of images of expanding plasma plume and corresponding integrated intensity profiles along the lateral direction in vacuum and at different delay times. The integration times of ICCD are set as 10 and 20 ns	54
3.3	Variation of plume length and half width as a function of time delay. Ambient pressure is set as $10^{-5}$ Torr. Solid lines represent best linear fit for the experimental data	56
3.4	The sequence of images of expanding plasma plume at different delay times along with the corresponding integrated intensity profiles along the axial direction. The ambient gas pressure and integration time of	57

	ICCD are set as $10^{-2}$ Torr and 10 ns respectively	
3.5	Axial position vs time plot for both the front and core of the plasma plume at $10^{-2}$ Torr of argon pressure. Solid and dashed lines represent the best fit for the experimental data with the linear fit and drag force model respectively	58
3.6	SVD analysis of the plume images in the lateral direction for different time delays at $10^{-5}$ Torr pressure. (a), (b) and (c) represent the computed first, second and third principal components respectively	61
4.1	(a) Schematic of the experimental set-up and (b) magnetic field profile between the two poles of Helmholtz coil measured by Gauss meter at $x = 0$ mm and $x = 14$ mm for magnetic field 0.13 T	75
4.2	The sequence of images of expanding plasma plume without magnetic field at different delay times	77
4.3	The sequence of images of expanding plasma plume at (a) 0.13 and (b) 0.57 T magnetic field at different delay times	78
4.4	The sequence of images of expanding plasma plume at (a) 400 and (b) 800 ns delay time at different magnetic fields	80
4.5	The sequence of images (y-imaging) of expanding plasma plume at 1200 ns delay time at different magnetic fields.	80
4.6	Experimentally measured inner major and minor radii (a) as function of time delay for $B = 0.13$ T and (b) as a function of magnetic field strength at $t = 400$ ns	81
4.7	The projected images in diamagnetic limit at 0.13 T and 400 ns and non-diamagnetic limits at 0.57 T and 800 ns	82
4.8	Variation of (a) electron temperature and (b) electron density as a function of delay time in the absence and presence of 0.27 T magnetic field	83
4.9	Typical Stark broadened profile of Al II 466.3 nm line at 400 ns time delay in the absence of magnetic field and corresponding Lorentzian fit	84
4.10	Variation of electron temperature and density as a function of applied magnetic field at 400 ns time delay	85
4.11	Variation of plume length as a function of time delay in presence of (a) 0.13 T and (b) 0.57 T magnetic field	90
4.12	Variation of maximum growth time of the electron-ion hybrid instability with the applied magnetic field	92
5.1	(a) Probe tip in a glass test tube and (b) the probe is connected along with differential amplifier	99
5.2	(a) Circuit schematics of a differential amplifier for one axis of the probe and (b) the voltage gain vs. frequency response of the amplifier	100
5.3	Block diagram of experimental Setup to measure the frequency response and calibrate the B-dot Probe	101
5.4	Helmholtz coil arrangement for B-dot probe response check.	101
5.5	The frequency response from (a) 500 Hz to 1 MHz and (b) 500 kHz to 10 MHz by the magnetic field produced by the Helmholtz coil	102
5.6	Variation of $V_{\text{meas,p-p}}$ with $V_{\text{ref}}$ at (a) 500 kHz and (b) 1 MHz	103
5.7	Schematic circuit diagram for generating magnetic field by capacitor discharge system at 1.27 MHz to test the response of B-dot probe and its calibration	104
5.8	The phase matching of current and $\int V_{\text{meas}}(t) dt$ at (a) 0.92, (b) 1.27, (c) 1.63, (d) 2.0 and (e) 2.327 A at 1.25 MHz	106

5.9	Variation of $\int V_{\text{meas}}(t) dt$ as a function applied magnetic field. Reciprocal of the slope give calibration factor of the B-dot probe	107
5.10	ICCD camera image of expanding plasma plume at 0.13 T and 400 ns in a plane (a) perpendicular and (b) parallel to external magnetic field. (c) Schematic of diamagnetic cavity	109
5.11	Time profile of (a) 0.13 T external magnetic field, (b) induced magnetic field and (c) magnified portion of induced field	111
5.12	Time profile of (a) induced voltage as measured by B-dot and (b) magnetic field obtained by integrating voltage signals in the applied magnetic field range 0.13-0.57 T	112
5.13	The variation of induced magnetic field measured by B-dot probe with different applied external magnetic fields	113
6.1	The sequence of images of the expanding tungsten plasma plume without magnetic field at different delay times	120
6.2	The sequence of images of the expanding tungsten plasma plume at 0.13 T transverse magnetic field at different delay times	120
6.3	The sequence of images of the expanding tungsten plasma plume at 0.50 T transverse magnetic field at different delay times	121
6.4	The sequence of images of the expanding nickel plasma plume without magnetic field at different delay times	122
6.5	The sequence of images of the expanding nickel plasma plume at 0.13 T transverse magnetic field at different delay times	122
6.6	The sequence of images of the expanding nickel plasma plume at 0.50 T transverse magnetic field at different delay times	123
6.7	The sequence of images of the expanding carbon plasma plume without magnetic field at different delay times	124
6.8	The sequence of images of the expanding carbon plasma plume at 0.13 T transverse magnetic field at different delay times	124
6.9	The sequence of images of the expanding carbon plasma plume at 0.50 T transverse magnetic field at different delay times	125
6.10	The X-imaging of expanding carbon, aluminium, nickel and tungsten plasma at 400 ns and 1200 ns delay time in presence of (a) 0.13 T and (b) 0.50 T transverse magnetic field	126
6.11	The Y-imaging of expanding carbon, aluminium, nickel and tungsten plasma at 400 ns and 1200 ns delay time in presence of (a) 0.13 T and (b) 0.50 T transverse magnetic field	127



# List of tables

2.1	Geometrical parameters of the compact coil assembly	39
4.1	Variation of electron Larmor radius ( $r_{L,e}$ ), ion Larmor radius ( $r_{L,i}$ ), thermal beta ( $\beta_{the}$ ), total beta ( $\beta_{tot}$ ) and diffusion time ( $t_d$ ) with applied external magnetic field (B)	87



# Chapter 1

---

---

## Introduction

This chapter presents an introduction to basic plasma, physics of laser-produced plasma and its interaction with the external magnetic field. A brief introduction of plasma parameters relevant to the present study has been included. A detailed literature survey related to this field has also been incorporated in this chapter. This review is followed by motivation and the objective of the thesis research work.



## 1.1 Plasma

A plasma is a quasineutral gas of charged and neutral particles which exhibits collective behaviour [1]. As the charges in the plasma moves around, they can generate local concentrations of positive or negative charge, which create electric fields. Motion of charged particles also generates currents and hence magnetic fields. These fields affects the motion of other far away charged particles. So by “collective” behaviour means the motion which depends on both local conditions and state of plasma in the remote regions [1].

### 1.1.1 Concept of temperature

A plasma in thermal equilibrium has particles of all velocities, and the most probable distribution of these velocities is known as the Maxwellian distribution [1].

The one-dimensional Maxwellian distribution is given by

$$f(u) = A \exp\left(-\frac{\frac{1}{2}mu^2}{KT}\right) \quad (1.1)$$

where  $f du$  is the number of particles per  $m^3$  with velocity between  $u$  and  $u + du$ ,  $\frac{1}{2}mu^2$  is the kinetic energy, and  $K$  is Boltzmann’s constant.

The density  $n$  (number of particles per  $m^3$ ) is given by

$$n = \int_{-\infty}^{\infty} f(u)du \quad (1.2)$$

The constant  $A$  is related to the density  $n$  by

$$A = n \left( \frac{m}{2\pi KT} \right) \quad (1.3)$$

The width of the distribution is characterized by the constant  $T$  (temperature of plasma).

The average kinetic energy of the particle in this distribution is

$$E_{av} = \frac{1}{2}KT \quad (1.4)$$

In three dimensions, average kinetic energy of the particle in Maxwellian distribution is

$$E_{av} = \frac{3}{2}KT \quad (1.5)$$

Hence  $E_{av}$  equal to  $\frac{1}{2}KT$  per degree of freedom. Thus temperature  $T$  may be considered as a measure of the means kinetic energy of the random thermal motion of particles. As  $T$  and  $E_{av}$  are closely related, the plasma temperature is generally expressed in units of energy (eV).

### 1.1.2 Debye shielding

A fundamental characteristic of the behaviour of a plasma is its ability to shield out electric fields that are applied to it [1]. A positive test charge at certain place ( $x = 0$ ) inside a plasma is shielded by the accumulation of negative charges and it decreases with distance as

$$\Phi = \Phi_0 e^{-\frac{|x|}{\lambda_D}} \quad (1.6)$$

where  $\Phi_0$  is the potential  $\Phi$  on the plane  $x = 0$  and

$$\lambda_D = \sqrt{\frac{\epsilon_0 K T_e}{n e^2}} \quad (1.7)$$

here  $n$  is electron number density and  $T_e$  is the electron temperature.

The test charge is shielded by the plasma particles situated in a sphere of radius  $\lambda_D$ . The test charge interacts only with these particles and it has negligible influence on particles lying at distance  $|x| > \lambda_D$ . The quantity  $\lambda_D$  called Debye length and sphere of radius  $\lambda_D$  is called Debye sphere. The Debye length is a fundamental unit of length in plasma physics and is a measure of the shielding distance or thickness of the sheath.

### 1.1.3 Quasi-neutrality in plasma

Plasma as a whole electrically neutral but this neutrality may not be maintained over microscopic regions. If the dimension  $L$  of a system is much larger than  $\lambda_D$  ( $L \gg \lambda_D$ ),

then whenever local concentrations of charge arise or external potentials are introduced into the system, these are shielded out in a distance short compared with  $L$ , leaving the bulk of the plasma free of large electric potentials or fields. The plasma is ‘quasineutral’ means neutral enough so that one can take  $n_i \approx n_e \approx n$ , where  $n_i$  is ion number density,  $n_e$  is electron number density and  $n$  is plasma density, but not so neutral that all the interesting electromagnetic forces vanish [1].

### 1.1.4 Criteria for ionised gas to be plasma

A criterion for an ionised gas to be a plasma is that it should be enough dense so that  $\lambda_D$  is much smaller than dimension of a system  $L$  [1].

$$\lambda_D \ll L \quad (1.8)$$

Another condition for an ionised gas to be called a plasma is that there should be enough charged particles in the Debye sphere for Debye shielding.

The number of particles in a Debye sphere is

$$N_D = n \frac{4}{3} \pi \lambda_D^3 = 1.38 \times 10^6 \frac{T^{3/2}}{n^{1/2}} \quad (T \text{ in } ^\circ K) \quad (1.9)$$

Hence collective behaviour requires,

$$N_D \gg 1 \quad (1.10)$$

The third condition is related with collisions. In the weakly ionized gas charged particles collide so frequently with neutral atoms that their motion is controlled by ordinary hydrodynamic forces rather than by electromagnetic forces. So it does not qualify as a plasma. Therefore, for an ionised gas to be a plasma, the period of typical plasma oscillation must be much smaller than mean time between collisions with neutral atoms ( $\tau$ ). So plasma requires,

$$\omega_p \tau > 1 \quad (1.11)$$

where  $\omega_p$  is the frequency of typical plasma oscillation.

Hence, the three conditions a plasma must satisfy are:

---



---


$$(1) \lambda_D \ll L$$

$$(2) N_D \gg 1$$

$$(3) \omega_p \tau > 1$$

### 1.1.5 Plasma frequency

If the electrons in the plasma are displaced from a uniform background of ions, electric fields will be built up in such a direction as to restore the neutrality of the plasma by pulling the electrons back to their original positions. Because of their inertia, the electrons will overshoot and oscillate around their equilibrium positions with a characteristic frequency known as the plasma frequency. This oscillation is so fast that the massive ions do not have time to respond to the oscillating field and may be considered as fixed.

The expression for plasma frequency ( $\omega_p$ ) is

$$\omega_p = \left( \frac{n_0 e^2}{\epsilon_0 m} \right)^{1/2} \quad (1.12)$$

Numerically, the approximate formula is

$$\frac{\omega_p}{2\pi} = f_p \approx 9\sqrt{n_0} \quad (1.13)$$

This frequency depends on only the plasma density ( $n_0$ ) and it is one of the fundamental parameters of the plasma. Example, if  $n_e = 10^{18} \text{ m}^{-3}$  then  $f_p = 9 \text{ GHz}$ .

Radiation at  $f_p$  normally lies in the microwave range [1].

## 1.2 Laser-produced plasma

When a high-intensity laser pulse is incident on a target material, it causes heating, melting and vaporization of the surface layers and results hot expanding plasma. This transient plasma is known as laser-produced plasma or laser-induced plasma or simply plasma plume. As laser-produced plasma is the result of the

---

interaction of laser with the material, so its properties depend on both, the laser parameters and the material properties of the target. The laser parameters such as laser wavelength, pulse duration, pulse shape, intensity of laser etc., and the properties of the material such as, absorption, reflection, atomic number of target materials etc. significantly affects the properties of the induced plasma. Typically, the plasma is produced by nanosecond, picosecond and femtosecond lasers. As far as the target materials are concerned, all types of solids, liquids and gases are used [2-7].

The laser-produced plasma is widely studied due to its potential applications in various areas like inertial confinement fusion (ICF), X-ray lasers, extreme ultra-violet (EUV) lithography, material processing, plasma diagnostics, tokamaks, space applications and pulsed laser deposition etc. [8-18]. Many experimental, theoretical and simulation-based studies have been carried out in the last few decades to understand the fundamental physics involved with it and to use it for applications [2-7]. Laser interaction with matter is one of the most important and complex phenomena. The complex mechanism of laser plasma formation which basically involves several stages of laser-matter interaction should be understood properly and it is explained in the section below.

### **1.3 Physics of laser plasma formation**

The formation of laser-produced plasma is a multi-step mechanism [3-5]. In the first stage, the high-intensity laser pulse falls on the target surface. A part of the laser energy got reflected back and rest is absorbed by the target. The heating rate and the surface temperature are defined by absorption and reflection coefficients, thermal conductivity and the specific heat of the target material. After a period of tens of picoseconds, the electrons and atoms in the solid equilibrate which leads to a strong heating of the irradiated volume. In this stage, laser-solid interactions are dominant. In the second stage, the material from the heated volume is ejected from the solid but

continue to absorb energy from the laser, resulting in the formation of a thin layer ionized vapor on the surface of the target. This is the laser-produced plasma. In this stage, laser-plasma interactions are dominant. In the plasma, the absorption of laser primarily occurs by an inverse Bremsstrahlung process [5], which involves the absorption of a photon by a free electron. The absorption coefficient  $\alpha_p$  of the plasma can be expressed as

$$\alpha_p = 3.69 \times 10^8 \left( \frac{Z^3 n_i^2}{T^{0.5} \nu^3} \right) \left( 1 - e^{-\frac{h\nu}{kT}} \right) \quad (1.14)$$

where  $Z$ ,  $n_i$ , and  $T$  are the average charge, ion density, and temperature of the plasma and  $h$ ,  $k$ , and  $\nu$  are the Planck constant, Boltzmann constant, and frequency of the laser light, respectively. The laser energy is highly absorbed if  $(\alpha_p X)$  is large, where  $X$  is the dimension perpendicular to the target of the expanding plasma. This equation shows that the absorption coefficient of the plasma is proportional to  $n_i^2$ . Thus, the plasma absorbs the incident laser radiation only at distances very close to the target where the densities of the charged particles are very high. In this equation, we have assumed that the plasma frequency is smaller than the frequency of the laser wavelength; otherwise, all the radiation would be reflected by the plasma [5]. The pulse duration and hence intensity of laser pulse play major role in material removal and plasma formation process as schematically shown in Fig. 1.1.

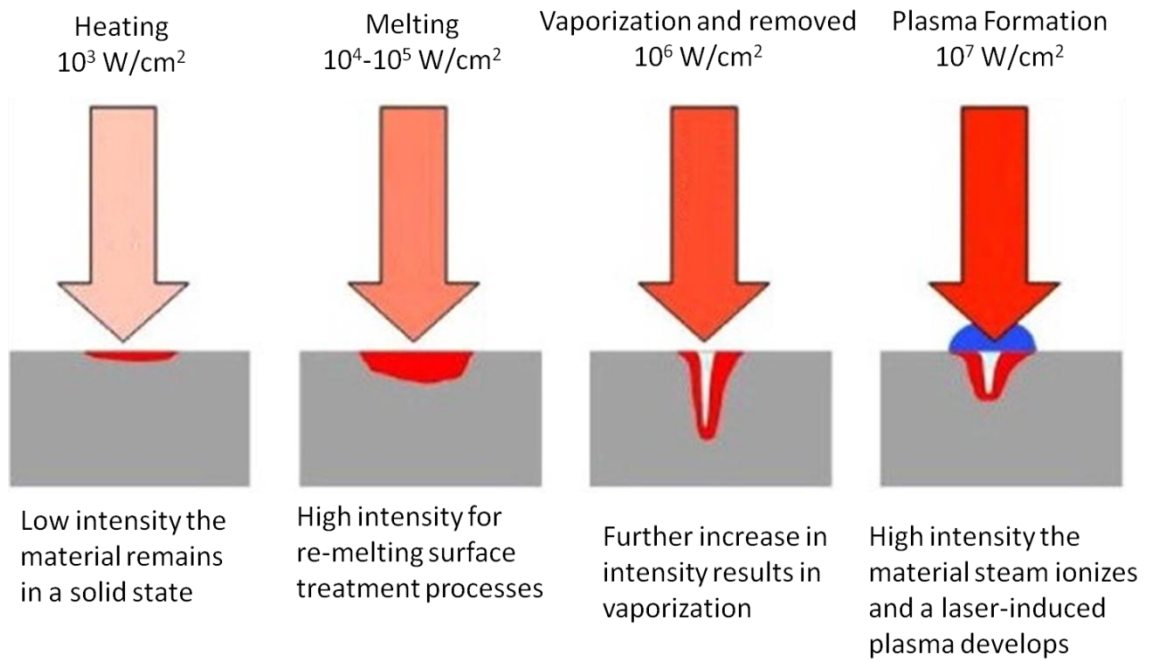


**Fig. 1.1.** The impact of intensity on the effect of the laser beam [19].

The third stage starts after the termination of the laser pulse. In this stage, the plasma expands into mediums like vacuum, background gas, background uniform or non-uniform magnetic field. So the plasma dynamics is effectively controlled by both plasma parameters as well as the nature expanding mediums.

## 1.4 Plasma plume in vacuum

In vacuum, the laser-produced plasma expands adiabatically and the Euler equations of hydrodynamics adequately describe the expansion process. The gas dynamics equations (conservation of mass density, momentum and energy equations) [6, 21] are:

$$\frac{\partial \rho}{\partial t} = - \frac{\partial(\rho v)}{\partial x} \quad (1.15)$$

$$\frac{\partial(\rho v)}{\partial t} = - \frac{\partial}{\partial x} [p + \rho v^2] \quad (1.16)$$

$$\frac{\partial}{\partial t} \left[ \rho \left( E_d + \frac{v^2}{2} \right) \right] = - \frac{\partial}{\partial x} \left[ \rho v \left( E_d + \frac{p}{\rho} + \frac{v^2}{2} \right) \right] + \alpha_{IB} I_{laser} - \epsilon_{rad} \quad (1.17)$$

Here,  $\rho$  is the mass density,  $v$  is the flow velocity,  $p$  is the local pressure,  $E_d$  is the internal energy density,  $I_{\text{laser}}$  is the laser irradiance,  $\alpha_{\text{IB}}$  stands for the absorption coefficient due to inverse Bremsstrahlung, which is a function of position in the plume and  $\epsilon_{\text{rad}}$  is the amount of energy emitted by the vapor per unit volume and time in the Bremsstrahlung process. This theory governing plasma expansion can be used for both ns and fs laser ablation.

The expression for expansion velocity [20, 21] is

$$v = \sqrt{\frac{(4\gamma + 10)E}{3M}} \quad (1.18)$$

Here,  $E$  is the energy of the plume,  $M$  is the mass evaporated and  $\gamma$  is the ratio of specific heats or heat capacity ratio. So the plasma expands linearly with a constant velocity in vacuum. This is also supported by several experimental and simulation studies. This is owing to the fact that, at very low pressure, the mean free path of the gas molecules is very large so that there is not much interaction between the expanding plasma and the ambient gas.

## **1.5 Plasma plume in background gas**

When the expansion takes place in ambient gas, the resistive force of the ambient gas controls the expansion dynamics of plasma plume. There are two models to explain the dynamics of laser-produced plasma in the presence of an ambient gas.

### **1.5.1 Shock wave model**

The plume expansion in the high background pressure can be explained by shock wave model [22-24]. In the high pressure, as the plume expands the mass of the background gas becomes more than that of the plasma plume and this results the formation of a shock between the two which propagates according to the blast wave model given by the relation

$$R = \xi_0 \left( \frac{E_0}{\rho_0} \right)^{1/5} t^{2/5} \quad (1.19)$$

where  $R$  is the position of the plume front at a time  $t$ ,  $\xi_0$  is a dimensionless constant depending on the specific heat capacity of the gas,  $\rho_0$  is the density of background gas and  $E_0$  is the energy released during the ablation of the target to the background gas.

### 1.5.2 Drag force model

On the other hand, the plume expansion in the low background pressure can be explained by drag force model [22-24]. At low background pressure, the mass of the plasma plume is more than that of background gas and the plume experiences a viscous force proportional to its velocity in the background gas. Hence the drag force model shows better agreement at earlier time. According to this model, the position of the plume front at a time  $t$  is given by the relation,

$$z = z_f [1 - \exp(-\beta t)] \quad (1.20)$$

where  $z$  is the position of the plume front at time  $t$ ,  $z_f (= v_0 / \beta)$  is the stopping distance of the plume,  $\beta$  is the slowing coefficient and  $v_0$  is the initial expansion velocity of the plume front.

## 1.6 Plasma plume in transverse magnetic field

### 1.6.1 Plasma parameters in magnetic field

In order to understand the dynamics of plasma plume in magnetic field, we need to understand and evaluate the various relevant parameters as discussed below.

#### 1.6.1.1 Larmor radius (Gyroradius or cyclotron radius)

The Larmor radius of a charged particle is defined as the radius of the circular motion of a charged particle in the presence of a uniform magnetic field [1]. The expression for Larmor radius ( $r$ ) is

$$r = \frac{mv_{\perp}}{|q|B} \quad (1.21)$$

where  $m$  is the mass of the charge particle,  $v_{\perp}$  is the component of the velocity perpendicular to the direction of the magnetic field,  $q$  is the electric charge of the particle, and  $B$  is the strength of the magnetic field.

The plasma dynamics in the presence of a uniform magnetic field depends on Larmor radius and the scale length of the plasma. When the Larmor radius of the plasma is comparable or greater than the scale length of the plasma, then the plasma can be treated as unmagnetized otherwise magnetized. In laser-produced plasma, the Larmor radius for ions and electrons are greater and smaller than the plume dimension respectively. Therefore, the ions and electrons can be considered as unmagnetized and magnetized respectively.

### 1.6.1.2 Plasma beta

There are three different types of plasma betas in laser-produced plasma.

The thermal beta of plasma is defined as the ratio of plasma thermal pressure to the magnetic pressure [1, 28]. The expression for thermal beta ( $\beta_{the}$ ) is

$$\beta_{the} = \frac{n_e T_e}{B^2 / 2\mu_0} \quad (1.22)$$

where  $n_e$  is the electron density,  $T_e$  is the electron temperature (eV),  $B$  is the applied magnetic field and  $\mu_0$  is permeability of free space.

After the initial conversion of thermal energy into directed energy, the directed beta ( $\beta_d$ ) becomes an important parameter. The directed beta for plasma is defined as the ratio of plasma kinetic pressure to magnetic pressure [28]. The expression for  $\beta_d$  is

$$\beta_d = \frac{mn_e v^2 / 2}{B^2 / 2\mu_0} \quad (1.23)$$

where  $m$  is the mass and  $v$  is the mass flow velocity.

As laser-produced plasma is highly transient in nature and usually directed beta is much larger than thermal beta. So the total beta which is the sum of thermal

beta and directed beta plays an important role in the formation of diamagnetic cavity of expanding plasma plume in magnetic field [28]. The expression for total beta ( $\beta_{tot}$ ) is

$$\beta_{tot} = \frac{n_e T_e + m n_e v^2 / 2}{B^2 / 2\mu_0} \quad (1.24)$$

### 1.6.1.3 Bubble radius (Confinement radius)

As the laser produced-plasma starts to expand, the diamagnetic cavity is formed and plasma behaves as a magnetic bubble. The maximum size of the diamagnetic cavity is known as bubble radius or confinement radius. The bubble radius is approximated by equating the total excluded magnetic energy and the kinetic energy of the laser-produced plasma.

The expression for bubble radius for spherical symmetric expanding plasma plume [29, 30] ( $R_b$ )

$$R_b = \left( \frac{3\mu_0 E_{lpp}}{\pi B^2} \right)^{1/3} \quad (1.25)$$

where  $E_{lpp}$  is the kinetic energy of the laser plasma which is approximated as half of the energy of initial laser pulse and  $B$  is the applied magnetic field.

### 1.6.1.4 Magnetic diffusion time

When the magnetic bubble reaches the confinement radius, the field diffuses into the plasma plume or diamagnetic cavity [28]. The time at which this starts is the magnetic diffusion time. The expression for the magnetic diffusion time is:

$$t_d = \mu_0 \sigma R_b^2 \quad (1.26)$$

where  $\sigma \left( = \frac{50\pi\epsilon_0 T_e^{\frac{3}{2}}}{\sqrt{m_e} e^2 Z \ln\Lambda} \right)$  is the plasma conductivity,  $\ln\Lambda$  is the coulomb logarithm and

its value is 10 for laser-produced plasma.

### 1.6.1.5 Cyclotron frequency

The angular frequency of the circular motion of a charged particle in the presence of a uniform magnetic field is known as the cyclotron frequency or gyrofrequency ( $\Omega$ ) [1].

The expression for  $\Omega$  is

$$\Omega = \frac{|q|B}{m} \quad (1.27)$$

### 1.6.1.6 Lower-hybrid frequency

In plasma, a lower hybrid oscillation is a longitudinal oscillation of ions and electrons in a magnetized plasma. The direction of propagation must be nearly perpendicular to the stationary magnetic field, within about  $\sqrt{m_e/m_i}$  radians. Otherwise the electrons can move along the field lines fast enough to shield the oscillations in potential.

The frequency of this oscillation is known as lower-hybrid frequency and the expression for lower-hybrid frequency ( $\omega_{LH}$ ) [31] is

$$\omega_{LH} = \frac{\omega_{pi}\Omega_e}{(\omega_{pe}^2 + \Omega_e^2)^{1/2}} \quad (1.28)$$

where  $\omega_{pe}$ ,  $\omega_{pi}$  and  $\Omega_e$  are the electron-plasma, ion-plasma and electron cyclotron frequencies respectively. It is called as ‘hybrid’ because of the mixture of two frequencies.

## 1.6.2 Plasma plume expansion in magnetic field

The dynamics of plasma plume is influenced significantly in the presence of external magnetic field and therefore it is useful to control the dynamic properties of highly transient plasma plume. The manipulation of geometrical shape, size and dynamics of plasma plume by the introduction of the external magnetic field has great importance in applied research and also in fundamental studies. Due to initial conversion of thermal energy into directed energy, the sum of directed pressure and thermal pressure of plasma plume is much larger than the magnetic pressure (that is plasma beta  $> 1$ ).

---

As the time evolves, electron temperature and density of the plasma plume decrease rapidly resulting in a decrease in plasma beta with time. Therefore, two different approaches have been taken to explain the dynamics of laser-produced plasma across the transverse magnetic field which are discussed as below.

### **1.6.2.1 Formation of diamagnetic cavity and confinement of the plume**

In the first approach the expansion of the plasma plume is treated as expansion in the diamagnetic limit where the applied magnetic field is displaced by the induced magnetic field due to the diamagnetic current in the plasma with this the plasma plume experiences the decelerating force [28, 31, 72]. The diamagnetism of plasma plume could be understood as follows [25]. Charge particles in the plasma plume experience the Lorentz force in the presence of magnetic field and therefore gyrate in opposite direction with different radii depending on the charge, mass and velocity of the plume particles. Since the Larmor radius for ions is greater than the plume dimension, the ions can be considered as unmagnetized and therefore, expand radially outward. But the electrons tie to the magnetic field and try to hold the ions back and eventually produce radially inward electric field. The ions on the outer edge are slowed down by the produced radial electric field, but ions inside catch up and thus the plasma get compressed into a thin shell. This results the formation of diamagnetic cavity or magnetic bubble. As the electrons are magnetized,  $E \times B$  drift is created azimuthally relative to the ions which, gives rise to a current. This current (known as diamagnetic current) generates a magnetic field opposite to the applied field inside. So the applied magnetic field is displaced by the induced magnetic field due to this diamagnetic current in the plasma and with this the plasma plume also experiences the decelerating force. This diamagnetic cavity exists up to the magnetic diffusion time and then its collapse starts.

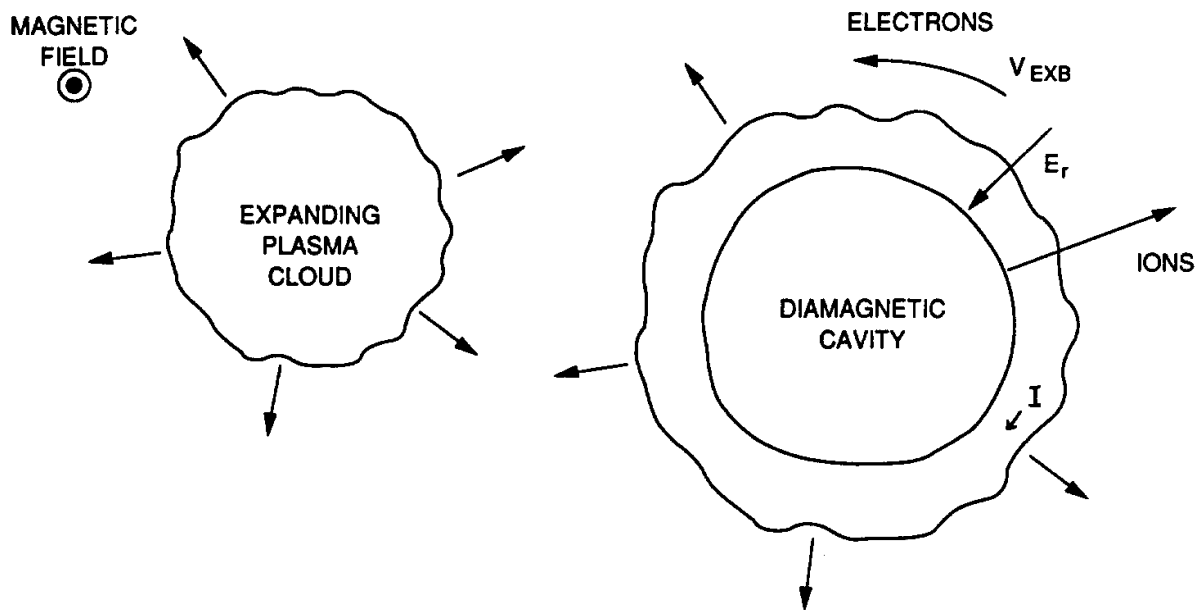


**Fig. 1.2.** Schematic of the constructing mechanism showing the outward motion of the ions, the radial electric field, the electron  $E \times B$  drift, the resulting current ( $I$ ), and the diamagnetic cavity. [25].

### 1.6.2.2 Polarization of plume and $E \times B$ drift

In the second approach, it is considered that external magnetic field is diffused in the plasma plume and produces polarized electric field (due to the deflection of electrons and ions in opposite direction) perpendicular to both the expansion direction and the magnetic field [26, 27, 31, 76, 77]. Therefore, the plasma plume experiences the  $E \times B$  field and drifts in the axial direction. The expression for drift velocity of the plasma plume ( $V$ ) is

$$V = \frac{E_{pol} \times B}{B^2} \quad (1.29)$$

where  $B$  is the external magnetic field and  $E_{pol}$  is the polarization electric field.

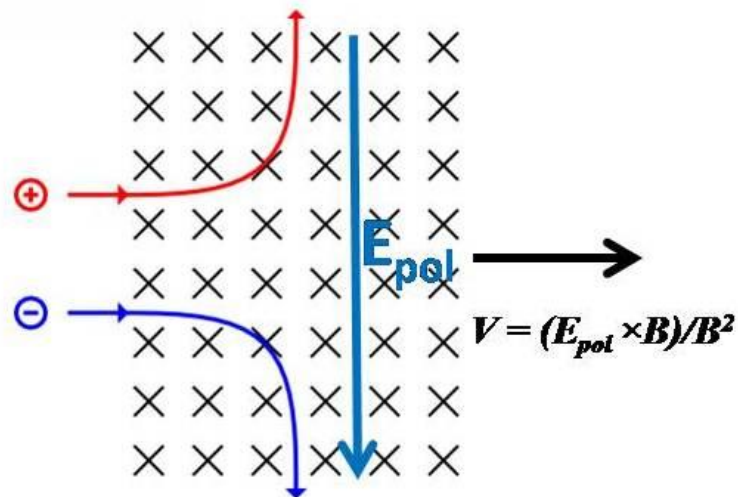


**Fig. 1.3.** Drift motion of plasma plume in polarized electric field and external transverse magnetic field.

## 1.7 Instabilities in plasma

The growth of plasma instability, mainly the velocity shear instabilities are responsible for structure formation during expansion of the plasma plume in the presence of magnetic field. An instability is said to be responsible for the intensity fluctuation or structure formation if its estimated growth time matches with the time at which the structure formation starts. Common instabilities present in laser-produced plasma are:

- 1.7.1 Rayleigh-Taylor (RT) instability,
- 1.7.2 Kelvin-Helmholtz (KH) instability and
- 1.7.3 Electron-ion hybrid instability

### 1.7.1 Rayleigh-Taylor (RT) instability

The Rayleigh-Taylor instability (after Lord Rayleigh and G. I. Taylor), is an instability of an interface between two fluids of different densities which occurs when the lighter fluid is pushing the heavier fluid. In laser-produced plasma RT instability is reported in presence of ambient gas [32]. In the plasma, a RT instability can occur

because the magnetic field acts as a fluid supporting a heavy fluid (plasma) [1]. The expression for growth time of RT instability [31] is

$$\lambda_{RT} = \left( \frac{g_{eff}}{L_n} \right)^{-1/2} \quad (1.30)$$

where  $g_{eff}$  is the effective deceleration due to magnetic field and  $L_n$  is the density scale length.

### 1.7.2 Kelvin-Helmholtz (KH) instability

The Kelvin-Helmholtz instability (after Lord Kelvin and Hermann von Helmholtz) can occur when there is velocity shear in a single continuous fluid, or where there is a velocity difference across the interface between two fluids. The KH instability depends on the free energy on the velocity shear layer. This does not require a transverse deceleration of the plasma. In plasma, KH instability is identified from the velocity shear of front layer of expanding plasma plume. The expression for growth time of KH instability [31] is

$$\gamma_{KH} = \frac{2\pi}{0.16 \left( \frac{V_E}{L_v} \right)} \quad (1.31)$$

Here,  $V_E$  is the edge velocity and  $L_v$  is the shear scale length.

### 1.7.3 Electron-ion hybrid instability

Peysner et al. [31] reported electron-ion hybrid instability in presence of 0.3 - 0.6 T field and comparatively higher laser energy (30-300 J) and this instability is responsible for the formation of striation-like structures in laser-produced plasma. In order to validate the existence of electron-ion hybrid instability in the present case, we have estimated the growth rate and maximum growth time for this instability.

This arises when the larmor radius of the ions is large compared to the scale length of the plasma. By assuming unmagnetized ions and magnetized electrons, the dispersion relation of K-H instability can be written as

$$\left( \frac{d^2}{dx^2} - k_y^2 + F(\omega) \frac{k_y V_E''(x)}{\omega - k_y V_E(x)} \right) \phi = 0 \quad (1.32)$$

where

$$F(\omega) = \frac{\delta^2}{(\delta^2 + 1) \left(1 - \left(\frac{\omega_{LH}}{\omega}\right)^2\right)} \quad (1.33)$$

and

$$\omega_{LH} = \frac{\omega_{pi} \Omega_e}{(\omega_{pe}^2 + \Omega_e^2)^{1/2}} \quad (1.34)$$

Here  $\omega_{pe}$  is electron plasma frequency,  $\omega_{pi}$  is ion plasma frequency,  $\Omega_e$  is the electron cyclotron frequency and  $\omega_{LH}$  is called as lower hybrid frequency.

The expression for maximum growth rate of this instability is given by

$$\gamma = 0.05 \omega_{LH} \quad (1.35)$$

The expression for maximum growth time is

$$\tau = \frac{2\pi}{0.05\omega_{LH}} \quad (1.36)$$

## 1.8 Overview of earlier works

The study of laser-produced plasma in presence of external magnetic field is useful to understand several important physical phenomena like conversion of kinetic energy into plasma thermal energy, plume confinement, ion acceleration/deceleration, emission enhancement/decrease and plasma instabilities [31, 33-38]. These phenomena play an important role in many applied researches, like tokamak plasma, space plasmas, propulsion of space vehicles, investigation of acceleration of stellar winds, increase in the detection sensitivity of laser-induced breakdown spectroscopy [33, 39], manipulation of plasma plume in pulse laser deposition [40-42], debris mitigation [43] etc.

Several pioneer works has been carried out to understand plasma plume-magnetic field interaction. Bhadra et al. (1968) [45] studied the effect of resistivity in the expansion of a laser-produced hot plasma against a magnetic field and postulated that laser-induced plasma would be stopped by a magnetic field  $B$  at a distance  $r \sim B^{-2/3}$ . Tuckfield, et al. (1969) [46] observed the periodic pulsations of the plasma

---

boundary against the magnetic field when  $\beta > 1$  observed. Peyser et al. (1992) [31] found that laser plasma from hollow glass cylinders in magnetic field results in structures. Further, they attributed that  $E \times B$  is responsible for the jet-like structures, whereas instabilities cause the edge structure. Mostovych et al. (1989) [47] found that the instability of barium plasma in presence of magnetic field as electron-ion hybrid velocity-shear instability. Bryunetkin et al. (1992) [48] reported the first experimental demonstration of the difference in the emission of spectral lines by ions of different degrees of ionization in a laser-plasma expanding in vacuum in the presence of a transverse external magnetic field strength of 0.3 T. Dimonte, et al. (1991) [29] studied the expansion of laser-ablation plasmas in a magnetic field with a new Faraday-rotation magnetic imaging probe and Fourier-analyzed optical plasma images over a wide range of ion magnetization. Plasma instabilities are observed during the plasma expansion which evolve from short to long wavelengths and significantly affect the magnetic structure. Neogi, et al. (1999) [35] observed that the presence of non-uniform magnetic field can cause oscillations of the expanding plasma and splitting of plume in the presence of an inhomogeneous magnetic field and explained the presence of lobes by considering  $J \times B$  force acting on the plume. Ripin et al. (1987) [49] observed the flute instability in aluminium targets in presence of 1 T magnetic field and was attributed to large larmor radius RT instability. VanZeeland, et al. (2004) [30] experimentally studied the diamagnetic cavity created by a dense laser-produced plasma expanding into an ambient magnetized background plasma capable of supporting Alfvén waves. Ripin et al. (1993) [50] studied sub-Alfvénic plasma expansion. Harilal et al. (2004) [28] found that the plume is not completely stopped at bubble radius and diffused across the magnetic field. Pandey et al. (2013) [51] showed Copper plasmoid rotation in presence of non-uniform magnetic field which was attributed to torque acting on the plasmoid because of the  $J \times B$  force. Peyser et al.

---

(1992) [31] studied the dynamics of plasma produced from glass target in the presence of different magnetic fields and undulations were observed in the plasma due to large larmor radius Kevlin-Helmholtz instability. Huba et al. (1990) [52] estimated the ‘stopping’ radius of a magnetically confined expansion by equating the initial kinetic energy of the plasma with magnetic energy and the stopping radius is named as magnetic confinement radius of plasma. Harilal et al. (2005) [53, 54] suggested the role of backflow of particles toward the target for the appearance of lobes. Qindeel et al. (2008) [55] studied the plume behavior with imaging charge-coupled device for varying magnetic field for aluminium, copper and brass targets. They suggested that plume structure might result from the Lorentz force exerted by the field. Jet-like structures in the plume in the presence of magnetic field has been attributed to instabilities by Rafique et al. (2008) [56].

Several diagnostic techniques, for example, optical emission spectroscopy, fast imaging, Langmuir probe, etc. was employed to study plasma plume - magnetic field interaction (Harilal et al. (2004) [28], Patel et al. (2013) [44], VanZeeland et al. (2004) [30], etc.).

Though many works have been done to understand plasma plume - magnetic field interaction, parametric study of the formation and evolution of diamagnetic cavity and its geometrical features is not conclusive in the reported work.

## **1.9 Motivation and objectives of the thesis**

In presence of magnetic field, dynamics and structure of the plasma plume are governed by formation & evolution of diamagnetic cavity, diffusion of magnetic field, collapse of diamagnetism and  $E \times B$  drift of the plasma plume across the magnetic field. To observe these phenomena, we need two dimensional imaging of plume during its expansion with high resolution image. There is possibility of occurrence of

---

---

some instabilities during its expansion. Similar phenomena have been reported by Peyser et al. [31]. Keeping in the view we have designed a high resolution two directional (along and across magnetic field) imaging system. Majority of previous experiments related to laser plasma-magnetic field interaction have been performed with permanent bar magnet where plume imaging along the magnetic field lines is not possible because of experimental constraints. Due to asymmetrical structure of plasma plume, the complete picture of formation and collapse of diamagnetic cavity is not feasible with only projection across the magnetic field. In addition,  $E \times B$  drift of the laser plasma is largely ignored in case of moderate magnetic field ( $< 1$  T) and the ablating laser energy of the order of few hundred mJ [28, 35, 39]. In conclusion, the systematic investigation of the formation of diamagnetism of plasma plume and at its transition into non-diamagnetic limit (diffused magnetic field) is scarce in the literature.

In view of the above, a systematic experimental investigation of the plume dynamics in both diamagnetic and non-diamagnetic limit has been carried out. The major objectives may be listed as follows:

- Development of a technique for two-directional imaging of expanding plasma plume in a uniform magnetic field.
- Visualization of the three-dimensional structure of the diamagnetic cavity.
- Study of the expansion of plasma plume in high and low magnetic beta limits.
- Study of the formation and evolution of the diamagnetic cavity and its transition to the non-diamagnetic limit.
- Study of magnetic striations in laser-produced plasma.
- Measurement of the time-varying magnetic field using B-dot probe.
- Study of the material dependence of diamagnetism in laser-produced plasma.

## **1.10 Organization of the thesis**

This thesis reports the systematic experimental investigations to study the dynamical and geometrical behaviours of laser-produced plasmas across the transverse magnetic field. Here the major emphasis is given on the diamagnetism in laser-produced plasma.

**Chapter 2** contains an overview of the experimental scheme used for the thesis study and the diagnostics like time-resolved emission spectroscopy, fast imaging and high frequency, three-axis magnetic probe those have been used to characterize the expanding plasma plume.

**Chapter 3** presents the study of the dynamical and geometrical behavior of laser-produced aluminum plasma across the 0.45 T magnetic field produced by two NdFeB permanent magnet bars using time-resolved fast imaging technique.

**Chapter 4** discusses the geometrical aspect of the expanding aluminum plasma plume along and across the magnetic field lines have been investigated with indigenously designed setup based on Helmholtz coil ( $B = 0-0.57$  T) and mutually synchronized two gated ICCD cameras.

In **Chapter 5**, the diamagnetism of laser-produced plasma is validated by indigenously designed three-axis, high-frequency B-dot probe.

**Chapter 6** contains the comparative study of material dependence of diamagnetism in laser-produced plasma using targets viz., copper, aluminium, nickel and tungsten.

In **Chapter 7**, the major outcomes of the thesis research work those are discussed in the previous chapters have been summarized. Also a few important possible future scope of this thesis research work has been provided.



## Chapter 2

---

### Experimental scheme

This chapter provides the detailed description of various instruments used in experimental setup (production of laser-produced plasma and diagnostics to diagnose plume dynamics and formation of structures in plasma plume) and various diagnostic systems used in this thesis. We have also described the design of Helmholtz coil, production of the uniform pulsed magnetic field by capacitor discharge method and its synchronization with generation of plasma plume, ICCD camera, spectrometer and B-dot probe.



## **2.1 Introduction**

The experimental study of laser-produced plasma mainly consists of two important parts: the first one is the production of laser plasma in the desired environment and the second one is the characterization of the produced plasma using suitable diagnostics. In this thesis work, the plasma is generated using an Nd:YAG laser from various metallic/non-metallic targets and the plasma expands in a transverse uniform magnetic field. Various challenges are associated to produce uniform variable magnetic field, particularly a high magnetic field in a small volume. This is important as it plays a key role to produce various expected features of expanding plasma plume experimentally. Majority of previous experiments have been performed with permanent bar magnet where plume imaging along the magnetic field lines is not possible because of experimental constraints. But the plume structure in magnetic field is highly asymmetrical and therefore complete geometrical information cannot extract from plume images projected across the magnetic field direction only. This problem is smartly resolved by developing a special designed Helmholtz coil configuration which not only produces uniform variable magnetic field but also allows the fast imaging of expanding plasma plume along and across the applied external magnetic field. We can characterize the expanding plasma plume using only the accurate and sophisticated diagnostics. These diagnostics provide required data to understand the physics associated with plasma dynamics. Therefore, we have taken high measures during development of desired diagnostics. The diagnostics like ICCD camera, optical emission spectroscopy and indigenously developed three-axis, high-frequency B-dot probe are used for this thesis work. The details of various equipment and diagnostic tools used are described below.

## 2.2 Components of experimental setup

### 2.2.1 Vacuum chamber and pumping system

The plasma is generated in a multipurpose cylindrical vacuum chamber (Fig. 2.1) made of non-magnetic stainless steel (SS 304 with 3 $\Delta$  finishing) of 1.6m length and 21 cm inner diameter. This chamber has 30 viewports (27 ports are fitted with CF 100 couplers, 2 ports are fitted with CF 160 couplers and rest one port is fitted with CF 35 coupler) in an equal-spaced cross geometry. A combination of double stage direct drive rotary vacuum pump (Model No: ED-30, Hind High Vacuum) and Turbo Molecular Pump (Mod: TC 400, Pfeiffer Vacuum) are used to achieve a base pressure less than  $10^{-6}$  Torr. The maximum pumping speed of rotary pump and TMP are 8 m<sup>3</sup>/hr and 600 l/s respectively. Gases can be introduced into the chamber at desired pressures through a fine controlled needle valve. Three pressure gauges: Digital Pirani Gauge (DHPG-102S, HI-TECH, Range: 0.9 to  $10^{-3}$  m.bar), Digital Penning Gauge (DPGN-001, HINDHIVAC, Range:  $10^{-2}$  to  $10^{-6}$  m.bar) and 375 Convectron gauge (Granville-Phillips, Range: atmosphere to  $10^{-4}$  Torr ( $10^{-4}$  m.bar,  $10^{-2}$  Pa)) are connected to the vacuum chamber to monitor pressure of the chamber.



**Fig. 2.1.** Photograph of the vacuum chamber

### 2.2.2 Laser system

A Q-switched Nd:YAG laser (PRII 9030, Continuum Electro-Optic, Inc. [57], Fig. 2.2) ( $\lambda = 1064$  nm, 8 ns pulse width) of 1.6 J maximum pulse energy is used to generate plasma. By varying the delay between the flash lamp and Q-switch, the desired laser fluence is achieved at the target. The diameter of the laser beam is 12.0 mm. The laser beam was focused using a 150 cm focal length lens and the spot size of the laser beam is set to about 1.0 mm in diameter at the target which can produce the power density  $\sim 10^9$  W/cm<sup>2</sup> the target surface. The laser can be operated at both 30 Hz and in single pulse mode. For all experiments in this thesis, the laser is operated only in the single pulse mode. An electromechanical shutter is introduced in the path of the laser beam for single shot operation. The intensity profile of this laser is flat-top (or top-hat) and the beam divergence is less than 5 mrad. A remote box is used to operate the laser, which is connected to the laser power supply.

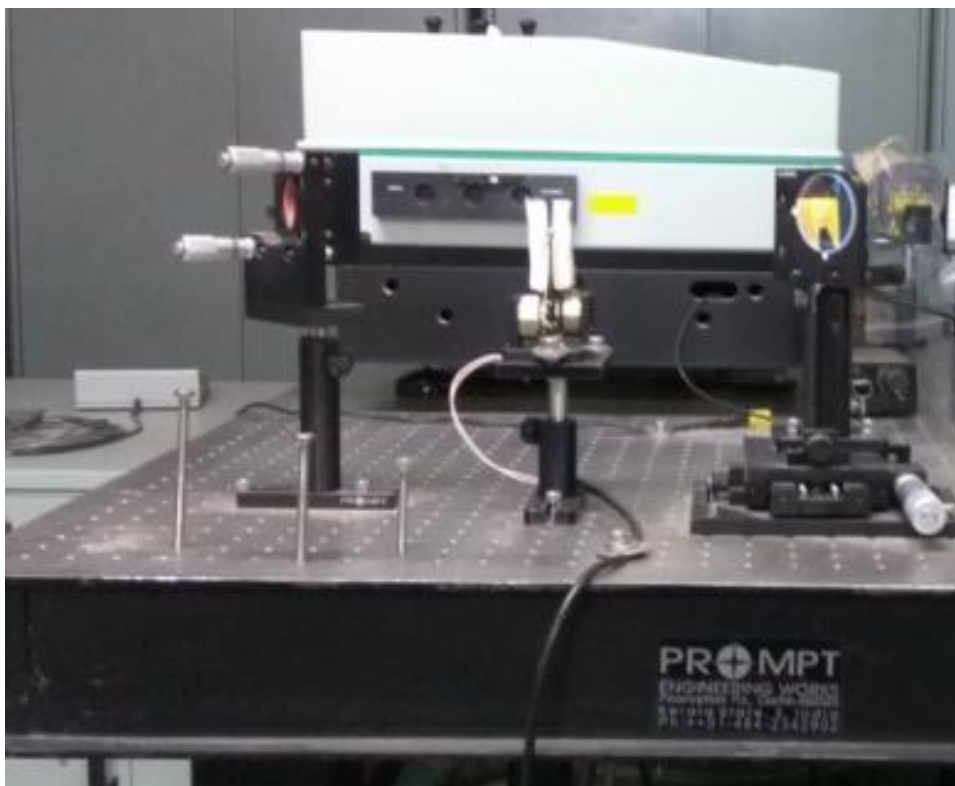


**Fig. 2.2.** Photograph of Nd:YAG laser (PRII 9030, Continuum Electro-Optic, Inc.) used for plasma production.

### 2.2.3 Magnet system

Two different schemes of uniform magnetic field generation have been employed for the present study.

#### 1.2.3.1 Magnetic trap

In the first scheme, a uniform magnetic trap was made by two rectangular Nd-Fe-B (Neodymium, Iron and Boron) permanent magnets having dimensions 38 mm height, 76 mm length and 76 mm width. A non-magnetic stainless steel structure holds the magnets parallel to each other with 30 mm separation, which produces  $\sim 0.45$  T uniform magnetic field (Fig. 2.3a). Magnitude and uniformity of the magnetic field is ensured by mapping the magnetic field along the expansion and lateral directions using Gauss meter (Fig. 2.3b).

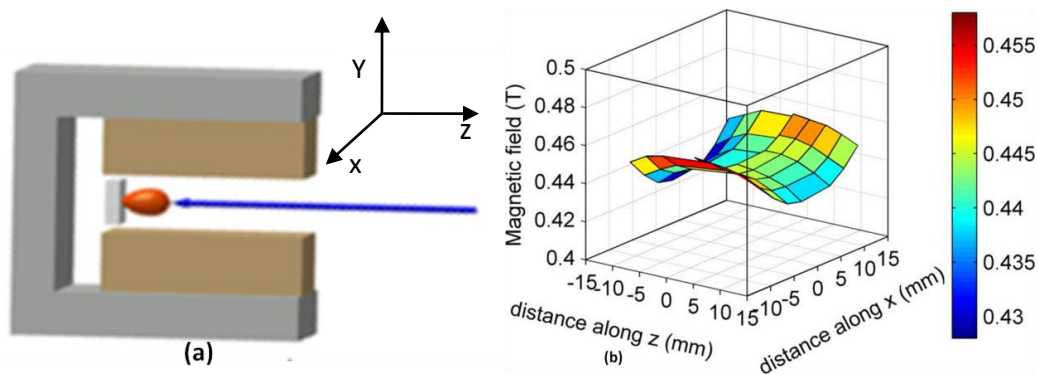


**Fig. 2.3.** (a) Schematic of the plasma plume in transverse magnetic trap, (b) magnetic field profile between the two magnets in the direction of plume expansion (z) and perpendicular to it (x) measured by Gauss meter [58]

#### 1.2.3.2 Helmholtz coil

In the second scheme, a Helmholtz coil along with the capacitor bank based pulse power system has been developed in house to produce variable magnetic field varying from 0 to 0.57 T (Fig. 2.4). The flat-top (uniformity) of the variable magnetic field is  $\sim 40$   $\mu$ s (which is much larger than the emissive lifetime of expanding plasma plume ( $\sim 5$   $\mu$ s)). The Helmholtz coil configuration allows the two-directional imaging of

expanding plasma plume in magnetic field. The details of its design, fabrication and measurement of the magnetic field are given in section 2.4.

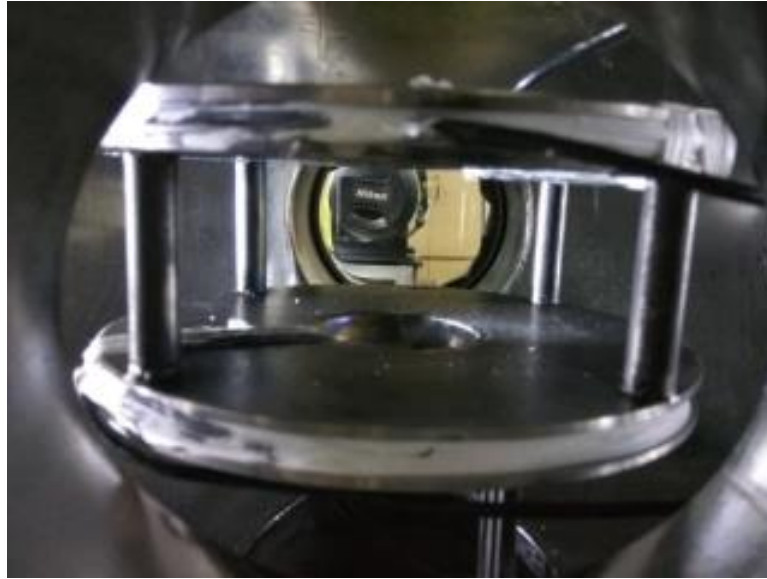


**Fig. 2.4.** Photograph of Helmholtz coil installed inside the vacuum chamber

### **2.2.4 Target and its handling system**

The targets are in the form of plates of thickness 1-3 mm. Carbon ( $Z = 6$ ), aluminium ( $Z = 13$ ), nickel ( $Z = 28$ ) and tungsten ( $Z = 74$ ) are used for this study. The targets are mounted on a movable target holder through a vacuum compatible feed-through and are placed in between the magnet bars/Helmholtz coils. Few (3-4) laser pulses are fired to remove the surface layer on the target materials to remove oxidization and all types of surface impurities and then the experimental data are recorded.

## **2.3 Plasma diagnostic systems**

### **2.3.1 Time-resolved fast imaging using ICCD camera**

Usual emission lifetime of the laser-produced plasma is  $\sim 5 \mu\text{s}$ . To study the plasma dynamics (i.e. to know its temporal evolution during its emission lifetime), it is necessary to record images of plasma plume at least in intervals of few hundred nanoseconds, even sometimes in intervals of few tens nanoseconds to record instabilities during plume expansion in magnetic field. This objective is effectively

---

achieved using picoseconds high speed intensified charge coupled device (ICCD) camera (4 Picos Stanford Computer Optics, Inc.). We have used single (for experiments with permanent magnets) or two (for experiments with Helmholtz coil) internally synchronized ICCD cameras in the experiments presented in this thesis to capture the temporal evolution of expanding laser plasmas (along and across the applied magnetic field lines). Time-resolved fast imaging of electronically excited plume species provides the two-dimensional snap-shot of the expanding plasma plume. Image analysis of these 2D-images provides various information related to plume dynamics, hydrodynamic movement of plasma and geometrical structure of the expanding plume.

Fast imaging camera consists of a high-performance CCD camera and an image intensifier that is mounted in front of it. The incoming light is first amplified by the image intensifier. The intensified image is then transmitted from the intensifiers phosphor screen where the multiplied electrons from the microchannel plate convert back into photons. This image is then projected onto the CCD sensor by means of a coupling lens. Thus, an ICCD camera directly amplifies the incoming light, thereby supplying the CCD sensor with a light intensity far above the thermal noise level of the sensors. The details of the image intensifier and high-speed shutter are described [49].

Time-resolved images of the visible expanding plume have been recorded using single or two internally synchronized ICCD cameras having variable gain and gate time and having a spectral range of 350 - 750 nm. The images have been captured by varying the time delay (from 50 to 5000 ns) between the laser pulse and the opening time of ICCD gate. Minimum of three images are recorded under similar experimental conditions. These images were found to be nearly identical in shape and the reproducibility of the emission intensity is better than 5%. A mesh image of

known dimensions ( $5\text{ mm} \times 5\text{ mm}$ ) is recorded to map the geometrical parameters of the plume and corresponding to the magnification of the imaging system is calculated (Fig. 2.5a). Dark current noise is subtracted from the recorded image using MATLAB. Length and width of the plume are estimated by segmentation algorithm using MATLAB. For better visibility, grey images (Fig. 2.5b) have been converted into pseudo-coloured images using MATLAB colormaps (jet) (Fig. 2.5c). A micro-controller based time control unit is used to trigger the camera in synchronous with the laser pulse. Timing jitter in time delay with respect to laser pulse is less  $<1\text{ ns}$ . To find the emission profile along the axial as well as lateral directions (Fig. 2.5d), plume images are binned along the horizontal and vertical columns of images respectively.

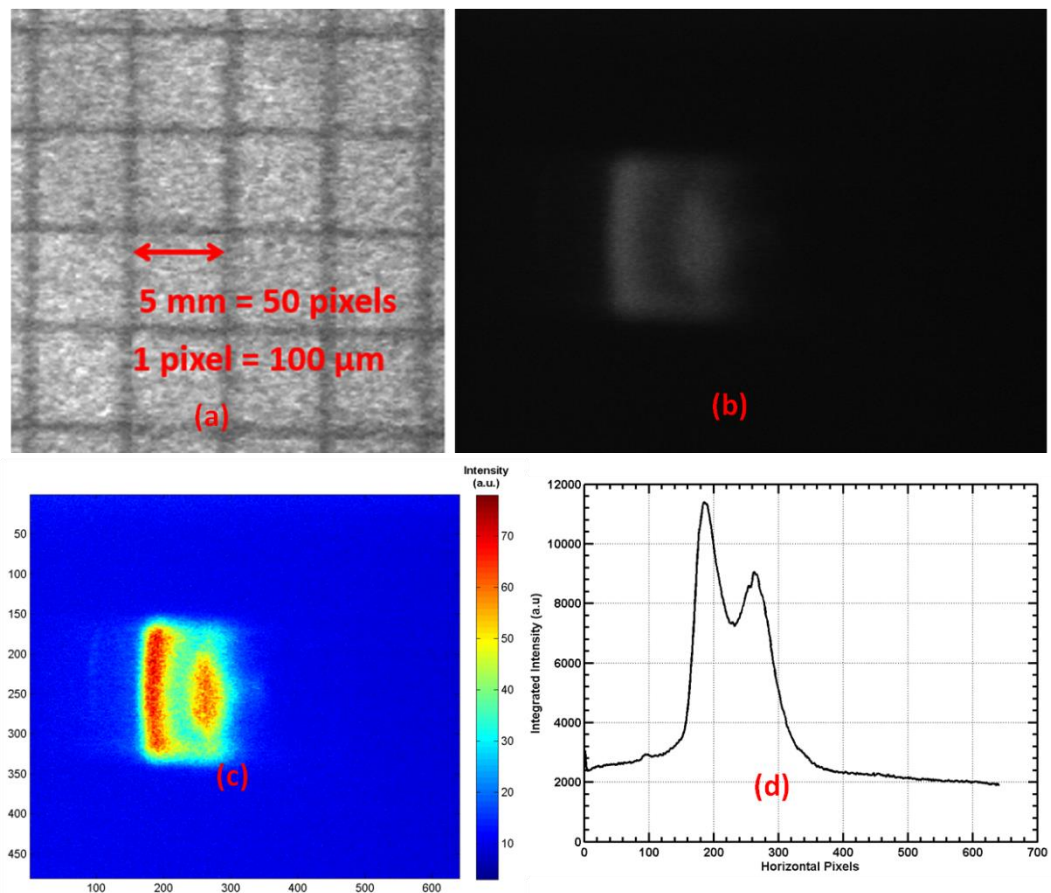


**Fig. 2.5.** (a) An image of  $5\text{ mm} \times 5\text{ mm}$  grid used for calibration, (b) grey scale image of expanding plasma plume captured using ICCD camera, (c) pseudo-coloured image of plasma plume obtained using MATLAB Colormaps (jet), (d) corresponding integrated intensity profile along the lateral direction.

### 2.3.2 Optical emission spectroscopy (OES)

Neutral atoms, ions and electrons in the laser produced plasma emit radiation which is characteristic of the target material. Optical emission spectroscopy (OES) is a simple and non-invasive technique to investigate the line emission from these atoms, ions and molecules within plasma. It provides information about properties such as excited species densities, electron - atom, atom - atom and ion - atom collision, energy distribution of species, charge transfer between plasma constituents, electric and magnetic fields etc. The analysis of the emission from the plasma can be used to determine the dynamics as well as plasma parameters [61-64].

The emission spectroscopy has been used to estimate the plasma parameters. For that spectral light is viewed normal to the expansion direction and fed at the entrance slit of the spectrometer (Acton Advanced SP2500A [60], Focal length: 0.500 m and Spectral resolution: 0.8 Å) through the optical fibre and collection optics (ME-OPT-0007, ANDOR, UV-VIS-NIR collector-collimator).

The plasma parameters like electron temperature ( $T_e$ ) and density ( $n_e$ ) are estimated by optical emission spectroscopy. The electron density is estimated either by the ratio of line intensity method or Boltzmann plot method [65]. We have estimated  $T_e$  through only ratio of line intensity method by taking the line intensity ratios of two lines using the relation

$$\frac{I_1}{I_2} = \frac{g_1 A_1 \lambda_2}{g_2 A_2 \lambda_1} \exp \frac{-(E_1 - E_2)}{kT_e} \quad (2.1)$$

Here,  $I_1$  and  $I_2$  are the intensities of the spectral lines of wavelengths  $\lambda_1$  and  $\lambda_2$ ;  $g_1$ ,  $g_2$  are the statistical weight factors,  $A_1$ ,  $A_2$  are the transition probabilities,  $E_1$ ,  $E_2$  are the energies of the excited states of the two spectral lines,  $k$  is the Boltzmann's constant, and  $T_e$  is the electron temperature. Here, non-resonant lines are chosen to avoid the self-absorption. The required spectroscopic data required for temperature measurement are taken from the NIST database.

The electron density  $n_e$  of the plasma plume is obtained from the Stark broadening profile of selected line using the relation [58],

$$\Delta\lambda_{1/2} = \frac{2 W n_e}{10^{16}} \quad (2.2)$$

where  $\Delta\lambda_{1/2}$  is the FWHM of the spectral line and  $W$  is the electron impact parameter. The observed line profile is fitted with a Lorentzian function to obtain the line width. Here, broadening due to ionic contribution and Doppler broadening are ignored because of its negligible contributions [66, 67].

It should be noted that above estimation of plasma parameters is valid only for plasma in local thermodynamic equilibrium (LTE). So, it is necessary to ensure the LTE condition by using the McWhirter criterion [58], which gives the minimum density required for LTE is given by

$$n_e \geq 1.4 \times 10^{14} T_e^{1/2} (\Delta E)^3 \text{ cm}^{-3} \quad (2.3)$$

where,  $T_e$  (eV) is the electron temperature and  $\Delta E$  (eV) is the maximum energy difference between the upper and lower energy levels.

### 2.3.3 B-dot probe

The magnetic field is an important parameter of laser-produced plasma. B-dot probe is used to measure the magnetic field of plasma plume during its expansion in external magnetic field [68]. The time-varying magnetic field produced by the laser-produced plasma can be measured with a B-dot probe by using Faraday's Law in integrated form [69]. The flux change in a loop of  $N$  turns and area  $a$  in a magnetic field  $B$  perpendicular to the plane of the coil produces voltage  $V$  is given by

$$V = - a N \frac{dB}{dt} \quad (2.4)$$

The time-varying magnetic field produced by the plasma can be calculated as

$$B = - \frac{\int V dt}{aN} \quad (2.5)$$

The magnetic field can be measured by integrating the B-dot probe signal by using either an electronic integrator or numerical integrator. A B-dot probe usually consists

of a single or multi-turn coil mounted on or enclosed in a support that allows the coil to be inserted into or near the plasma. The term ‘B-dot’ arises from the mathematical notation  $\frac{dB}{dt} = \dot{B}$ . We have indigenously built a three-axis, high-frequency B-dot probe (Fig. 2.6) to verify the diamagnetism of laser-produced plasma. The details of its design, fabrication, calibration is given in chapter 5.



**Fig. 2.6.** Photograph of designed B-dot probe

## **2.4 Generation of variable uniform magnetic field using Helmholtz coil**

The effect of external magnetic field on plume dynamics is well known. To study the explicit effect of variable magnetic field on the dynamics and geometrical aspect of the expanding plasma plume, we have developed a specially designed Helmholtz coil. Basically, the Helmholtz coil configuration is used to generate uniform pulsed variable magnetic field [70]. The majority of previous experiments have been performed with permanent bar magnet where plume imaging along the magnetic field lines are not possible because of experimental constraints [71]. Plume structure in magnetic field is highly asymmetrical and therefore complete geometrical information cannot extract from plume images projected across the magnetic field direction. Again, it is not possible to study the formation and evolution of the diamagnetic cavity and magnetic striation-like structure as a function of applied magnetic field using single permanent magnetic system. Our major focus is to study the transient behaviour of expanding plume, importantly these two features in variable

uniform transverse magnetic field. Previously, this problem was attempted; but the maximum produced magnetic field was 0.2 T and only 1D imaging system was used [70]. Therefore, another challenge is to produce a high magnetic field in a small volume. It is required that the magnetic field should be uniform throughout the plume dimension and the duration of the field should be longer than the emissive lifetime of the expanding plasma plume ( $>$  few microseconds). The pulse power capacitor bank and fast ignitron based switch is used to generate pulsed current in range of 3 KA. The stainless steel based coil structure with desired inductance value is fabricated to generate a variable uniform magnetic field (flat-top) for  $\sim 40 \mu\text{s}$  time. Magnitude and uniformity of the magnetic field is ensured by mapping the magnetic field as a function of distance along the expansion direction and lateral directions using a Gauss meter. A time synchronization unit has been developed for simultaneous operation of all the systems associated with the experiments.

### **2.4.1 Pulse power system**

The pulse power system is developed to generate high amplitude current pulse through coil. The schematic diagram is shown in Fig. 2.7. There are four main components: High voltage capacitor, high speed and high power switch, variable AC power supply and trigger section. The two capacitors ( $700 \mu\text{F} / 5 \text{KV}$ ) are connected in parallel to form high voltage source. The AC power supply is rectified using high power diode to charge the capacitors. The ignitron (BK506) is used as a switching device to transfer capacitor energy to inductance of coils.

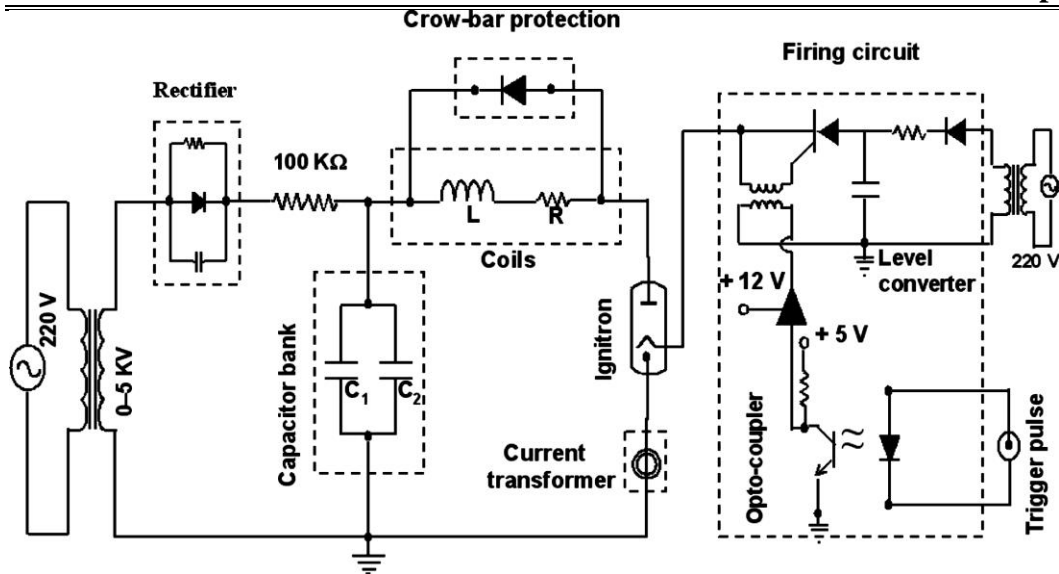


**Fig. 2.7.** Schematic diagram of the capacitor bank pulsed power system [70]

The ignitron is fired at pre-defined time using TTL signal generated from timing and synchronization section. The optically isolated TTL signal is converted to 12 V pulse to fire the ignitron. The AT8051 based micro-controller with timing algorithm is used to generate precise timing pulses.

### 2.4.2 Coil structure

Two identical coils are fabricated to form Helmholtz configuration to generate uniform magnetic field. The Helmholtz configuration is ideal for generating uniform magnetic field inside two coils. The separation between two coils is same as the radius of coil. Both coils are connected in parallel for minimizing the internal resistance of coil assembly.

A stainless steel (SS) based coil structure is developed (Fig. 2.9 and Fig. 2.11). The photograph of coil assembly is shown in Fig. 2.11. The insulated multi-core copper cable is used for coil fabrication. The materials of circular shape (inner diameter of Helmholtz coil) have been removed from SS assembly to capture images of expanding plasma plume in a plane perpendicular to applied magnetic field. This was not possible in case of permanent magnetic bars. It also supports stepper motor

based connection for future up-gradation. The geometrical parameter of the designed coil assembly is described in Table 2.1.

Parameters	Coil 1	Coil 2	Coil 1    coil 2
R (Ohm)	0.224	0.227	0.196
Z (Ohm)	0.640	0.675	0.445
L ( $\mu$ H)	63	67.6	34.9
N (no. of turns)	36	36	72
Magnetic field (G) at centre (I = 2710 A)	5700		
Cable type	Multi-core insulated Copper cable of AWG 13		
Diameter of coil assembly	150 mm (Opening of 44 mm diameter to imaging plasma using ICCD camera sensor)		
Separation between two coils	50 mm		

**Table 2.1.** Geometrical parameters of the compact coil assembly.

The profile of magnetic field is shown in Fig. 2.8a. A high frequency Gauss meter (9900, F. W. Bell, USA) is used to measure the magnetic field produced by Helmholtz coil for different input (Fig. 2.8b).

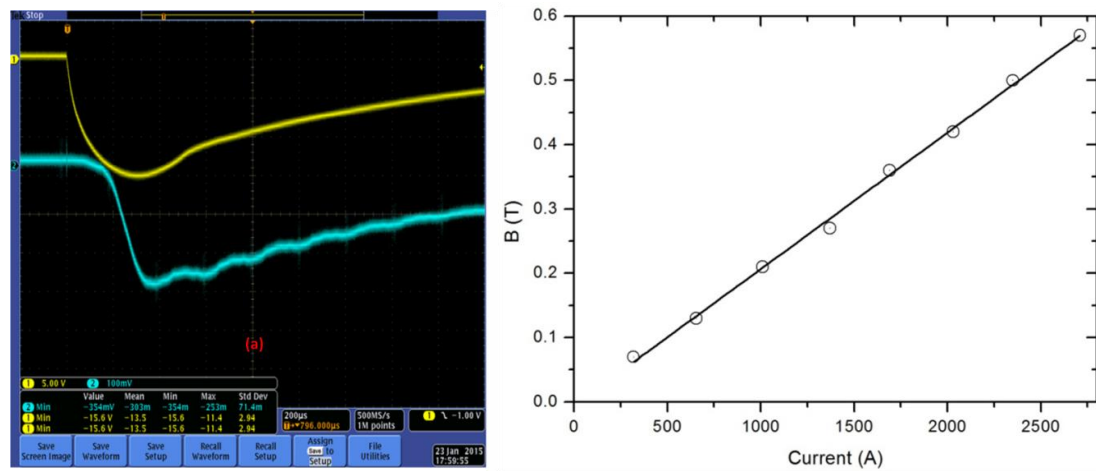


**Fig. 2.8.** The measurement of magnetic field at 654 A input current, (a) upper trace is the current transducer (CT) output, lower trace is Gauss meter output (b) plot for magnetic field produced by Helmholtz Coil for different input current measured using gauss meter.

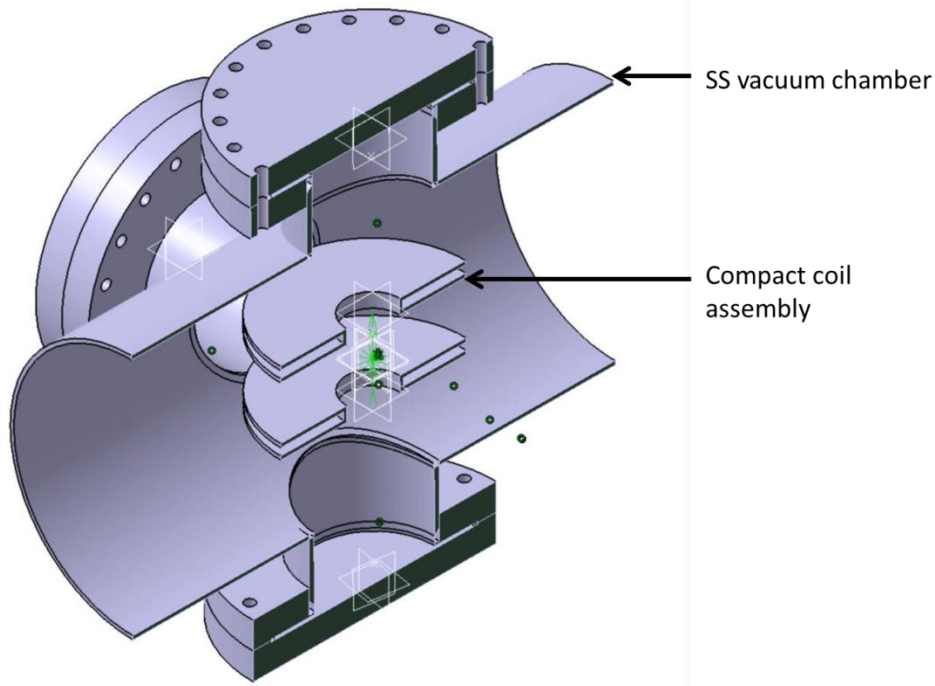


**Fig. 2.9.** Schematic of designed coil assemble structure integrated to SS vacuum chamber

The delay observed between input current to generated magnetic field is due to eddy current effect of coil assembly structure. The Fig. 2.9 shows the mechanical layout of developed coil assembly with integrated SS vacuum chamber structure. The coil assembly is easy to move in and out of vacuum chamber which is useful in case of object to laser distance modification.

### 2.4.3 RLC circuit analysis

The equivalent LCR circuit, for the current through the coil is governed by the second order differential equation:

$$L \frac{d^2I}{dt^2} + R \frac{dI}{dt} + \frac{I}{C} = 0 \quad (2.6)$$

In the present system  $R^2 < 4L/C$ , this is under-damped system. Under this condition, the solution of above equation is

$$I(t) = -\frac{V_0}{L\omega_d} e^{-\alpha t} \sin(\omega_d t) \quad (2.7)$$

where,  $V_0$  is the voltage across the charged capacitor,  $L$  and  $R$  are the inductance and resistance of the coils,  $\alpha = R/2L$  and  $\omega_d = [(1/LC) - (R/2L)^2]^{1/2}$ . Simulated temporal evolution of the coil current for the measured parameters,  $C = 1400 \mu\text{F}$ ,  $L = 35 \mu\text{H}$ ,  $R = 0.196 \text{ ohm}$  and  $V_0 = 200 \text{ V}$  is shown in Fig. 2.10. The current output waveform of the LCR circuit is damping in nature results in the reverse charging of capacitor. To avoid the reverse charging, a high power fast recovery diode (2.5 KV- 4KA @ 10 ms) is connected across the coil circuit. This overcomes the damping of the LCR circuit by bypassing induced reverse voltage across the inductor coil through the diode. The experimentally observed current profile measured by the current transformer is also shown in Fig. 2.10. The observed slow decay time as compared to simulated one is due to coupling of diode across the coil, which adds more resistance and inductance to circuit.

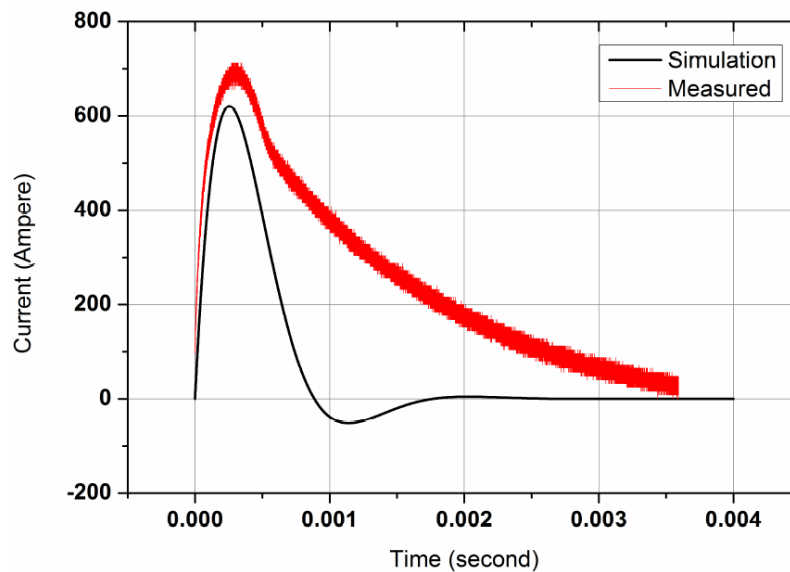


**Fig. 2.10.** Time response of RLC circuit

### **2.4.4 Uniformity of magnetic field**

A high frequency Gauss meter (9900, F. W. Bell, USA) is used to measure the actual magnetic field profile in the region of interest. The Gauss meter is calibrated and then used to measure the magnetic field. The Gauss meter is mounted on XYZ translator having a resolution of 1 mm (Fig. 2.11a). Magnitude and uniformity of the magnetic

field is ensured by mapping the magnetic field as a function of distance along the expansion direction and lateral directions shown in Fig. 2.11b.

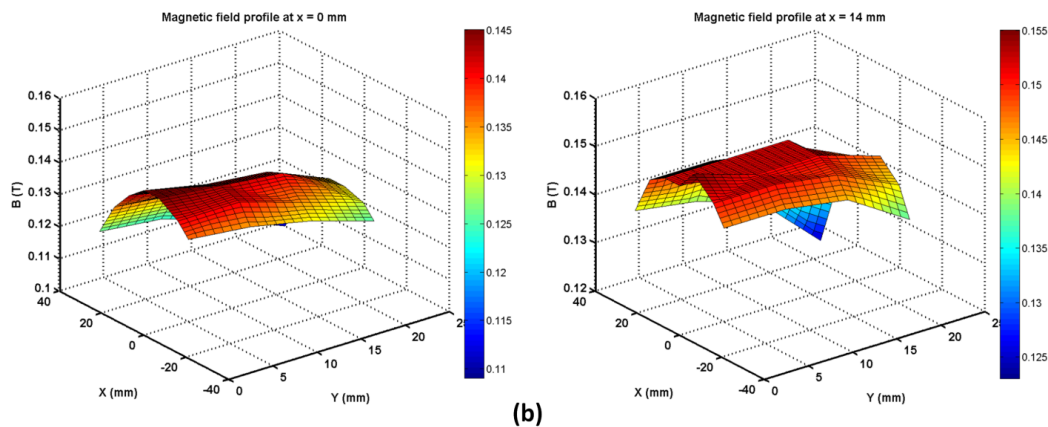
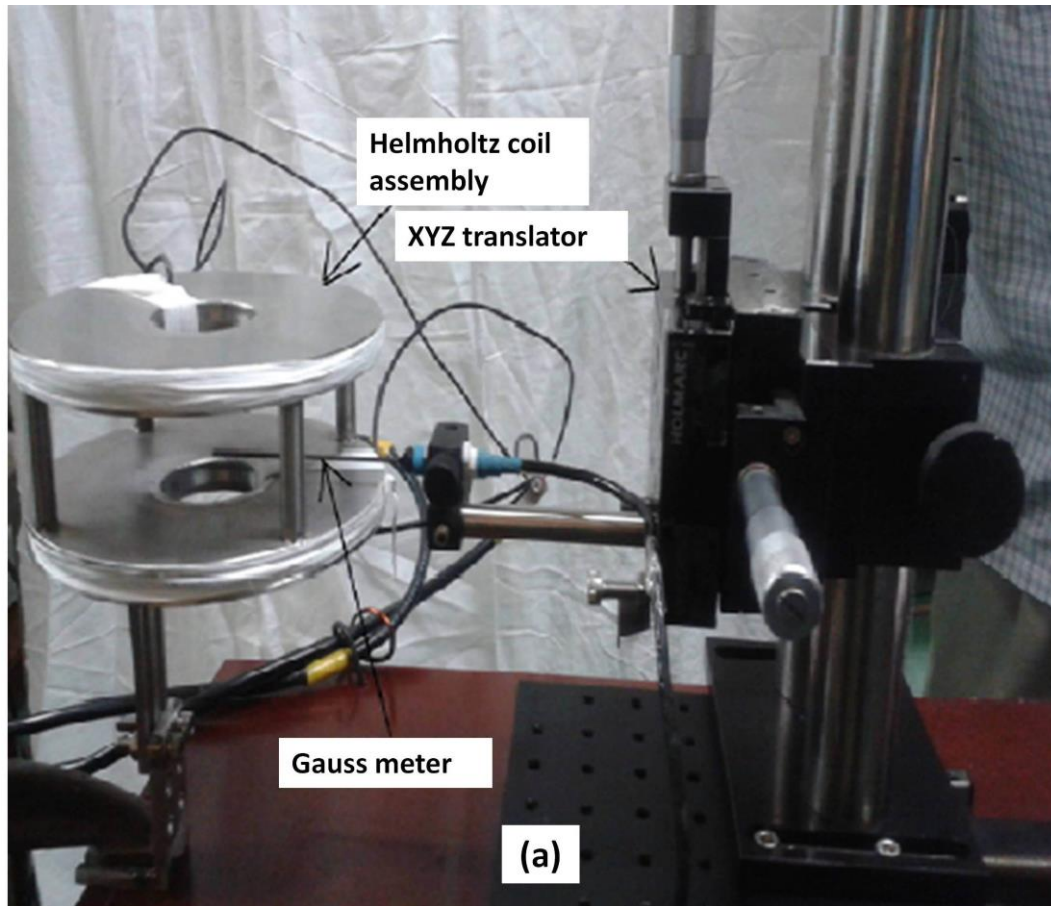


**Fig. 2.11.** (a) Setup for mapping of magnetic field around plasma plume region, (b) magnetic field profile between the two poles of Helmholtz coil measured by Gauss meter at  $x = 0$  mm and  $x = 14$  mm for magnetic field 0.13 T.

---

---

**2.4.5 Timing and synchronization scheme**

The laser-produced plasma experiment required the following detection and auxiliary systems for complete operation.

- (i) ICCD based detection system
- (ii) Spectrometer based detection system
- (iii) Photo-multiplier based detection system
- (iv) Photo-diode based timing monitoring system
- (v) Mechanical shutter based laser pulse shutter system

The ICCD and spectrometer are pre-triggered in programmable manner only at the flat region of magnetic field and laser Q-switch pulse are arrived. The trigger requirement for all auxiliary systems is very stringent as follows.

- (i) Jitter between trigger outputs:  $\leq \pm 1$  ns
- (ii) Delay resolution between outputs: 1 ns
- (iii) Delay accuracy between outputs: 1 ns
- (iv) Number of outputs: 5 nos. with 50  $\Omega$  load
- (v) Incorporation of algorithm for free running to single pulsed locking mechanism

The instrumentation based approach is used for implementing timing and synchronization system as shown in Fig. 2.12.

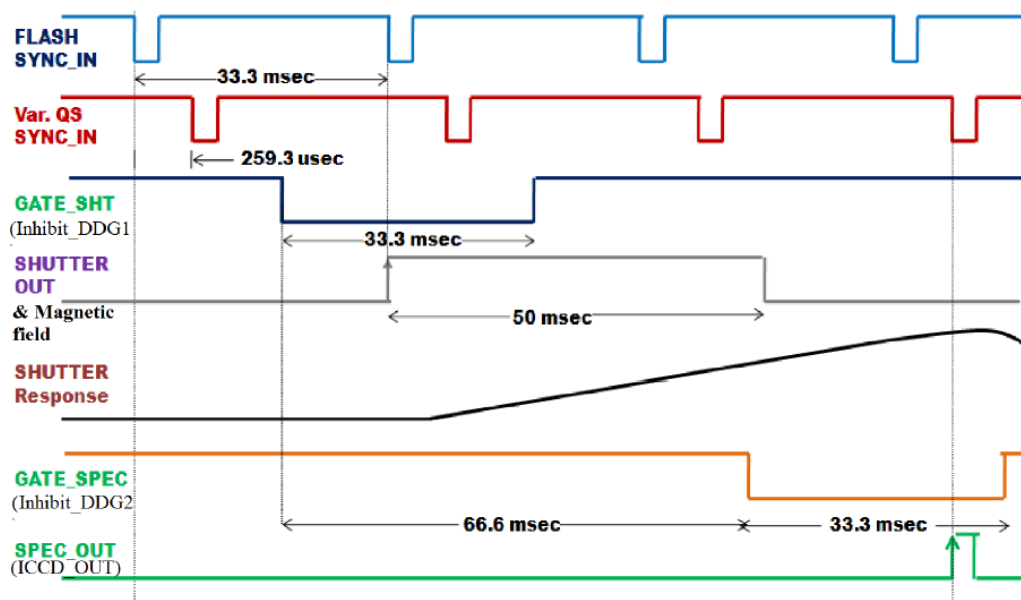


**Fig. 2.12.** Timing diagram for synchronization between laser and other auxiliary systems.

The laser is operated in continuous mode at 30 Hz repetition rate. The locking of free running laser pulse to other system is achieved using inhibit facility of digital delay generator (DDG) (DG 645, Stanford Research System). The function generator (AFG 3102, Tektronix, 100 MHz, 1 GS/s sampling rate) gives two outputs at predefined delay for inhibit inputs of two DDG; one is for magnetic field and mechanical shutter system while other is for ICCD and spectrometer system. The delay between each output is set in such a way that all outputs are activated at predefined time as shown in Fig. 2.12. The conformation of achieved synchronization is verified using photodiode output, current transformer (CT) output and image output.

## 2.5 Summary and conclusion

In summary, all the experimental systems required for the plasma plume production and associated diagnostics have been studied and developed. The detailed description of various instruments such as laser system, pumping stem, ICCD camera, spectrometer, B-dot probe and correlated components and their functionality has been explained. A Helmholtz coil configuration has been designed and fabricated. It

---

---

produces uniform variable transverse magnetic field and allows the fast imaging of expanding plasma plume along and across the applied external magnetic field. A time synchronization unit has been developed for automatic and simultaneous operation of all the systems associated with the experiments.



## Chapter 3

---

# **Dynamical behavior of plasma plume across the transverse magnetic field**

In this chapter, we present dynamical behaviour of aluminium plasma across 0.45 T magnetic field at low ambient pressure using fast imaging technique. The present finding related to the plume dynamics, splitting pattern and geometry of plume is significantly different from the reported results on similar experiments. In vacuum, after the initial expansion, the plume approaches stagnation followed by re-expansion with constant velocity. Above behaviour is correlated with the plume expansion in diamagnetic limit and  $E \times B$  drift in non-diamagnetic regime. Two slab-like structures, moving with different velocities are observed in presence of both the magnetic field and ambient gas.



---

## 3.1 Introduction

The presence of magnetic field during the expansion of laser-blow off (LBO)/laser produced plasma (LPP) can initiate several interesting physical phenomena, which include conversion of kinetic energy into plasma thermal energy, plume confinement, ion acceleration/deceleration, emission enhancement/decrease and plasma instabilities. [33-38, 31]. The physics of plasma flow across magnetic field lines is important in many laboratory, tokamak and space plasmas and has significant importance in many applied research, for example, increase in the detection sensitivity of laser-induced breakdown spectroscopy [33, 39], manipulation of plasma plume in pulse laser deposition [40-42], debris mitigation etc [43]. Also several pioneer works related to the basic understanding of plasma plume-magnetic field interactions have been done with regard to the formation of diamagnetic cavity and flute like structures [72, 73, 25], plasma oscillations [45], edge instability and dramatic structuring [29, 74], sub-Alfvenic plasma expansion [50] and laser plasma expansion in magnetized background [30].

Apart from the above, dynamics of plasma plume is influenced significantly in the presence of the magnetic field and therefore it is useful to control the dynamic properties of highly transient plasma plume. The manipulation of geometrical shape, size and dynamics of plasma plume by introduction of external magnetic field has great importance in applied research and also in fundamental studies. Due to initial conversion of thermal energy into directed energy at the initial stage of laser produced plasma, sum of directed pressure and thermal pressure of plasma plume is much larger than the magnetic pressure (that is plasma beta  $> 1$ ). As the time evolves, electron temperature and density of the plasma plume decrease rapidly as a result plasma beta is also decreases with time. Therefore, two different approaches have been made to explain the dynamics of laser produced plasma across the transverse magnetic field. In

the first approach expansion of the plasma plume is treated as expansion in the diamagnetic limit where the applied electric field is displaced by the induced field due to diamagnetic current in plasma and the plasma plume experiences the decelerating force [28, 31, 72]. In the second approach, it is considered that external magnetic field is diffused in the plasma plume and produces polarized electric field (due to the deflection of electrons and ions in opposite direction) perpendicular to both the expansion direction and the magnetic field [31, 76, 77]. In this case plasma plume experiences the  $E \times B$  field and drifts in axial direction. In most of the previous experiments with ns laser and moderate laser energy (up to few hundred mJ), the dynamics of plasma plume across the magnetic field is explained in terms of  $J \times B$  interaction induced by diamagnetic behaviour of plasma plume [28, 35, 39]. Drift of the bulk plasma across the magnetic field and field aligned instability (striation like structure) is commonly ignored, especially for moderate laser energy.

In view of above, in the present work we report a systematic study of the effect of the magnetic field regarding the dynamical and geometrical behaviour of laser induced plasma plume in different ambient conditions. We attempt to demonstrate the expansion of transient plasma plume in diamagnetic limit followed by drift across the polarized electric field.

### **3.2 Experimental scheme**

Schematic diagram of the experimental setup is shown in Fig. 3.1. The plasma plume is created in a cylindrical stainless steel chamber, which is evacuated to a base pressure less than  $2 \times 10^{-5}$  Torr. A uniform magnetic trap was made by two rectangular Nd-Fe-B permanent magnets having dimensions 38 mm height, 76 mm length and 76 mm width. A non-magnetic stainless steel structure holds the magnets parallel to each other with 30 mm separation, which produces  $\sim 0.45$  T uniform magnetic field. Magnitude and uniformity of the magnetic field is ensured by mapping

the magnetic field along the expansion and lateral directions using Gauss meter. The aluminium target was mounted on a movable target holder through a vacuum compatible feed-through and placed in between the two magnet bars. An Nd:YAG ( $\lambda = 1064$  nm) laser having 8-ns pulse width with pulse energy 300 mJ has been used to ablate the target. The spot size of the laser beam is set to about 1 mm in diameter at the target which can produce the power density  $\sim 4 \times 10^9$  W/cm<sup>2</sup> the target surface.

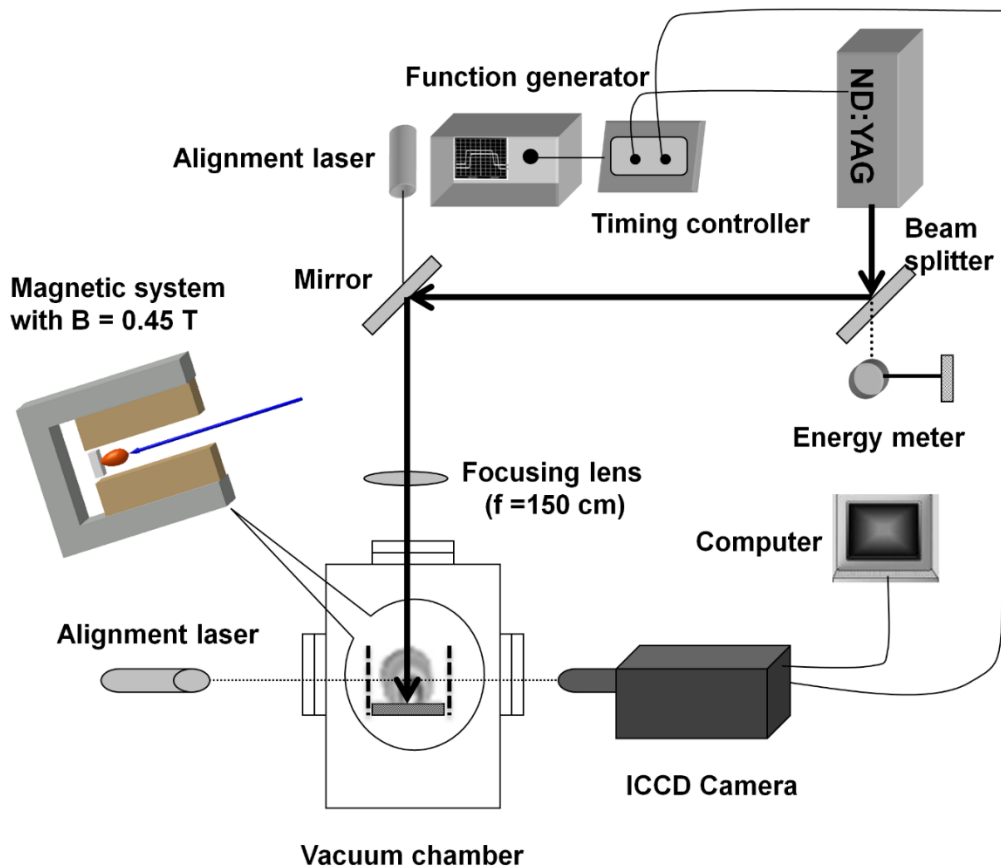


**Fig. 3.1.** Schematic of the experimental setup

The light emitted from the luminous plasma is transmitted through a quartz window mounted orthogonal to the direction of the plume expansion. Time resolved images of the visible plume luminescence have been recorded using an ICCD camera having variable gain and gating on time and having a spectral range of 350-750 nm. In the present experiment, gate opening (integration) time is set at 10 and 20 ns. Temporal evolution of the laser produced plume has been obtained by varying the time delay (from 400 to 5000 ns) between the laser pulse and the opening time of

---

ICCD gate. Minimum three images are recorded under similar experimental conditions. The reproducibility of the emission intensity is better than 5%. A mesh image of known dimensions (5 mm × 5 mm) is recorded to map the geometrical parameters of the plume. The magnification of the imaging system is found to be 3. Dark current noise is subtracted from the recorded image using MATLAB. Length and width of the plume are estimated by segmentation algorithm using MATLAB. For better visibility, gray images have been converted into pseudo-color images using jet-color map. A micro-controller based time control unit is used to trigger the camera in synchronous with the laser pulse. Timing jitter in time delay with respect to laser pulse is less <1 ns. To find the emission profile along the axial as well as lateral directions, plume images are binned along the horizontal and vertical columns of images respectively.

### **3.3 Results and discussions**

#### **3.3.1 Plume expansion across the magnetic field**

In order to understand the hydrodynamic movement of the expanding aluminium plasma in presence of strong transverse magnetic field, the images of the emitting plume are recorded by the ICCD camera for different ambient conditions. These images provide temporally resolved two-dimensional snapshots of the expanding laser produced plasma plume. Here it should be noted that for the present experimental configuration, it is possible the expanding plasma plume touches the magnet surface at higher delay time. The plasma–magnet interaction and its effect on plume dynamics is complex phenomenon and it is subject of separate investigation. However the separation between the two magnets is considerably large (30 mm) and therefore the lateral physical obstacle may not affect significantly the characteristic dynamics of the

---

plume along the axial direction. Since, the present work basically focused on axial dynamics of plume and hence the plume-magnet interaction is ignored in this report.

The effect of magnetic field as well as ambient condition on the dynamics and geometrical shape of the expanding aluminium plasma are studied by observing these emissions as a function of time.

### **3.3.1.1 In vacuum**

Fig. 3.2 shows the sequence of images recorded at different time delays, varying from 400 ns to 5000 ns in vacuum and in the presence of 0.45T magnetic field. Each image represents the spectrally integrated emission intensity in the range 350-750 nm emitted from plume species. For better presentation of emission intensity distribution in the plasma plume and its temporal variation in the axial direction, the integrated intensity profile along the expansion axis for each image is also included in Fig. 3.2.

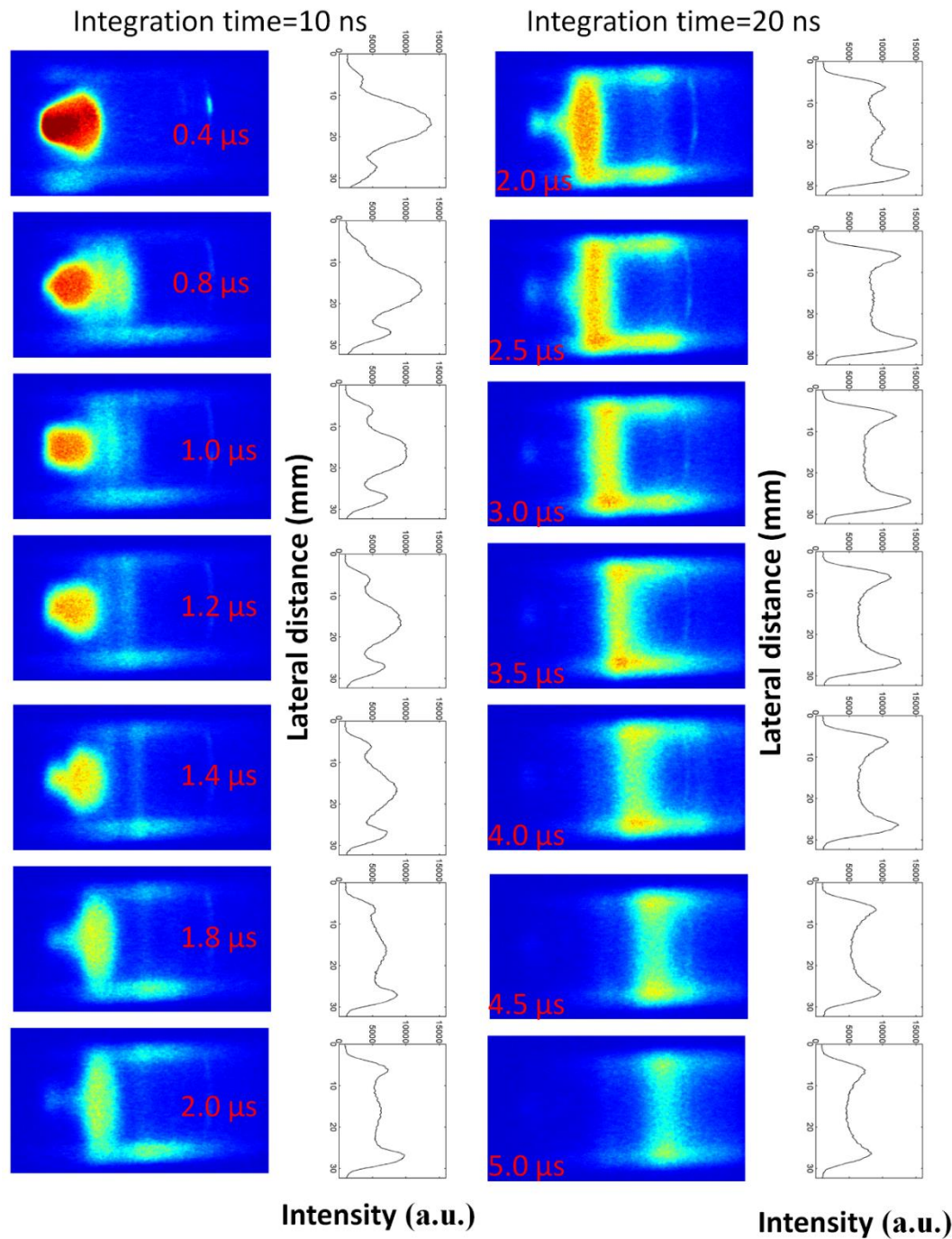


**Fig. 3.2.** The sequence of images of expanding plasma plume and corresponding integrated intensity profiles along the lateral direction in vacuum and at different delay times. The integration times of ICCD are set as 10 and 20 ns.

As can be seen from the Fig. 3.2, geometrical shape and intensity distribution of the plasma plume is significantly different from the previously reported results. Up to the 400 ns, plume expands under the influence of directed pressure [5] (due to the large pressure gradient) and has an ellipsoidal shape. The presence of resistive force

---

due to the magnetic pressure is clearly observed at 400 ns where the front is compressed and its shape is deviating from the ellipsoidal structure. At  $t = 800$  ns, well defined intensity columns parallel to the magnetic field line are observed ahead of bulk plume. This striation like structure is clearly observed from 800 ns to 1400 ns. Similar structure has been reported in past with much larger laser energy as compared to the present case [31] where, it is attributed as velocity shear induced instability. At the present stage it is not clear whether the plasma instabilities or plume-magnet interaction are responsible for the observed striation. Detailed investigation of this aspect will be reported in future communication. As the time evolves, bulk plume starts moving towards the magnetic pole whereas axial expansion is still negligible up to  $t = 1200$  ns. As a result, plume becomes more elongated in lateral direction with the time delay. With further increase in time delay  $t > 1200$  ns, the elongated plume starts moving in axial direction but the polarization of plume species near the magnetic poles goes on. At time delay  $t > 3500$  ns, intensity of the central portion of the plume starts decreasing and the overall structure look like a plume splitting in the vertical direction. Here it is noted that illumination of magnet boundary is mainly due to the light reflection and polarization of plume species near to magnet surface. For the present laser energy range, plume species cannot generate the secondary plasma on the magnet surface.

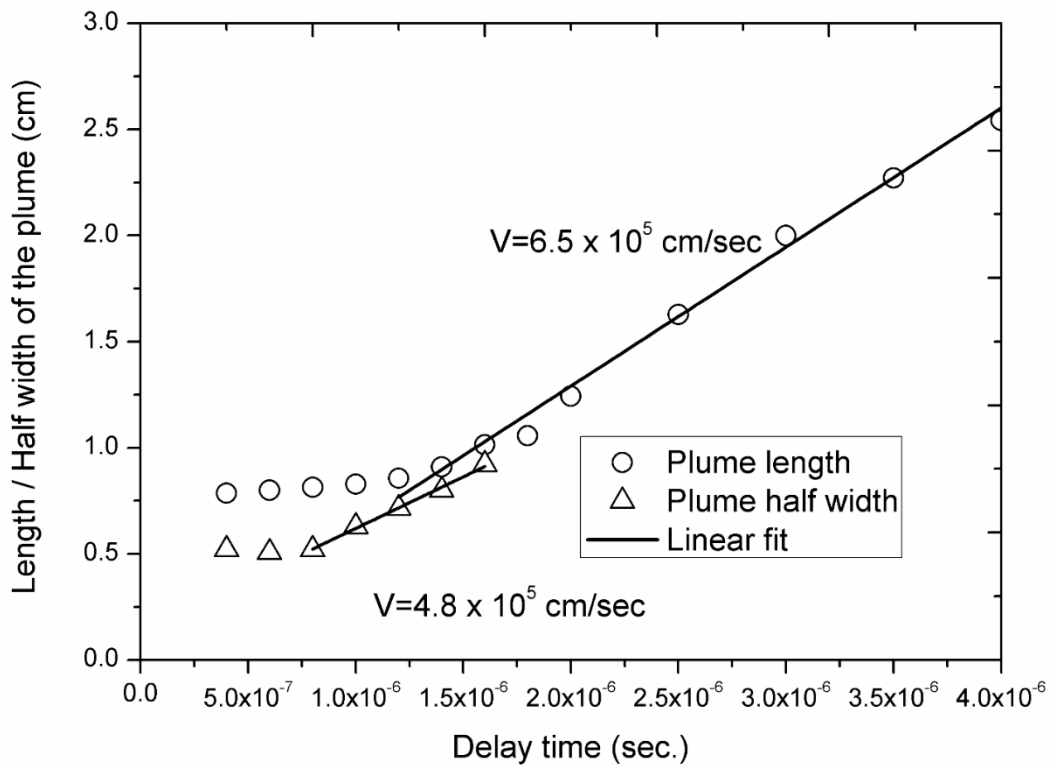


**Fig. 3.3.** Variation of plume length and half width as a function of time delay. Ambient pressure is set as  $10^{-5}$  Torr. Solid lines represent best linear fit for the experimental data.

The characteristics of the plume expansion in presence of magnetic field in axial as well as lateral direction are clearly visible in the distance versus time plot as shown in Fig. 3.3. It has been observed that under the influence of the magnetic field, the core of the plume is nearly stagnant with negligible axial velocity component up to the time delay 1200 ns. For the time delay  $> 1200$  ns, plume starts moving in axial direction as its length increases with time. The linear dependence of the plume front position with time delay suggests free expansion of the plume and the average axial velocity of  $6.5 \times 10^5$  cm/s is obtained from the slope of linear fit of the curve. It is interesting to note that after the stagnation ( $t > 1200$  ns), magnetic field effect on the axial direction is negligible as plume expands freely without any resistive force of magnetic pressure which is strikingly different from the behaviour of plume expansion in the magnetic field in comparison to majority of reported results. On the other hand

transverse velocity component of the plume is negligible up to 800 ns and with the further increase of time ( $> 800$  ns), plume starts moving in the lateral direction with a constant velocity of  $4.8 \times 10^5$  cm/s. Due to the early start of lateral movement with negligible axial velocity component, the shape of the plume is elongated in the transverse direction at later time delay.

### 3.3.1.2 In ambient gas

Scenario is different in case of plume expansion across magnetic field in  $10^{-2}$  Torr of argon pressure. The sequence of images of expanding plasma plume in  $10^{-2}$  Torr pressure of argon pressure is shown in Fig. 3.4.

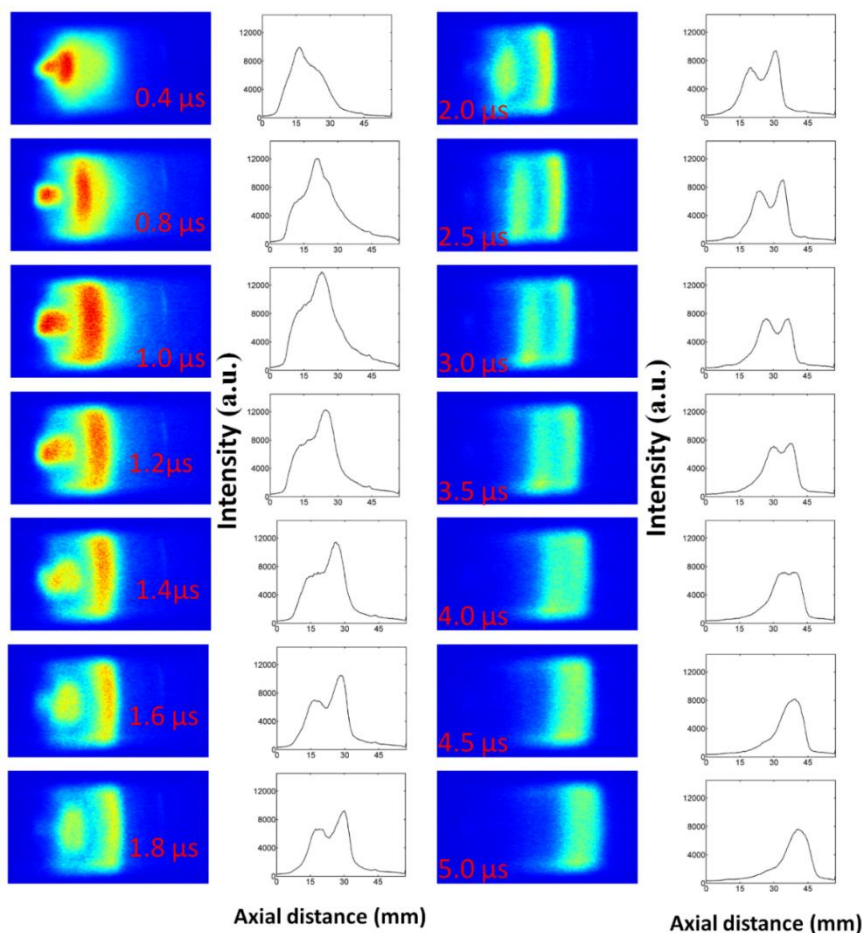


**Fig. 3.4.** The sequence of images of expanding plasma plume at different delay times along with the corresponding integrated intensity profiles along the axial direction. The ambient gas pressure and integration time of ICCD are set as  $10^{-2}$  Torr and 10 ns respectively.

In this case plume splits in two parts (designated as plume front and core of the plume) in axial direction at time delay  $t = 400\text{ns}$ . Plume splitting in the form of two components in presence of ambient gas is well known and extensively reported in literature [76, 78]. In the present case, that is in presence of magnetic field also, the fast component experiences the resistive force in expansion direction and therefore its shape is deformed and elongated in field direction. Front portion rapidly expands in lateral direction and attains maximum lateral dimension (separation between the two magnetic poles) at time delay  $t = 800\text{ ns}$ . However, geometrical shape of the core of the plume is almost identical up to  $t = 1000\text{ ns}$  and after that it propagates in axial as well as lateral directions and attains maximum lateral dimension at  $t = 2500\text{ ns}$ . Two vertical slab like structures appear which are move in forward direction with different velocities. For the time delay  $t > 4000\text{ ns}$ , these two components are merge together and expand as a single slab like structure which has nearly uniform intensity distribution.

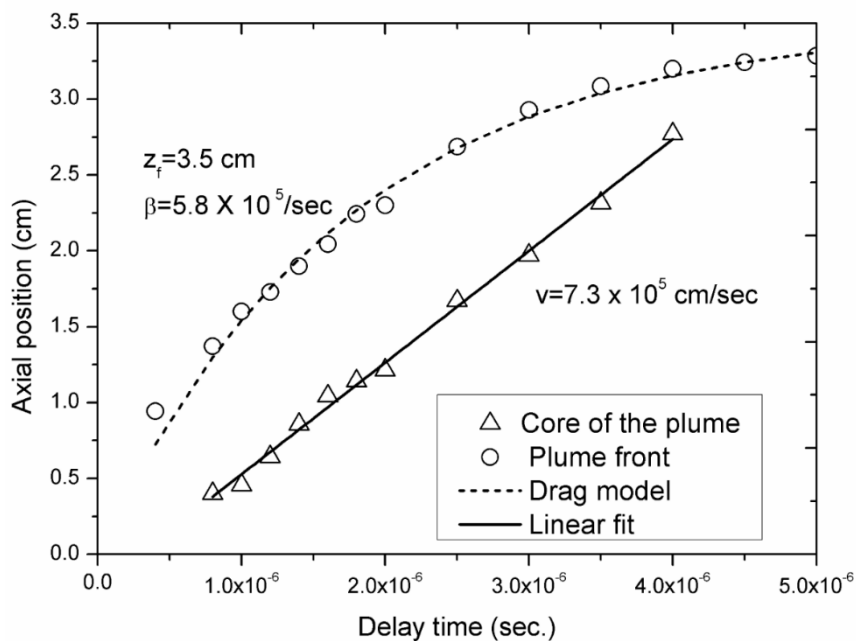


**Fig. 3.5.** Axial position vs time plot for both the front and core of the plasma plume at  $10^{-2}$  Torr of argon pressure. Solid and dashed lines represent the best fit for the experimental data with the linear fit and drag force model respectively.

---

In order to get the better presentation of axial expansion of these two components we have plotted the axial position of front and core of the plasma plume as a function of time delay as shown in Fig. 3.5. In this figure the axial positions of each component is obtained by their maximum, observed in the integrated intensity profile for the respective time delay. It has been observed that core of the plasma expands freely; the average expansion velocity of  $7.3 \times 10^5$  cm/s is deduced from the slope of the linear fit. On the other hand front component of the plume experiences the resistive force and its axial velocity decreases with time delay. The plume front position vs time curve is fitted well with classical drag force model  $z = z_f [1 - \exp(-\beta t)]$  [22-24, 79]. The best fitted parameters of the drag model give the slowing coefficient  $\beta \sim 5.8 \times 10^5$ /s and stopping distance  $z_f \sim 3.5$  cm. Therefore, these two components react with ambient gas to different extents; the core of the plume expands with uniform velocity whereas the velocity of the front component continuously decreases with the time. As a consequence both components merge together at later time delay. Thus the observed forward expansion of uniform intensity distribution in a large volume is an important finding which may be desirable for large area film deposition.

### **3.3.3 SVD analysis of the plasma plume**

Apart from the rapid change in plasma parameters during expansion, laser produced plasma have large radial velocity gradients. Therefore, core and edge region of expanding plasma plume interact with magnetic field to different extents and also the interaction is highly dynamical. This initiates the formation of complex internal structures inside the plume. A conventional analysis of two dimensional images of the plasma plume is unable to provide enough information related to these internal structures/components and their evolution with time. The unresolved components of the expanding plasma plume can be obtained by transpose and decomposition of

---

---

image data matrix using singular value decomposition (SVD) technique [80]. In SVD technique, the image data matrix (i.e.,  $A$  denotes a  $m \times n$  matrix of image having  $m \times n$  pixels) is decomposed into various principal components for optimal estimate of the signal and the noise components given by

$$A = u_1 s_1 v_1^T + u_2 s_2 v_2^T + \dots + u_k s_k v_k^T \quad (3.1)$$

The projections of  $A$  along  $v$  (i.e. the product  $su$ ) are the principal components (PC) of  $A$  [81]. Details of SVD in image analysis are given in our previous report [82].

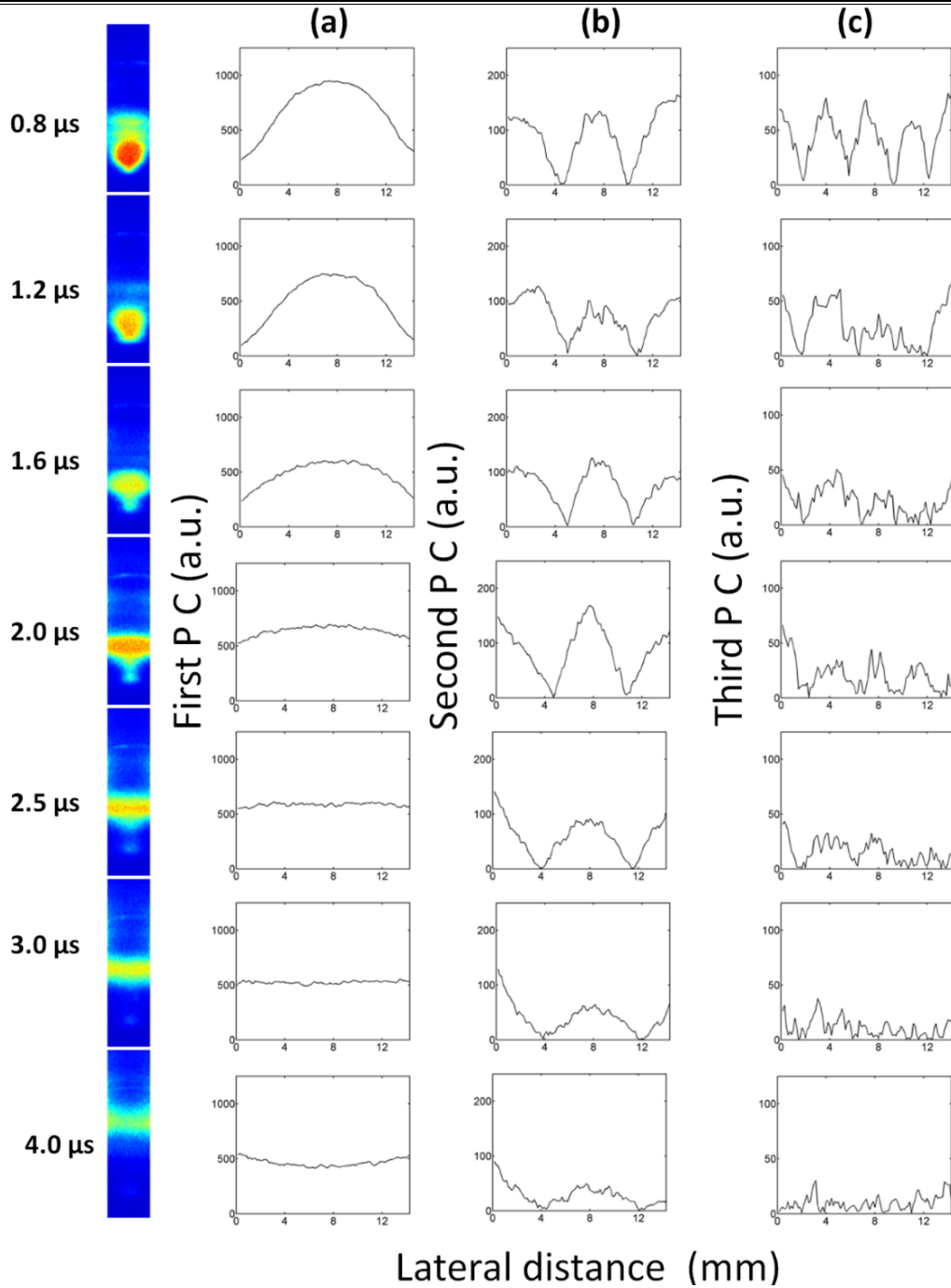


**Fig. 3.6.** SVD analysis of the plume images in the lateral direction for different time delays at  $10^{-5}$  Torr pressure. (a), (b) and (c) represent the computed first, second and third principal components respectively.

In order to see the structure formation along the magnet pole, the data matrix of each image is transposed and decomposed in transverse direction as shown in Fig. 3.6. The first principal component gives the general features of the plume and it is similar to the intensity profile along transverse direction. It is observed that the first principal

---

component has a single component and there is an increase in its width with time which represents the lateral expansion of the plume. Further to get the hidden components of the plume, we computed the second principal component for different time delays as shown in Fig. 3.6. Three distinct components are clearly visible in the second principal component which represents the core and edges of the plasma plume. The plume species moving towards the poles of the magnet are clearly visible in the second principal component. These components are further decomposed into several sub-components in third principal component which might be further resolved in higher order principal components. Due to decrease in intensity, it is not possible to compute the principal components higher than third order. Although higher order principal components are resolved as various structures of the plasma plume, these components do not systematically vary with time. This may be due to lower intensity at this stage and shot to shot variation of hydrodynamical movement of the plume and their interaction with the field. In conclusion the SVD analysis reveals that plume species are not smoothly distributed along the field lines (as they appear in the images); rather have complex structured profiles. It seems that different regions of the plasma plume interact with magnetic field to different extents because of the radial velocity and temperature gradients of plume species and hence form the complex internal structure.

### **3.3.4 Plume dynamics in diamagnetic and non-diamagnetic limits**

Further, the observed dynamical behavior as well as geometrical shape of the plasma plume in magnetic field can be explained as follows. At the initial stage, plasma temperature and density are very high, and hence plasma beta is expected to be greater than unity [28, 31]. Here plasma beta is the dimensionless parameter in magneto-hydrodynamical equation, which is defined as the ratio of the particle pressure or plasma thermal pressure ( $nkT_e$ ) to the magnetic pressure ( $P_B = B^2/2\mu_0$ ) where  $n$  is the

electron density and  $T_e$  is the electron temperature. In order to approximate the plasma beta, we have taken the electron density  $\sim 9 \times 10^{17} \text{ cm}^{-3}$ , and electron temperature  $T_e \sim 2.8 \text{ eV}$  at 1 mm distance from the reported results [28] in nearly identical experimental condition as the present case. At early stage of plasma, the estimated plasma beta is  $\sim 5$ . Here it should be noted that in laser produced plasma, plasma plume has large directed velocity (due to initial conversion of thermal energy into directed energy) and therefore directed pressure ( $nmv^2/2$ ) is larger than the thermal pressure. Therefore, final plasma beta  $[(nmV^2/2 + nkT_e)/(B^2/2\mu_0)]$  is much larger than unity, especially at early stages. In high beta region the expansion of the plasma plume is treated as expansion in the diamagnetic limit where the applied magnetic field is displaced by the field induced due to diamagnetic current. The plasma plume experiences the decelerating force and it expands until the displaced magnetic field reaches the maximum i.e. displaced magnetic energy balances the kinetic energy of the plasma plume [31, 72].

In the present scenario, diamagnetism of plasma plume could be understood as follows. Charge particles in the plasma plume experience the Lorentz force in the presence of magnetic field and therefore gyrate in opposite direction with different radii depending on the charge, mass and velocity of the plume particles. For the magnetic field  $\sim 0.45 \text{ T}$  and ion velocity  $\sim 6 \times 10^6 \text{ cm/s}$ , the estimated Larmor radii of aluminium ions ( $\text{Al}^+$ ) and electrons are 3.7 cm and 0.75  $\mu\text{m}$  respectively. Here for simplicity we assume that ions and electron are moving with same velocity in the plasma plume. Since the Larmor radius for ions is greater than the plume dimension, the ions can be treated as unmagnetized whereas electrons are trapped by the magnetic field. So as the time evolves, due to larger Larmor radius, ions overshoot the electrons and form the positive charged layer at the boundary of the plasma plume. The electrons try to hold the ions back and eventually produce radially inward electric

field. As a result induced diamagnetic current decelerates the plasma plume. Here, the maximum force appears at the direction normal to the applied magnetic field whereas plume does not experience any resistive force along the field lines as a result plume species start moving towards the pole of the magnet. Further, in the present case, position vs time plot clearly indicates that plasma plume is almost stagnant up to 1200 ns where the average plume length is  $\sim 8.5$  mm (see, Fig. 3.3). Confinement radius (or bubble radius) of the plasma can be estimated from the conservation of plasma energy and magnetic energy relation, and for the simplest case (assuming spherical symmetry) it is defined as  $R_b = (3\mu_0 E_{lpp}/\pi B^2)^{1/3}$  [29, 30]; where  $E_{lpp}$  is the kinetic energy of the laser plasma which is approximated as half of the initial laser beam energy and  $B$  is the applied magnetic field. In the present case, for the laser energy 300 mJ and 0.45 T magnetic field, the estimated confinement radius is  $\sim 9.5$  mm which is in nearly agreement with the observed confinement radius ( $\sim 8.5$  mm).

One of the important observations is re-expansion of the plume after stagnation. It can be seen from fig. 3.3 as the time evolves, the plasma plume begins to expand in both axial as well as lateral directions. The linear dependence of both velocity components and hence the free expansion of plume suggests that at this stage bulk plasma moves across the magnetic field without any resistive force. This could be understood on the basis of temporal variation of diamagnetic current in expanding plasma plume. Several experimental results suggest diamagnetism of the plasma plume first increases with time and reaches to a peak value (at bubble radius) [50, 30]. Due to rapid decrease of plasma temperature and density with time, the diamagnetic current and hence amount of displaced magnetic field is decreased and external magnetic field starts diffusing in the plasma plume. Therefore, at later stage i.e. in low plasma beta regime, plume expands in non-diamagnetic limit where the magnetic field diffuses into the plasma plume. In the present case magnetic diffusion time [28] is

estimated by the relation,  $t_d = \mu_0 \sigma R_b^2$ , where  $\sigma = \frac{50 \pi^{1/2} \epsilon_0^2 (kT_e)^{3/2}}{m_e^{1/2} e^2 Z \ln \Lambda}$  is the plasma conductivity [83], which is  $8.56 \times 10^3$  Siemens/m for  $Z = 1$ . The estimated diffusion time  $t_d$  is  $\sim 1 \mu\text{s}$ . Therefore, in the present case we assume the plasma plume expands in non-diamagnetic regime for the time delay  $> 1000$  ns. Cross field propagation of plasma plume in this regime is correlated to  $E \times B$  drift of bulk plasma as also observed by earlier workers [79]. In this case, charged particle in plasma experiences the Lorentz force  $v \times B$  and hence electrons and ions move in the opposite direction. The charge separation occurs until the counter electric field balances the Lorentz force. Thus the bulk plasma experiences the  $E \times B$  field and is drifted in axial direction with velocity  $v = (E \times B)/B^2$ .

In view of the above observations could be explained on the basis of plume expansion in diamagnetic and non-diamagnetic regimes. At the early stages of plasma, a diamagnetic cavity is formed due to the outward escape of the ions with respect to the magnetically trapped electrons. The induced diamagnetic current decelerates the plasma plume and it reaches the peak value where the plasma plume is nearly stagnant. With increase of time, diamagnetic property of the plasma weakens and magnetic field diffuses into the plasma and polarises it due to the influence of Lorentz force. Therefore, at later time plume also experiences the polarized electric and hence it freely moves across the magnetic field under the influence of  $E \times B$  drift. In the presence of the ambient gas, ambient atoms exert resistive force on the expanding plume. Evidently maximum resistive force experienced by front portion of the plume and therefore its position vs time plot deviate from the linearity as shown in Fig. 3.5. On the other hand, core of the plume is almost unaffected by ambient gas, probably shielded by plume front and moves with constant velocity.

---

### 3.4 Summary and conclusion

In summary, the dynamical and geometrical behaviour of laser produced aluminium plasma across the magnetic field have been investigated in vacuum and at  $10^{-2}$  T of argon pressure. Several distinct features have been observed related to axial and radial expansion of the plume, splitting pattern and geometrical formation which are significantly different from the reported results for similar kind of experiments. It has been observed that expanding plume experiences resistive force and approaches the stagnation limit. Stagnation condition is maintained for some time and thereafter plume begins to expand with uniform velocity. The above observations are explained on the basis of temporal behaviour of diamagnetism of laser plasma and  $E \times B$  drift of bulk plasma across the diffused field. The estimated field diffusion time and confinement radius well support the above interpretation. Well separated intensity columns, which are probably due to the velocity shear driven instabilities are observed at the leading portion of the plume. Also, SVD analysis of the image data matrix shows structured profile of the bulk plasma along the applied field lines, which is not visible in the plume images. Further, unique slab like splitting is observed in the presence of magnetic field and ambient gas. The leading component experiences the resistive force whereas trailing portion expands freely. As a consequence, both components merge together and produce uniform density distribution in the transverse direction. Uniform intensity distribution in a large volume and almost flat expansion of the plume is an important observation which can be utilized in large area film deposition. In brief the above study provides some additional information regarding the plasma dynamics in magnetic field.

This work has been published in N. Behera et al., *Phys. Lett. A* **379** (37), 2215-2220 (2015) [71], N. Behera et al., *Proceedings of the DAE-BRNS National Laser*

---

Symposium **23**, CP-07-15 (2014) [84] and N. Behera et al., Proceedings of the DAE-

BRNS National Laser Symposium **25**, CP-7.20 (2016) [85].



## Chapter 4

---

# Two directional fast imaging of plasma plume in variable magnetic field

A new experimental set-up which consists of pulse magnetic field system has been developed to capture the different phases of expanding plasma plume across the transverse magnetic field, varying from 0 to 0.57 T. Two internally synchronized ICCD cameras, mounted in orthogonal direction have been used to record the two directional projection (across and along the magnetic field directions) of the plasma plume. The plume takes the conventional ellipsoidal shape in absence of magnetic field. Well-defined cavity-like structures have been observed in a plane perpendicular to field direction, which are dominant at the early stage of plasma in a relatively lower magnetic field. As the time evolve, the cavity changes to jet/cone-like structures, which turn to slab-like structure at later times. On the other hand, well separated intensity columns (striation-like structures) are appeared in a plane parallel to magnetic field direction which is more apparent at higher magnetic field. Based on the projections of plume images in two perpendicular planes, the three dimensional structure of the plasma plume is modeled as an elliptical cylinder-like structure. The dynamics and geometry of plasma plume in presence of magnetic field are correlated with the expansion in diamagnetic and non-diamagnetic regime. The validity of plasma instability which is responsible for observed striation-like structures are also discussed.



---

## 4.1 Introduction

The study of laser-produced plasma in presence of external magnetic field is useful to understand several important physical phenomena like conversion of kinetic energy into plasma thermal energy, plume confinement, ion acceleration/deceleration, emission enhancement/decrease and plasma instabilities [33-38, 31]. It is also important for many applied researches like tokamak plasma, space plasmas such as the study of an artificial comet, propulsion of space vehicles using laser ablation, investigation of acceleration of stellar winds, laboratory plasmas such as increase in the detection sensitivity of laser-induced breakdown spectroscopy [33, 39], manipulation of plasma plume in pulse laser deposition [40-42], debris mitigation [43] etc. Several pioneer workers have tried to understand plasma plume - magnetic field interactions in vacuum as well as in presence of background gas pressure with uniform [58] and non-uniform magnetic field [35] and have observed various phenomena like formation of diamagnetic cavity and flute like structures [72, 73, 25], plasma oscillations [45], edge instability and dramatic structuring [29, 74], sub-Alfvenic plasma expansion [30] etc.

The dynamics and geometrical structure of the plasma plume across the magnetic field is depends on plasma parameters and applied magnetic field. At early stage of the plasma, where the plasma pressure and kinetic pressure is much higher than the magnetic pressure, plasma expansion in this region is considered as expansion in diamagnetic limit. Diamagnetism of laser plasma has been extensively analyzed in terms of  $\mathbf{J} \times \mathbf{B}$  interaction with the assumption plasma plume having spherical symmetry in most of the reported works. As the time evolved, plasma temperature and density are reduced considerably and magnetic start diffuse into the plasma plume. Diffused magnetic field polarized the plasma plume; as a result plume penetrates the magnetic field barrier under the influence of  $\mathbf{E} \times \mathbf{B}$  drift.  $\mathbf{E} \times \mathbf{B}$  drift of the laser

---

---

plasma is largely ignored in the reported work in case of moderate magnetic field ( $< 1$  T) and the ablating laser energy of order of few hundred mJ. Also the systematic experimental observation of formation of diamagnetism of plasma plume and at its transition into non-diamagnetic limit (diffused magnetic) field is scarce in the literature. Further shape, size and geometrical structure of plasma plume in presence of magnetic are another important aspects in terms of their utilization in practical application. Several fast imaging spectroscopy, which provide time resolved 2D images of the plume has been done to study the geometrical aspect of the plasma plume. However majority of previous experiments have been performed with permanent bar magnet where plume imaging along the magnetic field lines are not possible because of experimental constraints. Plume structure in magnetic field is highly asymmetrical and therefore complete geometrical information cannot extract from plume images projected across the magnetic field direction.

Keeping in view of above, we have designed experimental setup for studying the explicit effect of variable magnetic field on the dynamics and geometrical aspect of the expanding plasma plume. Helmholtz coil along with the two mutually synchronized ICCD cameras placed on orthogonal direction facilitate to get images across and along the magnetic field lines simultaneously. Temporal evolution of diamagnetic cavity, its dependence of external magnetic field strength and drift of plasma plume in non-diamagnetic field limit is experimentally demonstrated. Validity of different model and appearance of plasma instability is also discussed.

## **4.2 Experimental scheme**

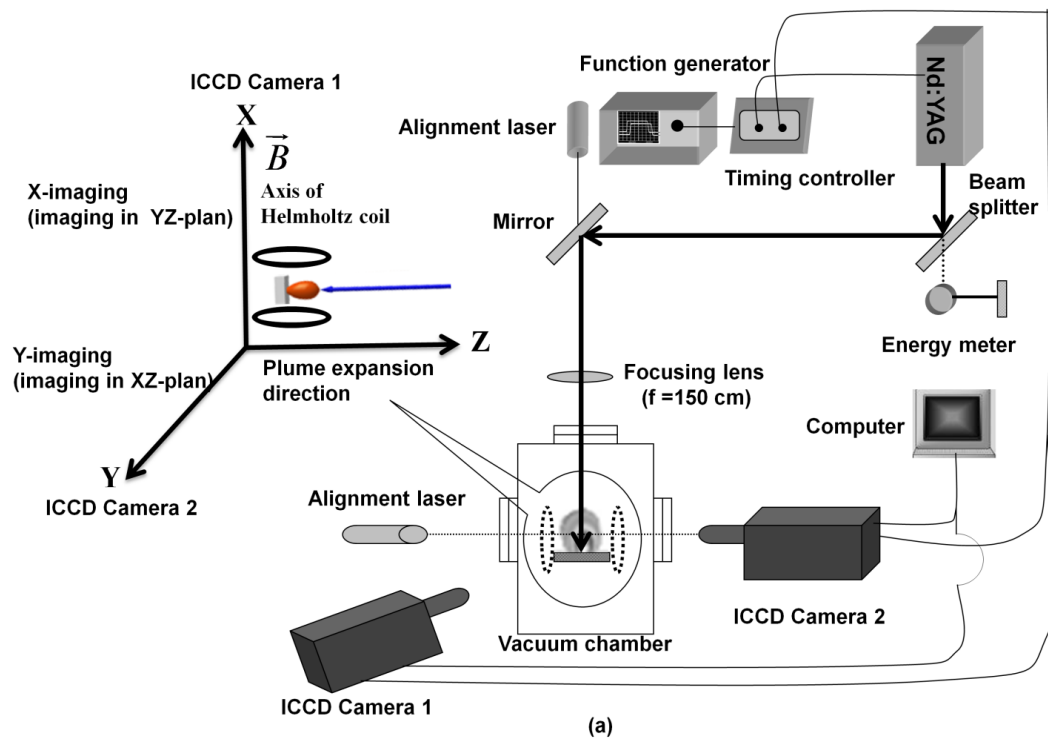
Schematic diagram of the experimental setup is shown in Fig.4.1a. The plasma plume is generated in a multi-ports cylindrical stainless steel vacuum chamber having base pressure less than  $10^{-6}$  Torr. An Nd:YAG ( $\lambda = 1064$  nm) laser having 8 ns pulse width

---

has been used to ablate the target. The pulse energy and spot size of the laser beam are set to 150 mJ and 1 mm in diameter at the target respectively, which can produce the laser fluence  $19.1 \text{ J/cm}^2$  at the target surface. Helmholtz coil along with the indigenously developed pulse power system (consist of capacitor bank) is used to produce transverse magnetic field varying from 0 to 0.57 T. Magnitude and uniformity of the magnetic field is ensured by mapping the magnetic field as a function of distance along the expansion direction and lateral directions using a Gauss meter shown in Fig. 4.1b. Here it should be noted the time varying magnetic field has a flat top profile of  $\sim 40 \mu\text{s}$ , which is larger than the considered measurement time. This is also ensuring the expansion in a uniform field. The aluminium target was mounted on a movable target holder through a vacuum compatible feed-through and placed in between the Helmholtz coil.

The light emitted from the luminous plasma is recorded through a quartz window mounted orthogonal to the direction of the plume expansion. Time resolved images of the visible plume luminescence have been recorded using two internally synchronized ICCD cameras having variable gain and gate time and having a spectral range of 350 - 750 nm. A micro-controller based time control unit is used to trigger the camera in synchronous with the laser pulse. Timing jitter in time delay with respect to laser pulse is less  $< 1 \text{ ns}$ . In this experiment z-direction is the plume propagation direction and camera 1 and 2 are recorded images along the x and y-direction respectively as shown in fig. 4.1. Here camera 1 and 2 are designed as x-imaging and y-imaging respectively. In the present experiment, gate opening time is set at 5 to 25 ns. Temporal evolution of the laser-produced plume has been obtained by varying the time delay (from 100 to 2000 ns) between the laser pulse and the opening time of ICCD gate. Minimum three images are recorded under similar experimental conditions. The reproducibility of the emission intensity is better than

5%. A mesh image of known dimensions ( $5 \text{ mm} \times 5 \text{ mm}$ ) is recorded to map the geometrical parameters of the plume. The magnification of the imaging system is found to be 3. Dark current noise is subtracted from the recorded image using MATLAB. Length and width of the plume are estimated by segmentation algorithm using MATLAB. For better visibility, grey images have been converted into pseudo-colour images using jet-colour map. The emission spectroscopy has been used to estimate the plasma parameters. For that spectral light is viewed normal to the expansion direction and fed at the entrance slit of the spectrometer (Acton SP2500A) through an optical fibre.



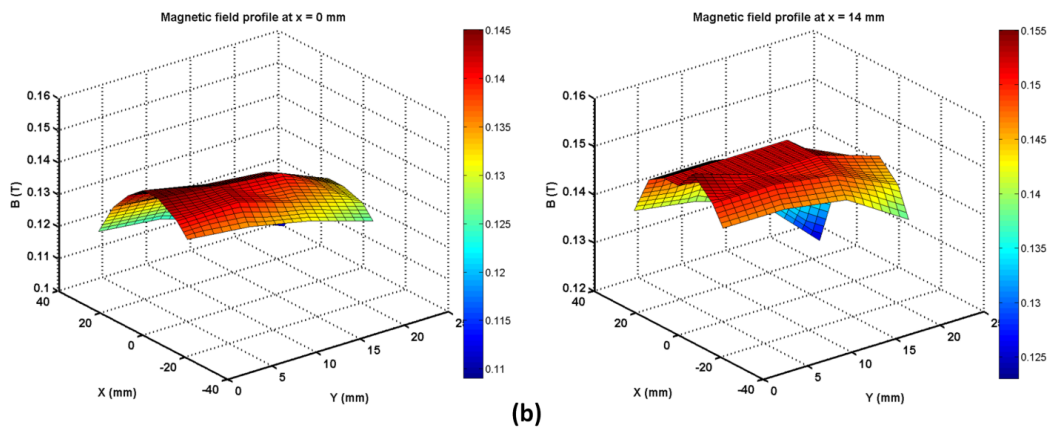


**Fig. 4.1.** (a) Schematic of the experimental setup and (b) magnetic field profile between the two poles of Helmholtz coil measured by Gauss meter at  $x = 0$  mm and  $x = 14$  mm for magnetic field 0.13 T.

### 4.3 Results and discussions

When laser-produced plasma expands in magnetic field it undergoes through several interesting phases like thermalization, diamagnetization, confinement, propagation across the field, formation of different type of structures etc. Time resolve study of expanding plume in presence of magnetic field is important to understand these phases. Time resolved fast imaging of electronically excited plume species provide the two-dimensional snap-shot of the expanding plasma plume. Image analysis of these 2D-images provides various information related to plume dynamics, hydrodynamic movement of plasma and geometrical structure of the expanding plume. Most of the previous experiments related to plasma expansion in magnetic field have done with permanent magnet bar which have several experimental constrains. In these experiments, plume imaging along the magnetic field is not possible. Since plume expansion in magnetic field is highly asymmetrical and therefore complete picture of shape and dynamics of the plume cannot extract from the plume images projected across the magnetic field direction.

---

Keeping in view of above we have deigned the experiment based on the Helmholtz coil and mutually synchronized two gated ICCD camera which facilitates to record images of evolving plume along and cross the magnetic lines. Helmholtz coil not only give the variable magnetic field but it also facilitate to record the images along the magnetic field lines. The simultaneous use of these cameras gives the complete information about the dynamics and geometrical aspect of the plume in presence of transverse magnetic field.

### **4.3.1 Expansion in the absence of magnetic field**

The sequence of images of the plasma plume projected in two different directions, that is along and across the magnetic field lines (thereafter called as x-imaging and y-imaging respectively) are captured in absence of magnetic field as shown in Fig 4.2. These images are recorded at different time delays, varying from 200 ns to 1000 ns. The background pressure and laser fluence are set as  $10^{-5}$  Torr and  $19.1 \text{ J/cm}^2$  respectively. Each image represents the spectrally integrated emission intensity in the range 350-750 nm, emitted from plume species. In absence of magnetic field, plume expansion is mainly governed by the initial pressure gradient inside the plume, and is treated as adiabatic expansion [5]. Due to large pressure gradient in axial direction (opposite to laser beam direction), plume has an early ellipsoidal shape. Ellipsoidal shape of plume is confirmed by two projection of images where both x-imaging and y-imaging data are nearly identical. With time, emission intensity was reduced considerably and at  $t > 1000 \text{ ns}$ , emission intensity is beyond the detection limit of the ICCD. This is because electron temperature and density reduces rapidly with time and hence the probability of excitation of plume species is also reduced.

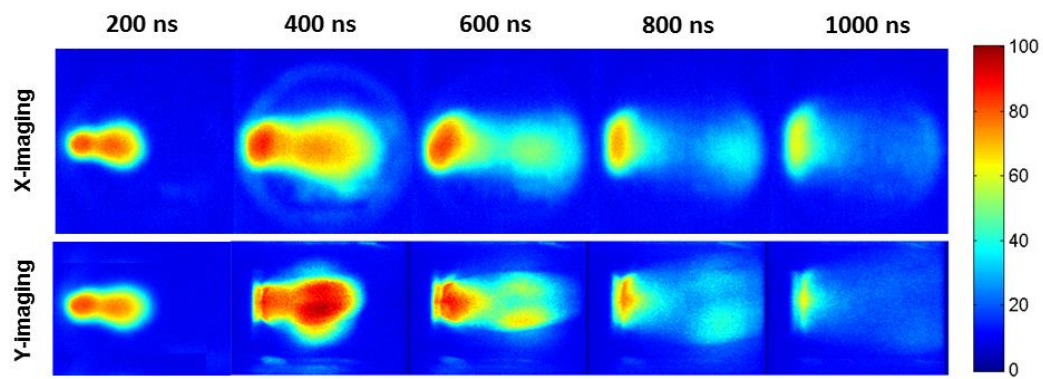


**Fig. 4.2.** The sequence of images of expanding plasma plume without magnetic field at different delay times.

### 4.3.2 Expansion in the presence of magnetic field

Effect of magnetic field on the dynamics and geometrical aspect of the plume is studied by observing plume images as a function of time in presence of magnetic field. Fig. 4.3 shows the sequence of images recorded at different time delays, varying from 150 ns to 1200 ns at 0.13 T and 0.57 T magnetic fields. All the experimental parameters, laser fluence, ambient pressure etc. are same as in case of field free case. In comparison to observed images in field free case, it has been observed that the presence of magnetic field drastically changes the structure, dynamics and emission intensity of the plasma plume. Enhancement in emission intensity has been observed in presence of magnetic field where the emissive lifetime of the expanding plume is significantly increased in comparison to field free case. In presence of magnetic field, increase in electron temperature and electron-ion collision frequency is expected because of Joule heating and cyclotron motion of electrons and ions. This will result in increased the excitation processes in the plume species.

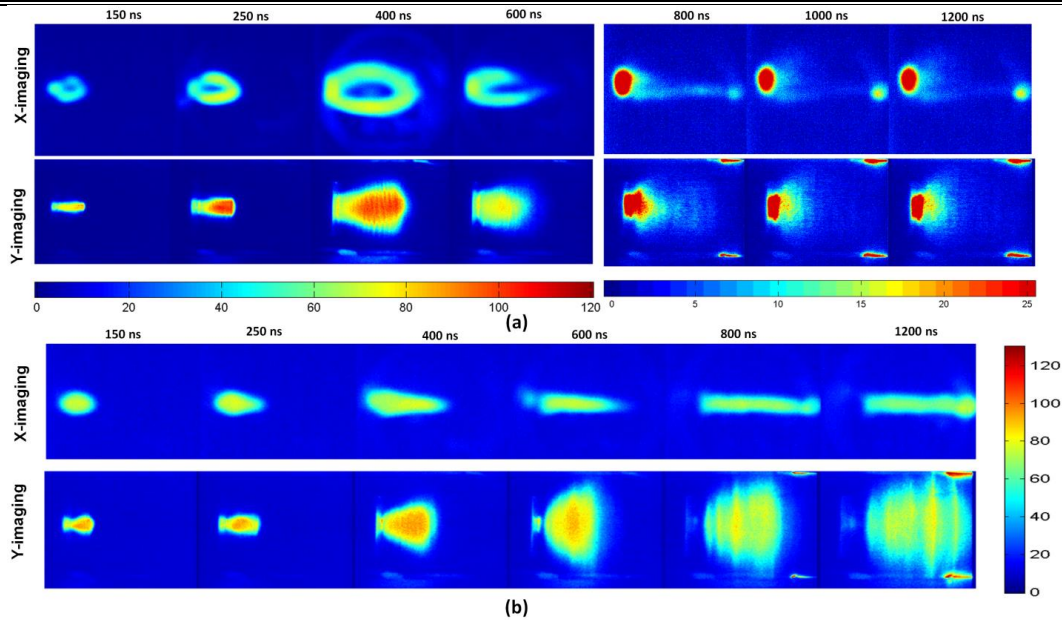


**Fig. 4.3.** The sequence of images of expanding plasma plume at (a) 0.13 and (b) 0.57 T magnetic field at different delay times.

A well-defined elliptical cavity like structure is observed in the plume images projected along the magnetic field lines (x-imaging) at comparatively low magnetic field (0.13 T) as shown in Fig 4.3a. Initially the cavity expands with time and attain the maximum dimension at  $t = 400$  ns. However the elliptical shape of plume cavity is retained. At time  $t > 400$  ns, plasma cavity start reducing mainly along the lateral direction and finally cavity-like structure is dismissed with further increase of time delay. Here, it should be noted that the circular intense structure at the plume front observed in x-imaging (Fig 4.3a) from 800 ns is due to the reflection from the inner radius of the Helmholtz coil. This reflection is also visible in y-imaging data. So this portion doesn't contribute to the plume length calculation. In case of higher magnetic field that is at 0.57 T, cavity-like structure is not observed throughout our considered measurement range (see, fig 4.3b). It seems that cavity is collapsed before 150 ns time delay at 0.57 T field. Another noteworthy observation is that after collapse of cavity-like structure, a cone like structure is formed which is clearer in higher magnetic field

---

intensity (0.57 T). At later time instant, cone like structure converted into slab like shape with expand freely in axial direction.

Scenario is completely different in case of plume images projected across the magnetic field direction (y-imaging). It has been observed that in presence of magnetic field, plasma plume expand with higher lateral velocity in comparison to axial velocity and hence plume becomes more elongated towards the magnetic pole with time delay. The dominant lateral velocity of the plume is more visible in higher magnetic field (0.57 T) as seen in y-imaging data of fig 4.3b, where lateral dimension of the plume rapidly increased and attain the maximum dimension (separation between the two Helmholtz coil) at time delay  $t = 800$  ns. The magnetic field induced plasma instability is also visible in this case. At low magnetic field (0.13 T), initially the instability is developed at the edges of the plume. As the time evolves, instability grows as an intensity column (Striation like structure) parallel to the magnetic field lines. These striations are more defined and well separated at later stage and higher magnetic field intensity (0.57 T).

In order to get more insight into the formation and evolution of cavity-like structure, growth of plasma instability and their dependence on the magnetic field intensity, plume images are recorded in variable magnetic field. Fig. 4.4 shows the x- and y- imaging data for different magnetic field in the range 0.13 to 0.57 T recorded at two different time delay, 400 and 800 ns. In case of x-imaging and comparatively lower time delay ( $t = 400$  ns), size of the cavity gradually decreases with increasing the magnetic field. The cavity-like structure has disappeared at  $\sim 0.36$  T field and formed a jet like structure. Jet like plume structures slightly shrink laterally with the further increase of magnetic field up to 0.57 T magnetic fields. However, at fixed time instant, we could not observe any significant change in axial dimension of the plume with increase of magnetic field intensity. On the other hand in case of y-imaging data,

plasma plume elongated in direction of field lines with increasing the magnetic fields.

Also at a given time, the density columns are closely packed in low magnetic fields which are gradually separated with increase of magnetic field intensity from 0.13 to 0.57 T. This effect is more apparent at higher at higher time delay (800 ns as shown in Fig. 4.4b and 1200 ns as shown in Fig. 4.5).

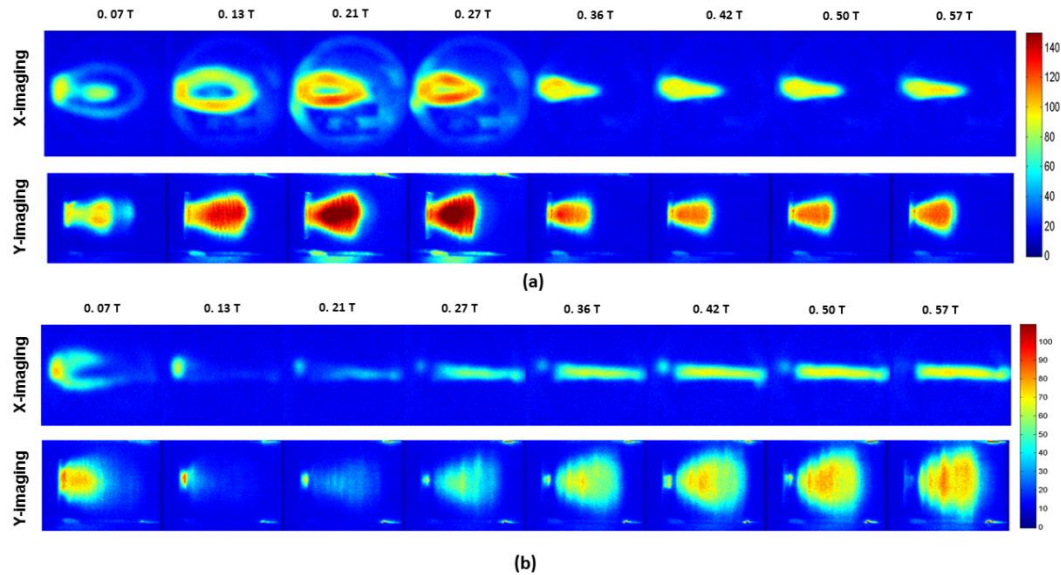


**Fig. 4.4.** The sequence of images of expanding plasma plume at (a) 400 and (b) 800 ns delay time at different magnetic fields.

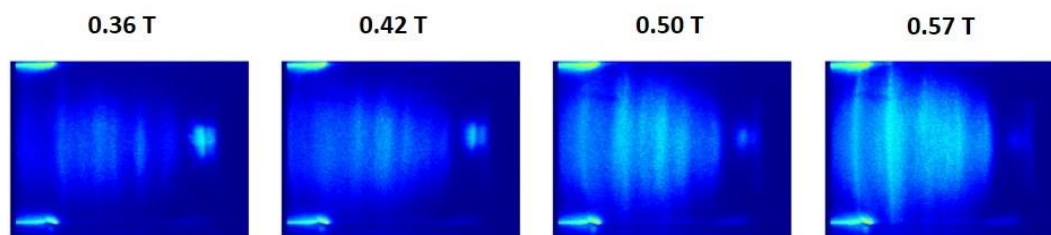


**Fig. 4.5.** The sequence of images (y-imaging) of expanding plasma plume at 1200 ns delay time at different magnetic fields.

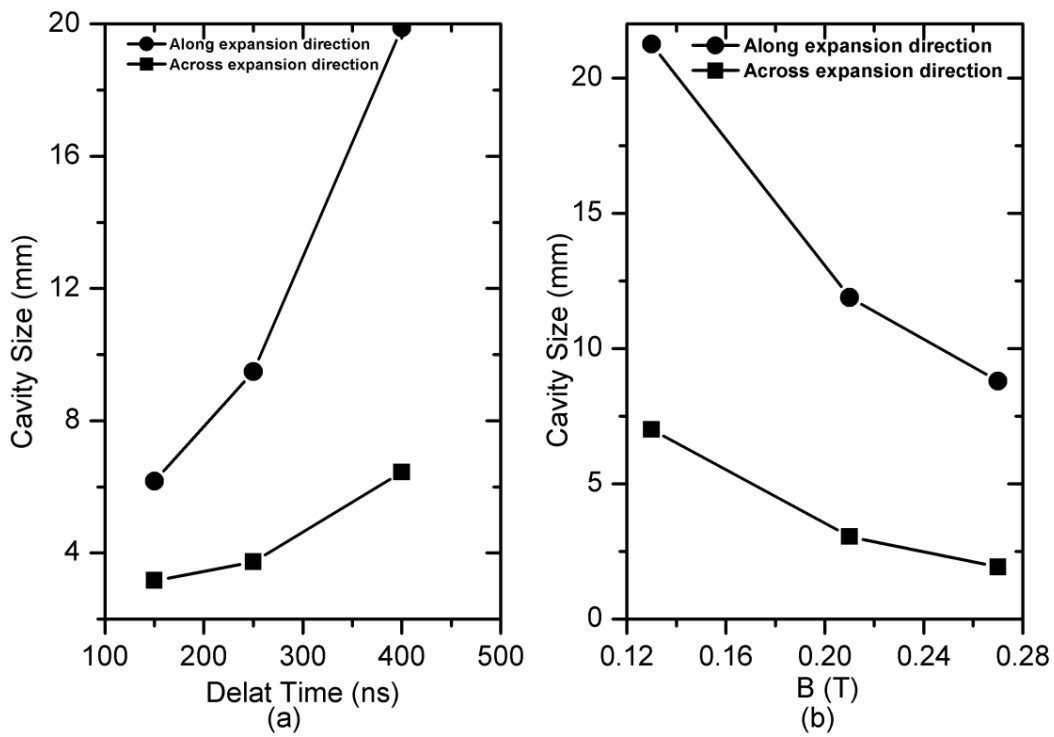


**Fig. 4.6.** Experimentally measured inner major and minor radii (a) as function of time delay for  $B = 0.13$  T and (b) as a function of magnetic field strength at  $t = 400$  ns.

From the above observation it is clear that cavity-like structure of the plasma plume is more pronounced in lower magnetic field which shows the strong dependence on time and magnetic field strength as shown in Fig 4.6. Temporal behavior of plasma cavity, that is, variation of inner major and minor radii with time for fixed magnetic field (0.13 T) field is clearly depicted in Fig. 4.6a. Figure 4.6b represents the variation of cavity radii with magnetic field for fixed time delay  $t = 400$  ns. On the other hand, appeared plasma instability is more evident at comparatively higher magnetic field and later stage of plasma expansion. Also based on the projections of the images in  $yz$ -plane ( $x$ -imaging) and  $xz$ -plane ( $y$ -imaging), the three dimensional structure of the plasma plume is modeled as an elliptical cylinder-like structure which is converted into structured slab like shape as schematically shown in Fig 4.7.

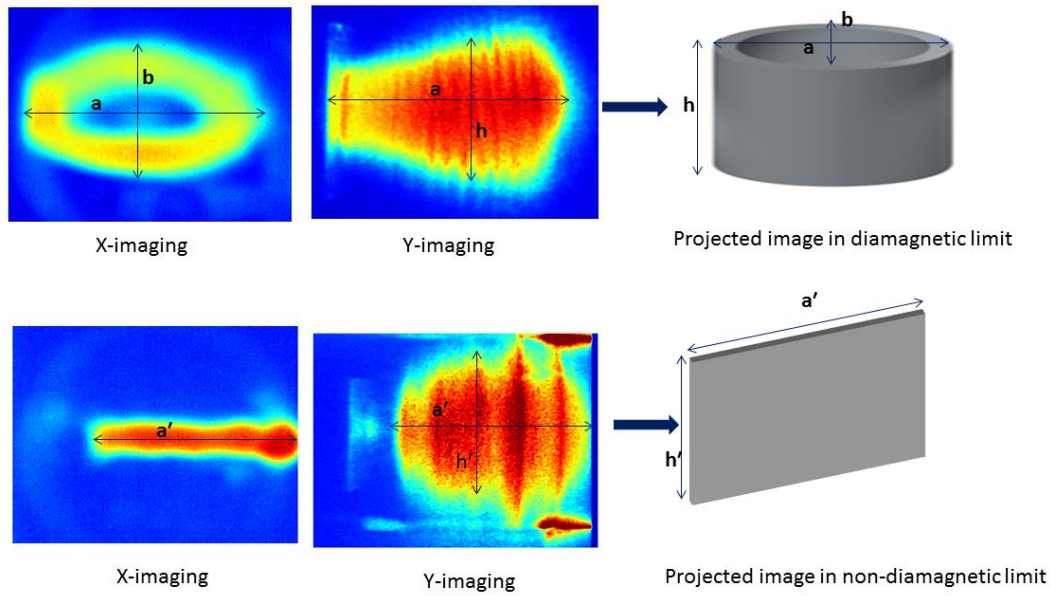


**Fig. 4.7.** The projected images in diamagnetic limit at 0.13 T and 400 ns and non-diamagnetic limits at 0.57 T and 800 ns.

### 4.3.3 Plasma parameters

In order to explain the observed features of the plume, the plasma parameters like electron temperature and density are estimated using optical emission spectroscopy. The electron temperature was estimated by taking the line intensities ratios of two ionic lines Al II  $3s4p\ ^1P^0 \rightarrow 3p^2\ ^1D$  (at 466.3 nm) and Al III  $2p^64d\ ^2D \rightarrow 2p^64p\ ^2P^0$  (at 452.9 nm) using the relation [58],

$$\frac{I_1}{I_2} = \frac{g_1 A_1 \lambda_2}{g_2 A_2 \lambda_1} \exp \frac{-(E_1 - E_2)}{kT_e} \quad (4.1)$$

where,  $I_1$  and  $I_2$  are the intensities of the spectral lines of wavelengths  $\lambda_1$  and  $\lambda_2$ ;  $g_1$ ,  $g_2$  are the statistical weight factors,  $A_1$ ,  $A_2$  are the transition probabilities,  $E_1$ ,  $E_2$  are the energies of the excited states of the two spectral lines,  $k$  is the Boltzmann's constant, and  $T_e$  is the electron temperature. Here, non-resonant lines are chosen to avoid the self-absorption. The required spectroscopic data required for temperature measurement are taken from the NIST database.

Variation of electron temperature as function of time in both, absence and presence of magnetic field is shown in Fig. 4.8a. In field free case, as usual plasma cool down rapidly where electron temperature decreases exponentially with increase of time delay. Estimation of electron temperature beyond the 400 ns is difficult because of reduction of emission intensity in field free case. In presence of 0.27 T magnetic field, significant increase of electron temperature is observed in comparison to observed temperature in field free case. However it follows a decreasing trend with time delay similar, to that in the field free case. Most of previous researchers have explained the increase of electron temperature in magnetic in terms of Joule heating [28]. Moreover presence of magnetic field can also increases the electro-ion recombination (three body recombination) because of plume confinement (as comparison to the field free case), which can also increase the electron temperature. Therefore effect of magnetic field on electron temperature is attributed as net contribution of both joule heating and three-body recombination.

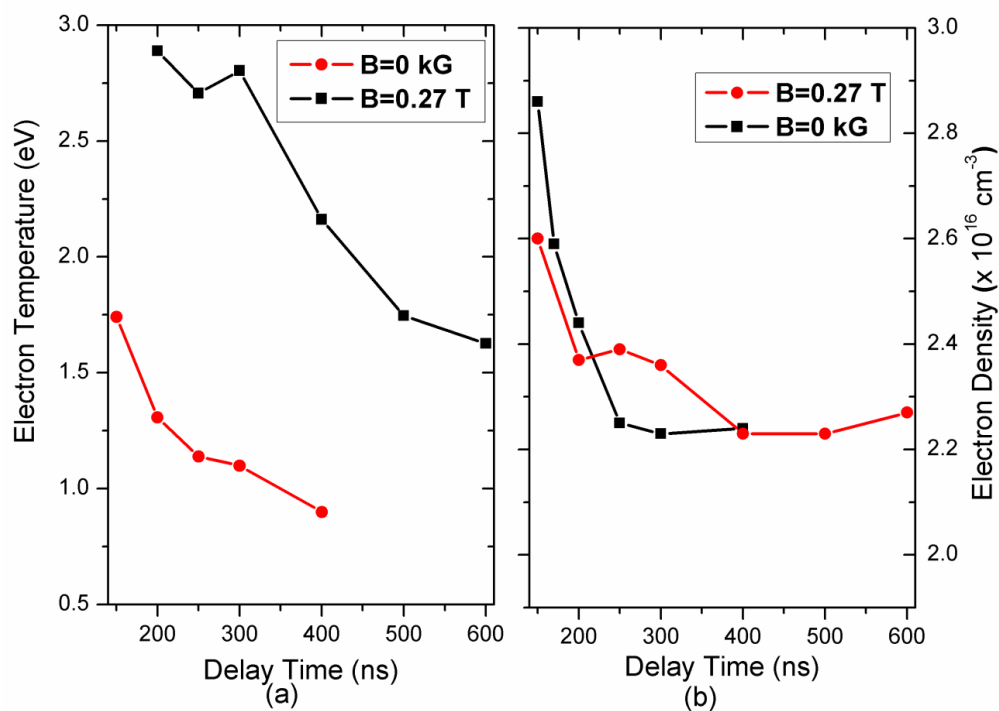


**Fig. 4.8.** Variation of (a) electron temperature and (b) electron density as a function of delay time in the absence and presence of 0.27 T magnetic field

Further, the electron density  $n_e$  of the plasma plume is obtained from the Stark broadening profile of Al II at 466.3 nm line using the relation [58],

$$\Delta\lambda_{1/2} = \frac{2 W n_e}{10^{16}} \quad (4.2)$$

where  $\Delta\lambda_{1/2}$  is the FWHM of the spectral line and  $W$  is the electron impact parameter. The observed line profile is fitted with a Lorentzian function to obtain the line width. The electron impact parameter ( $W$ ) for Al II (466.3 nm) line is taken from Ref. [25]. Here, broadening due to ionic contribution and Doppler broadening are ignored because of its negligible contributions [66, 67]. A typical line profile of Al II (466.3 nm) and the fitted Lorentzian curve is shown in Fig. 4.9.

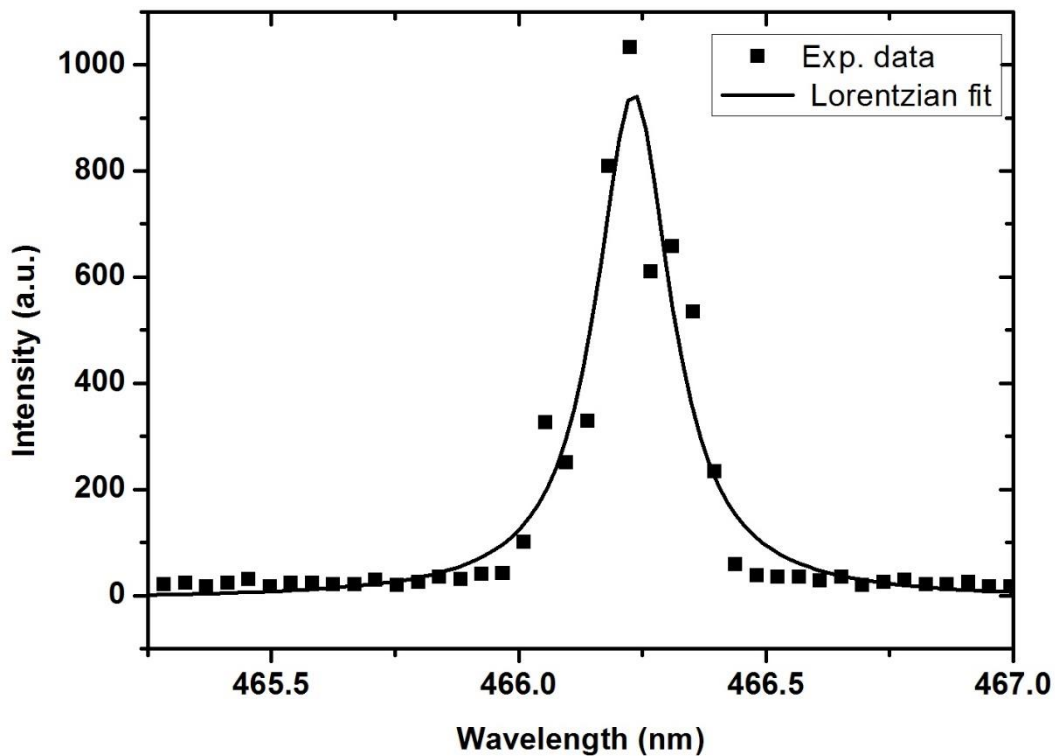


**Fig. 4.9.** Typical Stark broadened profile of Al II 466.3 nm line at 400 ns time delay in the absence of magnetic field and corresponding Lorentzian fit.

The variation of electron density as a function of delay for the both absence and presence of 0.27 T magnetic field is shown in Fig. 4.8b. Exponential decay of electron density with time follows the adiabatic expansion model in field free case. Not much significant change in the electron densities are noticed by introduction of

0.27 T magnetic field in comparison to field free case. However at  $t > 200$  ns, slight increase in densities is observed in presence of magnetic field.

We have also studied the effect of magnetic field strength on the plasma parameters of the plume. Electron temperature as well as density as function of magnetic field strength, varying from 0.17 to 0.57 T at 400 ns time delay is shown in Fig. 4.10. It has been found that electron temperature increases with field strength and attain the saturation at 0.27 T magnetic field and no further change in electron temperature is observed beyond the 0.27 T field. Interestingly, at a fixed time delay 400 ns, the electron density is almost constant for all magnetic field considered in the present case. The increase of electron density with field is expected due to the magnetic confinement. However at the same time probability of collision and hence electron-ion recombination is also increased, which leads to decrease the electron density. This might be the reason of observed density pattern in varying magnetic field.

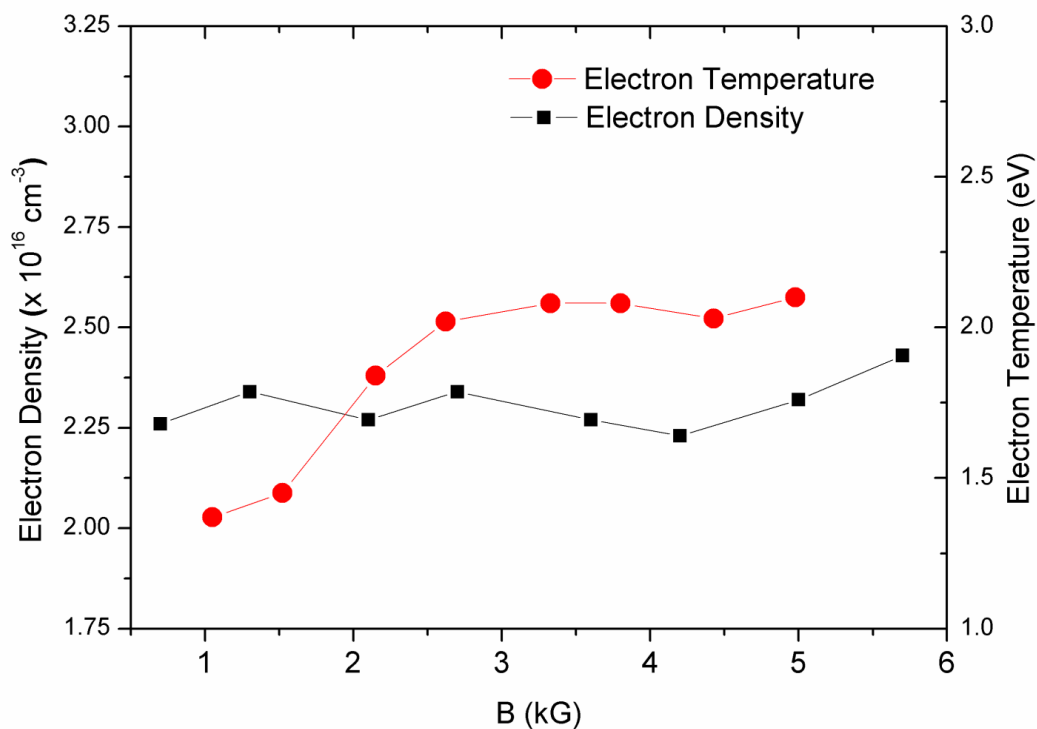


**Fig. 4.10.** Variation of electron temperature and density as a function of applied magnetic field at 400 ns time delay.

Here it should be noted that above estimation of plasma parameters is valid only for plasma in local thermodynamic equilibrium (LTE). So, it is necessary to ensure the LTE condition by using the McWhirter criterion [58], which gives the minimum density required for LTE is given by

$$n_e \geq 1.4 \times 10^{14} \sqrt{T_e} (\Delta E)^3 \text{ cm}^{-3} \quad (4.3)$$

where,  $T_e$  (eV) is the electron temperature and  $\Delta E$  (eV) is the maximum energy difference between the upper and lower energy levels. For the estimated electron temperature (1.74 eV) and the largest energy gap of the considered lines (2.74 eV), this criterion predicts a lower limit for  $n_e$  of  $3.8 \times 10^{15} \text{ cm}^{-3}$ . Our estimated values of  $n_e$  are always greater than limiting value and hence LTE is safely approximated in the present case.

#### **4.3.4 Plume dynamics in diamagnetic and non-diamagnetic limits**

Further, dynamics and geometrical shape of plasma plume across the magnetic field is governed by various parameters, for example, plasma beta, diamagnetism of plasma, magnetic diffusion through the plasma plume etc. For the electron temperature of 1.74 eV and electron density of  $2.8 \times 10^{16} \text{ cm}^{-3}$  obtained at the early stage of plasma, the estimated plasma beta for all the considered magnetic field are tabulated in Table 4.1. However the laser-produced plasma is highly transient in nature and usually directed pressure ( $P_d = mnV^2/2$ ) is much larger than the thermal beta. Therefore the total plasma beta ( $((mnV^2/2+nT_e)/(B^2/2\mu_0))$ ) plays an important role in the present case. Here,  $V$  is expansion velocity of plasma plume, which is  $\sim 8.4 \times 10^4 \text{ m/s}$ . With the present experimental parameters, the estimated total plasma beta are found to be varied from 659.67 to 34.31 for the magnetic field in the range of 0.13 - 0.57 T (see, Table 4.1). Here it should be noted that plasma total beta is always greater than unity even at maximum considered magnetic field.

Magnetic field, B (T)	Electron larmor radius, $r_{L,e}$ ( $\mu\text{m}$ )	Ion larmor radius, $r_{L,i}$ (cm)	Thermal beta, $\beta_{\text{the}}$	Total beta, $\beta_{\text{tot}}$	Diffusion time, $t_d$ (ns)
0.13	3.67	18.08	1.16	659.67	1148.14
0.21	2.27	11.19	0.44	252.80	605.75
0.27	1.77	8.71	0.27	152.93	433.28
0.36	1.33	6.53	0.15	86.02	295.25
0.42	1.14	5.60	0.11	63.20	240.39
0.5	0.96	4.70	0.08	44.59	190.53
0.57	0.84	4.12	0.06	34.31	159.99

**Table 4.1.** Variation of electron Larmor radius ( $r_{L,e}$ ), ion Larmor radius ( $r_{L,i}$ ), thermal beta ( $\beta_{\text{the}}$ ), total beta ( $\beta_{\text{tot}}$ ) and diffusion time ( $t_d$ ) with applied external magnetic field (B).

In high beta region the expansion of the plasma plume is treated as expansion in the diamagnetic limit where the applied magnetic field is displaced by the induced field in the plasma due to diamagnetic current. The plasma plume experiences the decelerating force and it expands until the displaced magnetic field reaches the maximum displaced magnetic energy balances the kinetic energy of the plasma plume. Diamagnetism of expanding plasma plume in presence of magnetic field arises because of Larmor motion of electrons and ions. Assuming that electron and ions in the plume moving with same velocity of  $\sim 8.4 \times 10^4$  m/s, Larmor radii of electrons and  $\text{Al}^+$  ions for the maximum magnetic field (0.57 T) are estimated as 0.84  $\mu\text{m}$  and 4.12 cm respectively. Here, even for the maximum field the Larmor radius for ions is greater than the plume dimension and hence the ions are considered as non-magnetised and therefore not much affected by the magnetic field. Since the electron are trapped by magnetic field, ions overshoot the electrons and formed the positive charge layer at the surface of the plasma plume which are hold by induced inward

electric field. As a result, cavity like structure is developed where diamagnetic current opposes the applied magnetic field. In the present context, cavity like structure as shown in Fig. 4.3a represents the plume expansion in diamagnetic limit. As mentioned before, dimension of the cavity is varying with time for any fixed magnetic field. This is because plasma temperature and density are decreases with time and hence the magnitudes of displaced magnetic field due to the diamagnetism of plume also decrease. As a result, applied magnetic field starts diffusing into the plasma plume. This could be understood by estimating the magnetic Reynolds number which is defined as the ratio of magnetic field convection to magnetic field diffusion, that is  $R_m = (\mu_0 LV)/\eta$  where,  $\eta = 5.2 \times 10^{-5} Z \ln\Lambda (T_e)^{-3/2}$  is plasma resistivity [83],  $Z$  is charge state,  $\Lambda$  is coulomb logarithm,  $T_e$  is electron temperature in eV,  $L$  is magnetic field gradient scale length,  $V$  is plasma speed. For the present experimental parameters, the estimated magnetic Reynolds number are found to be 8.92, 8.12, 4.28, 2.50 for time delay 200, 250, 400 and 600 ns respectively in presence of 0.27 T magnetic field. The decrease of  $R_m$  (or increase of diffusion coefficient,  $1/R_m$  in the generalized Ohm's law [77]) with the time delay indicates that the plasma becomes more and more diffusive as it evolves.

Furthermore, in most of the previously reported work, size of diamagnetic cavity, commonly known as bubble radius ( $R_b = (3\mu_0 E_{lpp}/\pi B^2)^{1/3}$ ) and magnetic diffusion time ( $t_d = \mu_0 \sigma R_b^2$ ) are approximated by equating the total excluded magnetic energy and kinetic energy of the laser-produced plasma ( $E_{lpp}$ ). Here, for simplicity they assume that plasma plume having spherical symmetry,  $E_{lpp}$  is equal to the half of the energy of laser pulse and  $\sigma$  is the plasma conductivity.

However, Fig. 4.3 & 4.4 clearly suggest that spherical symmetry of the plasma plume is not a good approximation in the present case. Zakharov et al., [73] reported the asymmetric structure of plume in presence of magnetic field where the maximum

cavity size along the expansion axis was 1.4 times larger than the size across the expansion axis. Based on the projected shape of the plasma plume in magnetic field as shown in Fig. 4.6, the maximum cavity size along the expansion axis (a) and magnetic diffusion time (t) can be expressed as,

$$a = \left( \frac{2\mu_0 E_{lpp}}{k_1 k_2 \pi B_2} \right)^{1/3} \quad (4.4)$$

$$t_d = \mu_0 \sigma a^2 \quad (4.5)$$

where,  $k_1 = b/a$  and  $k_2 = h/a$  and a, b, and h are the dimensions of elliptical cylinder as depicted in Fig. 4.6. For the present parameters, that is  $E_{lpp} = 75$  mJ,  $\sigma = \frac{50\pi\epsilon_0 T_e^{3/2}}{\sqrt{m_e e^2 Z \ln \Lambda}} = 2.0 \times 10^3$  Siemens/m (for  $Z = 2$ ) is the plasma conductivity [83] and  $k_1 = k_2 = 1.6$ , the estimated magnetic diffusion time (see, Table 4.1) with the help of equation (8) is in close agreement with experimental observation for the magnetic field  $> 0.27$  T. Still there is significant difference between the estimated diffusion time and observed results at lower magnetic field. This is might be due to the error in estimation of plasma conductivity.

As we discussed earlier, after collapse of cavity like structure, the bulk plasma plume expands freely without any decelerating force. The cross-field propagation of bulk plasma plume is more evident in 0.57 T magnetic field (Fig. 4.3b). This is the region where the diamagnetism of plasma plume is disappearing and the magnetic field lines get diffuse through the plasma (treated as non-diamagnetic region). In order to see the plume dynamics in diamagnetic and non-diamagnetic regime, we have plotted the plume length (axial dimension) as function of time delay for the two magnetic field 0.13 T and 0.57 T as shown in fig. 4.11. For 0.13 T magnetic field, deviations from linear dependence of plume length vs time plot suggest that plume experience the resistive force by the magnetic pressure. This in agreement with

expansion in diamagnetic region where the diamagnetic cavity persists up to considered time range as shown fig. 4.3a. Interestingly at 0.57 T field, linear dependence of plume length with time is observed, that is plume expands freely without any drag force. Though, we expect the large resistive force by magnetic pressure at high magnetic field. This could be explained as follows. At 0.57 T field, magnetic field diffuse into the plume before 200 ns as shown in fig. 4.3b. Diffuse magnetic field causes the polarization of ions and electrons in opposite direction because of Lorentz force ( $\mathbf{v} \times \mathbf{B}$ ). Thus charge separation induces the electric field  $E$  in  $xy$ -plane. Hence the plume species experience the  $E \times B$  force and propagate across the magnetic field with drift velocity  $(E \times B)/B^2$  [71]. Here it should be noted that plasma is polarized if plasma dielectric constant  $\epsilon$  satisfy the condition,  $\epsilon = 1 + (\omega_{pi}/\omega_{ci})^2 \gg 1$ , where  $\omega_{pi}$  = ion plasma frequency,  $\omega_{ci}$  = ion cyclotron frequency [26]. The estimated  $\epsilon$  is found to be  $4.36 \times 10^8$  for 0.57 T field and hence the cross field propagation is valid in present scenario.

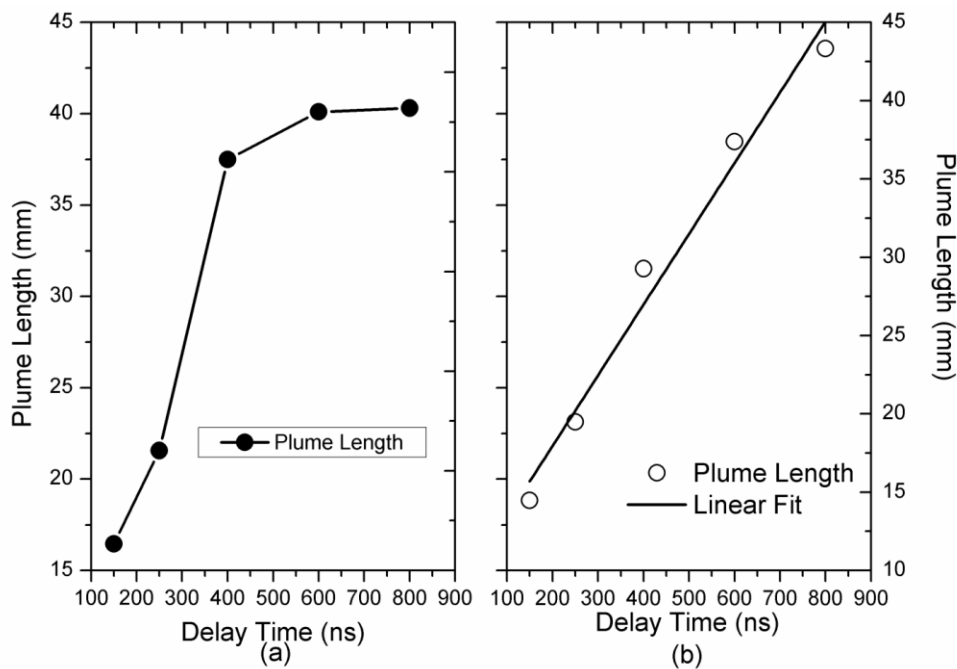


**Fig. 4.11.** Variation of plume length as a function of time delay in presence of (a) 0.13 T and (b) 0.57 T magnetic field.

---

Furthermore, conical structure which is converted into a slab like structure (discussed earlier) at latter time in non-diamagnetic regime could also be explained on the basis of polarization of plasma plume. The strength of induced electric field  $E$  gradually decreases away from the plume center because of the shielding effect. As a result the particles on the surface of polarized plasma experience less electric field and hence less  $E \times B$  force in comparison to inner layer. Thus the inner layers of the plasma move ahead with respect to outer layer and re-polarized [26, 27]. Thus the successive lagging of outer layer, initially form the conical structure which is converted into a slab like structure with increase of time delay.

### 4.3.5 Formation of striation-like structures

Again referring Fig. 4.3, where striation-like structures, parallel to magnetic field lines are observed in y-imaging data, which are dominant at comparatively higher magnetic fields. It has also been noticed that the number of density column is showing the increasing trends with magnetic field as shown in Fig. 4.4b and Fig. 4.5.

The growth of plasma instability, mainly the velocity shear instabilities (e.g. Rayleigh-Taylor instability, Kelvin-Helmholtz instability and electron-ion hybrid instability) are responsible for structure formation in the plasma plume in presence of magnetic field. Peyser et al. [31] reported the similar striation-like structures in presence of 0.3 - 0.6 T field and comparatively higher laser energy (30-300 J). They explained the observed structure in terms of electron-ion hybrid instability.

In order to validate the existence of electron-ion hybrid instability in present case, we have estimated the growth rate,  $\gamma = 0.05\omega_{LH}$  and maximum growth time,  $\tau = 2\pi/0.05\omega_{LH}$  for this instability, where  $\omega_{LH} = (\omega_{pi}\Omega_e)/(\omega_{pe}^2 + \Omega_e^2)^{1/2}$  is the lower hybrid frequency. Here,  $\omega_{pe}$ ,  $\omega_{pi}$  and  $\Omega_e$  are the electron-plasma, ion-plasma and electron cyclotron frequencies respectively. The estimated growth time for different magnetic

field are shown in Fig. 4.12. A reasonably good agreement is observed between the estimated growth time and appearance of structure for the magnetic field  $> 0.27$  T. Therefore at relatively higher magnetic field, the electron-ion hybrid instability may be responsible for striation-like structures in the present case. However large discrepancies between the estimated and observed growth time is observed for the magnetic field  $< 0.27$  T. More details theoretical study is needed to explain these observations, especially in incase of low magnetic field.

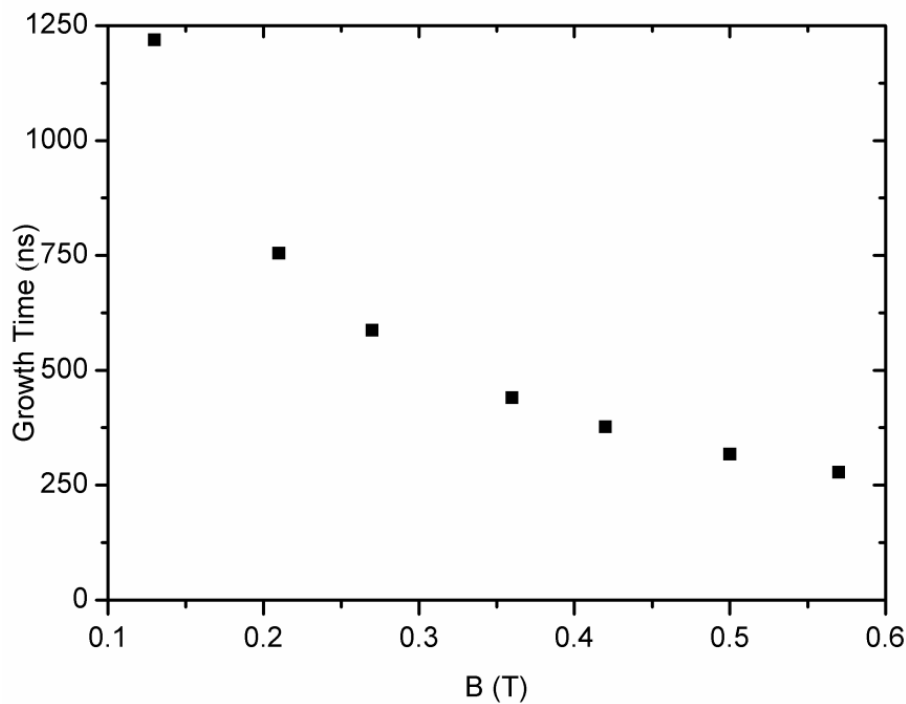


**Fig.4.12.** Variation of maximum growth time of the electron-ion hybrid instability with the applied magnetic field.

#### 4.4 Summary and conclusion

In summary, based on plume imaging in both across and along the magnetic field lines, the dynamical and geometrical behavior of laser-produced plasma across the transverse magnetic field has been investigated. Different phases of plasma expansion, e.g. formation of diamagnetic cavity and its dependence of the delay time and field strength, disappearance of diamagnetism and  $E \times B$  drift of the plasma plume are

---

experimentally demonstrated. On the basis of present observation, we proposed the three dimensional structure of expanding plasma plume in both diamagnetic region as well as non-diamagnetic region. Many distinct features have been observed which are significantly different from the reported results for plume expansion in transverse magnetic field. Time and field strength dependence of cavity formation and its collapse, jet and slab-like structure formation and plasma instability are correlated with time varying plasma parameters and field diffusion into the plasma plume. The diamagnetic cavity is dominant at comparatively lower delay time and lower magnetic field. The cavity like structures turn to jet/cone-like structures which again change to slab-like structure with increase of either external magnetic field or time delay. Time and field strength dependence of observed results are correlated with time varying plasma parameters and hence the extent of field diffusion into the plasma plume. The diffusive term of the generalized Ohm's law have calculated and found it increases with increase in time, which indicates that the plasma becomes more and more diffusive as it expands. The striation-like structures are dominant at comparatively higher delay time and higher magnetic field which are related to electron-ion hybrid instability at higher magnetic fields. In brief the above study provides several addition features about the plume dynamics in uniform transverse magnetic field.

This work has been published in N. Behera et al., *Phys. Plasmas* **24** (3), 022511 (2017) [86] and N. Behera et. al., in *Frontiers in Optics / Laser Science*, OSA Technical Digest (Optical Society of America, 2018), paper JW3A.37 [87].

*Phys. Plasmas* **24** (3), 022511 (2017) [86] is listed in “**Top 20 Impactful articles in 2017**” and top in the section “**Highly Downloaded Articles in 2017**” in the Journal of “**Physics of Plasmas**”.



## Chapter 5

---

### **Study of diamagnetism using B-dot probe**

When laser-produced plasma expands in the presence of external magnetic field a diamagnetic current is produced on the surface of the plasma which produces a time-varying magnetic field opposite to the applied external magnetic field. The presence of diamagnetism in laser plasma can be verified by measuring this induced magnetic field. In this regard, we designed and constructed a three-axis, high-frequency magnetic probe. Attempt was made to ensure the designed probe should be capable to measure the time varying field of desired frequency range and its strength. The details of the design, construction, optimization, calibration and outcome of this study are thoroughly discussed in the following sections.



---

---

## 5.1 Introduction

The laser produced plasma in the presence of magnetic field is an important area due to its high application in many applied researches such as tokamak plasma, space plasmas viz., study of an artificial comet, propulsion of space vehicles using laser ablation, investigation of acceleration of stellar winds, and laboratory plasmas i.e., increase in the detection sensitivity of laser-induced breakdown spectroscopy [33, 39], manipulation of plasma plume in pulse laser deposition [40-42], debris mitigation [43] etc. A detail literature survey is given in section 1.8. Though many works have been done to understand plasma plume - magnetic field interaction, parametric study of the formation and evolution of diamagnetic cavity in laser-produced plasma has not been observed to the best of our knowledge.

When the laser-produced plasma expands in the presence of external magnetic field, it produces a diamagnetic current on the surface of the plasma plume and this diamagnetic current generates a magnetic field opposite to the applied magnetic field. So the applied magnetic field is displaced by this induced magnetic field [25]. It is necessary to measure this induced magnetic field to understand several physical phenomena involved in plasma plume-magnetic field interactions. B-dot probe is commonly used to measure the time-varying magnetic field. But major challenges involve in probe designing are probe should response to the desired frequency range, the size of the probe should be in the scale of the ion Larmor radius and it should sensitive to the desired magnetic fields range [68].

In the present investigation [71, 84-86], the external magnetic fields are 0 - 0.57 T, electron and ion temperature are  $\sim 2$  eV, electron density are  $10^{22}$ - $10^{23}$   $\text{m}^{-3}$  respectively and ion Larmor radius are 3.5-20 cm. In this case, the diamagnetic cavity exists in the range of 200-1000 ns. Hence, the designed probe should response to such a fast varying magnetic field and it must be calibrated for few MHz bandwidth.

Based on the above considerations, we have designed a high frequency, three axis B dot probe having dimensions 3.2 mm and its bandwidth up to 10 MHz. Different experimental approach have utilized for tedious calibration of designed probe at desired frequency range. The designed B-dot probe is placed at the expected diamagnetic cavity, which can measure the resultant magnetic field ( $\Delta B_{\text{plasma}}$ ).

## 5.2 Probe theory and calculation of magnetic field

The time-varying-magnetic field produced by the laser-produced plasma can be measured with a B-dot probe by using Faraday's Law in integrated form. The flux change in a loop of  $N$  turns and area  $a$  in a magnetic field  $\mathbf{B}$  perpendicular to the plane of the coil produces voltage  $V$  and is given by the relation  $V = - a N \frac{dB}{dt}$ . The time-varying magnetic field produced by the plasma can be calculated as  $B = - \frac{\int V dt}{aN}$ . The B-dot probe is highly sensitive to high frequencies [69]. The magnetic field can be estimated by integrating the B-dot probe voltage signal by using either an electronic integrator or numerical integrator. In this experiment, we want to record induced voltage signal for external applied magnetic field and the magnetic field produced by plasma simultaneously. While induced voltage signal for the external magnetic field is in kHz range, the magnetic field produced by plasma is in MHz range. But it is not possible to integrate both low frequency (kHz) and high frequency (MHz) signal simultaneously using electronics integrator. So the numerical integrator is the only option to achieve this desired objective.

## 5.3 Construction of probe

The Faraday's law is used to design the magnetic probe for detection of time varying magnetic field. The major challenges involve to design a probe to measure magnetic field during any phenomena are: the response of the probe should be faster than the time scale of occurrence of the desired phenomena, the size of the probe should be in

the scale of the ion Larmor radius and it should be sensitive to measure the desired magnetic fields etc. Based on the above considerations we have designed and fabricated the probe as follows.

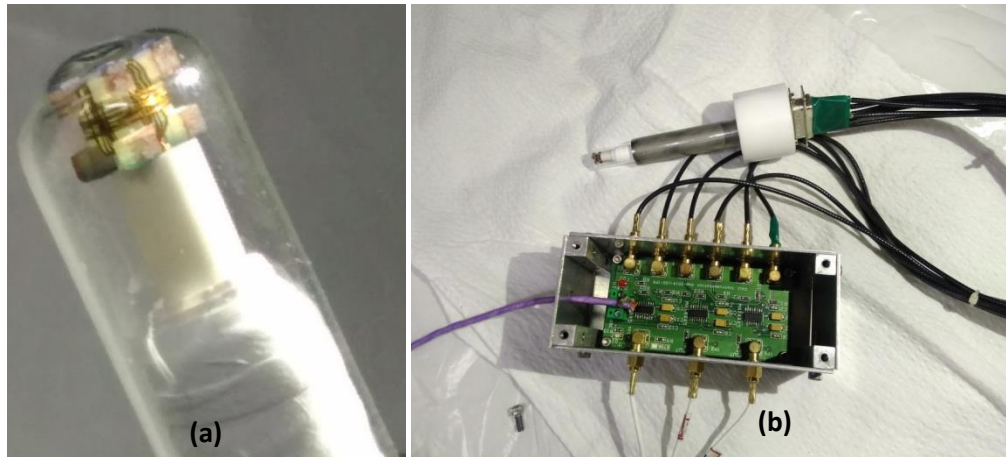


**Fig. 5.1.** (a) Probe tip in a glass test tube and (b) the probe is connected along with differential amplifier

The probe tip is a  $3.2 \times 3.2 \times 3.2$  mm cubical G10 material is used as a core for the probe as shown in Fig. 5.1 The G10 material is used due to its high thermal capacities, easy to machine and unity relative magnetic permeability at high frequencies. 5 turns of a twisted pair of Gauge 40 polyimide insulated copper wire wound around the core which creates a differential pair along the each axis. This differential pair helps to cancel the capacitive or electrostatic pickup and add or doubles the voltage induced by the changing magnetic flux. The probe shaft consists a long ceramic tube and the whole probe is kept inside a closed 11.50 mm outer diameter glass test tube to protect it from direct expose to charged particles. Wires of the loops are connected with  $50 \Omega$  coaxial cables through 15-pin connectors and coaxial cables are connected with a high frequency differential amplifier through SMA connectors. An ultra-high-speed (high frequency) differential amplifier (MAX4445, 550MHz-3dB Bandwidth) (Fig. 5.1b, Fig 5.2a) is designed to cancel the electrostatic/capacitive pickup developed in plasma and to amplify only the magnetic

component of voltage to give the final differential voltage. The output of differential amplifier is connected to 50  $\Omega$  coaxial cables with a termination impedance of 50  $\Omega$ .

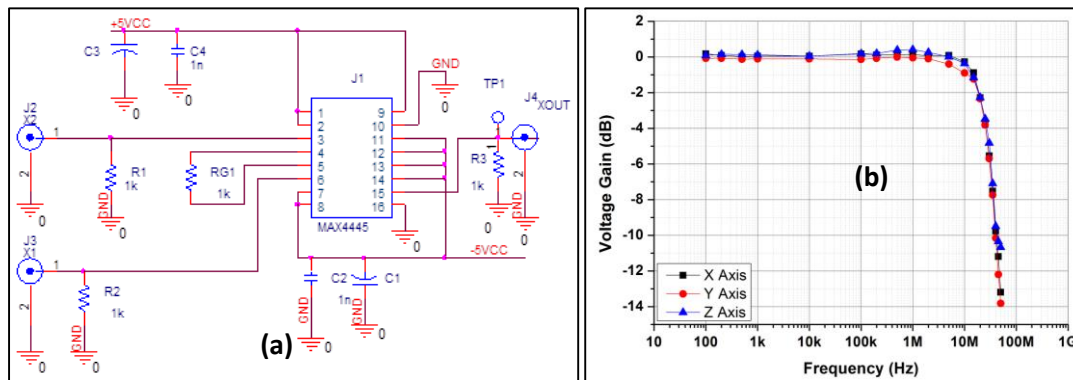


**Fig. 5.2** (a) Circuit schematics of a differential amplifier for one axis of the probe and (b) the voltage gain vs. frequency response of the amplifier.

## 5.4 Response of the probe

The response of probe should be faster than the time scale of occurrence of the desired phenomena. As we are studying the phenomena like demagnetization of laser-produced which occurs at 200-1000 ns, so designed probe should respond to minimum few MHz range. We have tested the response of the B-dot probe in the magnetic field produced by several different configurations like Helmholtz coil (from 500 Hz to 10 MHz) and circular inductor coil (at 1.27 MHz).

The response of the probe is tested by the scheme is shown in Fig. 5.3. The components required for this are: variable frequency generator (e.g. Dual channel arbitrary/function generator (AFG 3102, Tektronix, 100 MHz, 1 GS/s sampling rate), pulsed power supply), magnetic field generator (e.g. Helmholtz coil, circular inductor), designed magnetic probe and ultra-high-speed differential amplifier (MAX4445).

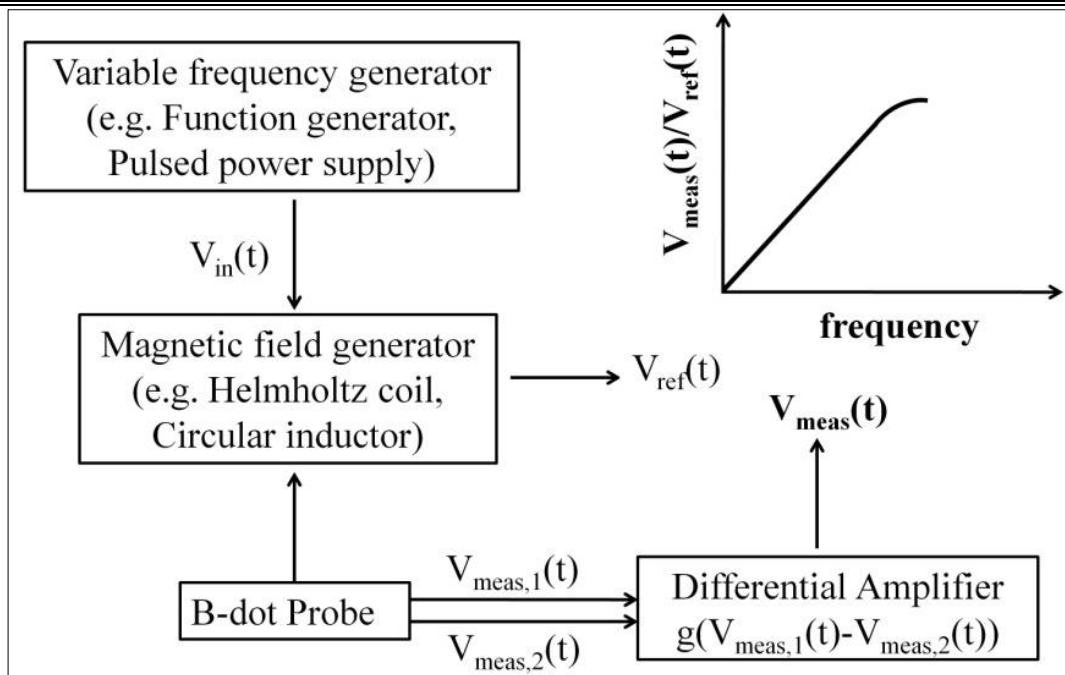


**Fig. 5.3.** Block diagram of experimental Setup to measure the frequency response and calibrate the B-dot Probe.

#### 5.4.1 Frequency response of the probe in Helmholtz coil

A Helmholtz coil configuration is used to check the response of the probe for frequencies 10 kHz-10 MHz. A Helmholtz coil consists of two identical circular magnetic coils of 20 turns each having radius of  $R_0 = 40$  mm that are placed symmetrically along a common axis and separated by a distance 40 mm from each other.

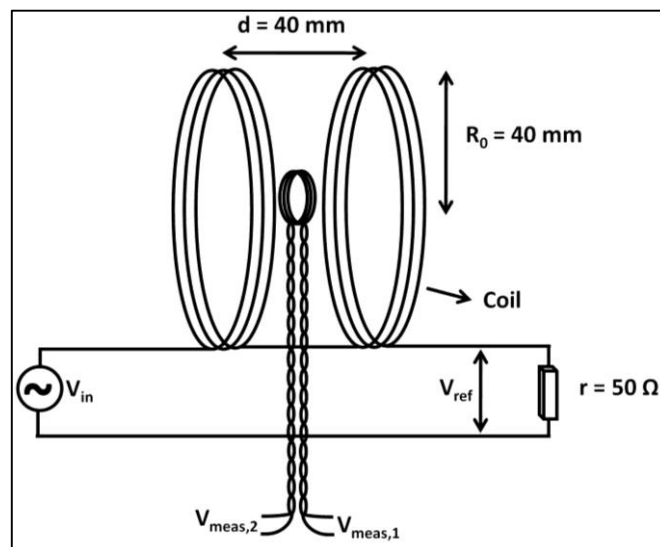


**Fig. 5.4.** Helmholtz coil arrangement for B-dot probe response check.

A time-varying voltage of frequencies 1 kHz-1 MHz and constant peak to peak amplitude  $V_{\text{ref}} = 1.50 \text{ V}$  is applied to the Helmholtz coil by a function generator. A resistor of  $r = 50 \Omega$  is connected in series with the coils. The magnetic field produced at the centre of the coil is  $B = \frac{8}{5\sqrt{5}} \frac{\mu_0 n I}{R_0}$ . In this case, the current can be found as voltage drop across the resistor divided by the  $50 \Omega$ . In this configuration of the Helmholtz coil, for 1 A current flow, the magnetic field produced by the coil at the centre is 4.5 G. The B-dot probe is kept at the centre of the Helmholtz coil. The output voltage  $V_{\text{meas,pp}}$  at different frequencies are measured using a Digital Phosphor Oscilloscope (DPO 3054, Tektronix, 500 MHz, 2.5 GS/s sampling rate) and are plotted for frequencies as shown in Fig. 5.5a. The linear variation of  $V_{\text{meas, p-p}}$  with frequencies shows the proper response of probe in 1 kHz-1 MHz. At higher frequencies the input voltage reduced significantly. So at 1 kHz-10 MHz, a time-varying voltage of constant peak to peak amplitude  $V_{\text{ref}} = 840 \text{ mV}$  is applied to the Helmholtz coil and  $V_{\text{meas,p-p}}$  is plotted with frequencies as shown in Fig. 5.5b. This is again showing a linear variation of  $V_{\text{meas,p-p}}$  with frequencies. From the above study we have confirmed that our probe is working perfectly in 500 Hz - 10 MHz.

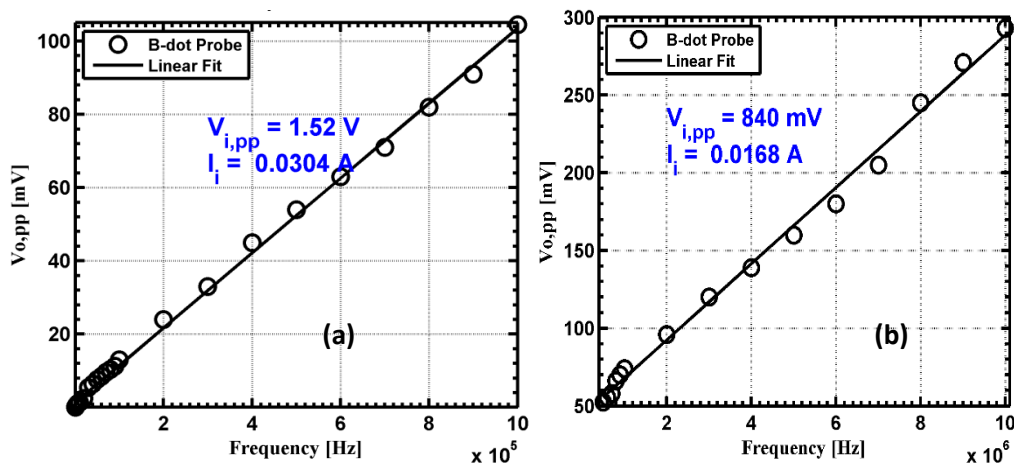


**Fig. 5.5.** The frequency response from (a) 500 Hz to 1 MHz and (b) 500 kHz to 10 MHz by the magnetic field produced by the Helmholtz coil.

The linearity of the probe is verified with varying the input voltage at fixed frequency. Fig. 5.6a and Fig. 5.6b represent  $V_{\text{meas,p-p}}$  for reference voltages  $V_{\text{ref}} = 1.1, 2.2, 3.25$  V at 500 kHz and 0.640, 1.23, 1.868 V at 1 MHz respectively and it is found to be linear.

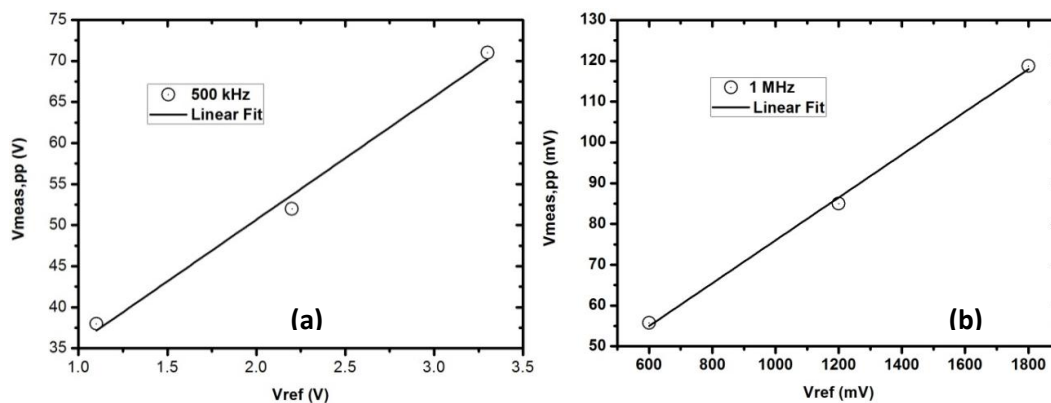


**Fig. 5.6.** Variation of  $V_{\text{meas,p-p}}$  with  $V_{\text{ref}}$  at (a) 500 kHz and (b) 1 MHz.

At higher frequencies the input current decreases, so it not a very good idea to calibrate the probe with low input current. So we have used a pulsed power supply instead of a function generator at 1.27 MHz. The frequency response of the probe is checked using a circular inductor magnetic field configuration.

### 5.4.2 Frequency response of probe in circular inductor

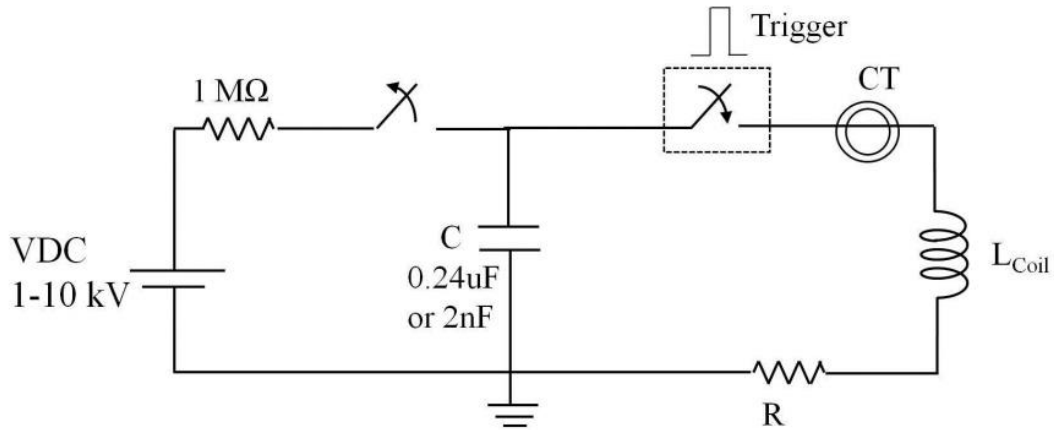
The probe is said to be responding perfectly at a given frequency if the estimated magnetic field (or the integrated voltage) and output voltage waveform of B-dot probe are in phase and  $90^\circ$  phase difference with input current (which produces the magnetic field) respectively. This basic principle is used to check the response of the probe at higher frequencies and at higher currents.

We have produced magnetic field of 2.62, 3.62, 4.65, 5.71 and 6.64 G at 1.27 MHz though a capacitor discharges circuit (Fig. 5.7). 2 nF capacitor is charged to 50, 75, 100, 125 and 150 V by a variable DC voltage source. A circular inductor of 10 turns (N) having diameter 0.8 mm wire wound in a circle of radius 22 mm ( $R_0$ ). The current in the circuit is measured using a CT (FCT-016-20:1, Bergoz instrumentations,

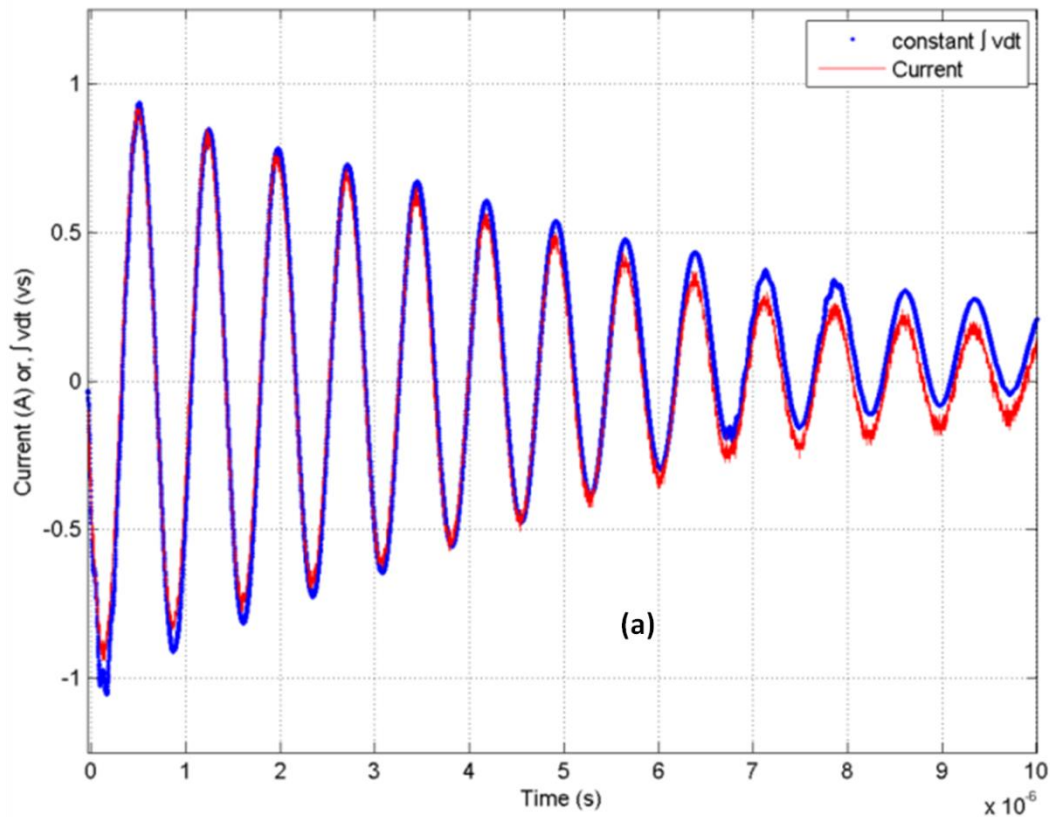
1.25V/A)) and are found to be 0.92, 1.27, 1.63, 2.0 and 2.32 A. The magnetic field at the centre of the circular inductor is given by

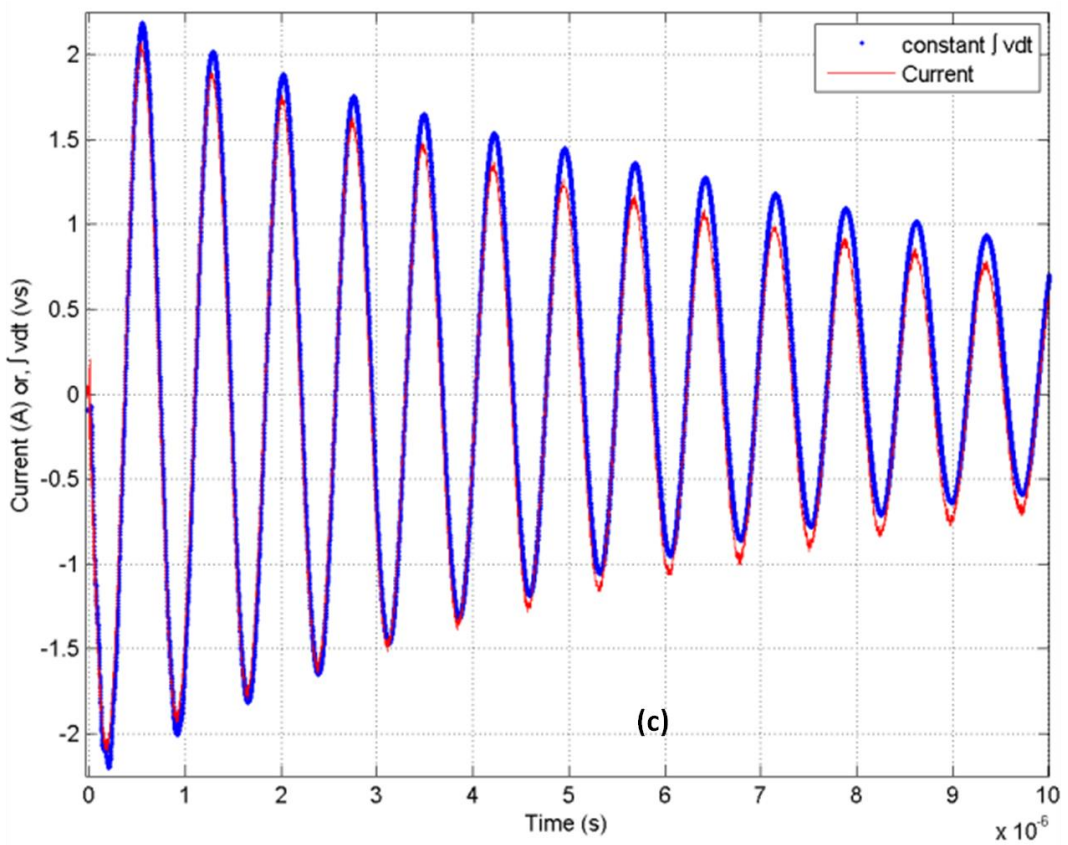
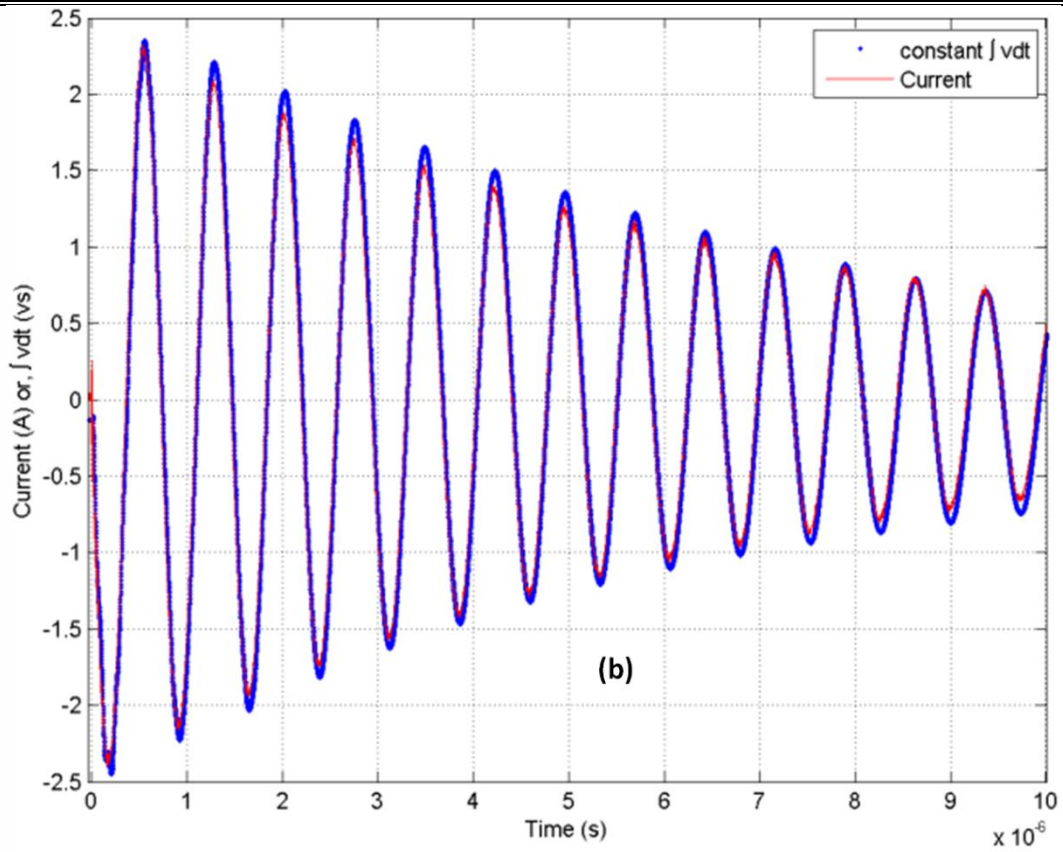
$$B (r = 0) = \frac{1}{2} \mu_0 NI \left( \frac{x-a_1}{\sqrt{(x-a_1)^2 + R^2}} - \frac{x-a_2}{\sqrt{(x-a_2)^2 + R^2}} \right) = \frac{\mu_0 NI}{2R_0} \quad (5.1)$$

The maximum magnetic field at the centre of the inductor are 2.62, 3.62, 4.65, 5.71 and 6.64 G.



**Fig. 5.7.** Schematic circuit diagram for generating magnetic field by capacitor discharge system at 1.27 MHz to test the response of B-dot probe and its calibration.





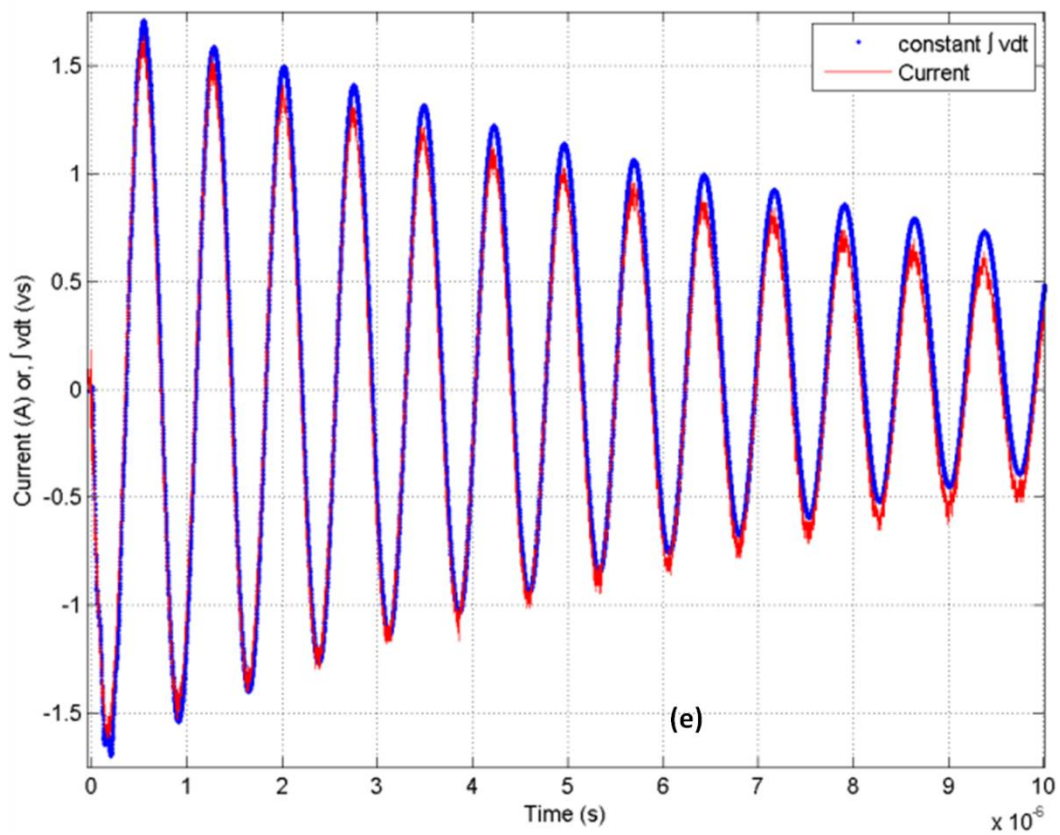
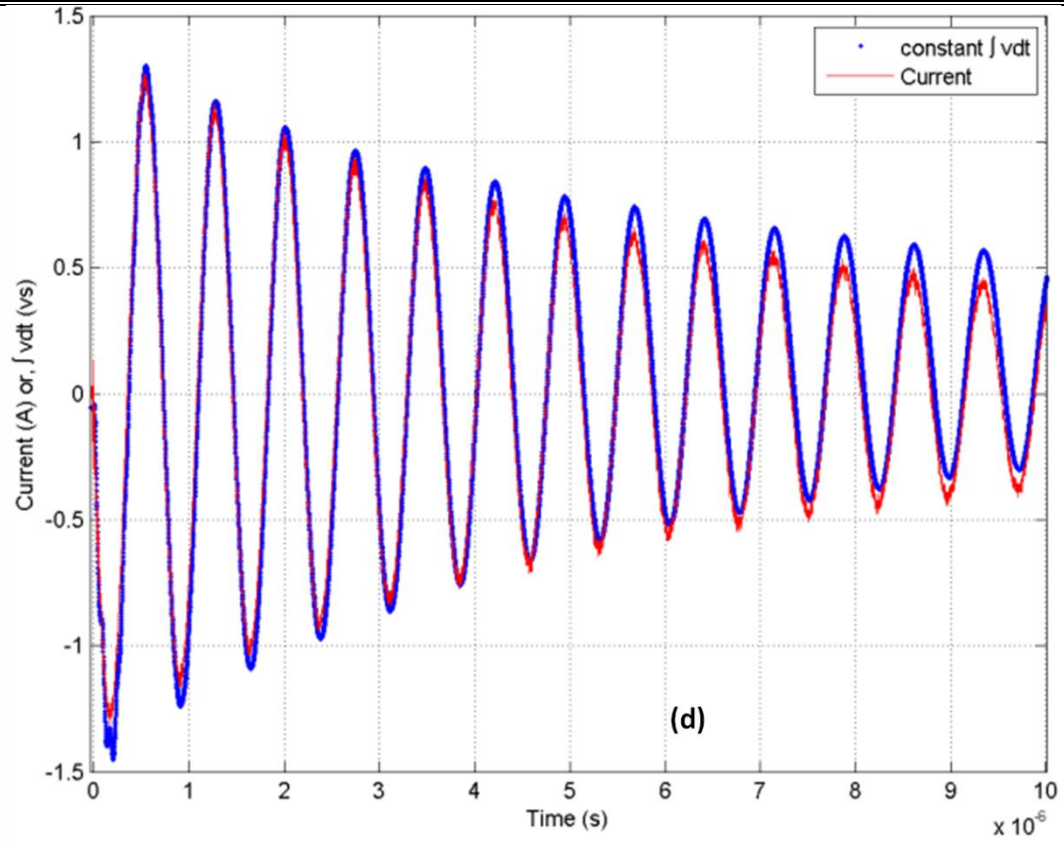


**Fig. 5.8.** The phase matching of current and  $\int V_{\text{meas}}(t) dt$  at (a) 0.92, (b) 1.27, (c) 1.63, (d) 2.0 and (e) 2.327 A at 1.25 MHz.

## 5.5 Calibration of the probe

To measure the unknown magnetic field produced by the plasma, the probe is calibrated with known test magnetic fields of strength 2.62, 3.62, 4.65, 5.71 and 6.64 G as described in Section. 5.4.1. The B-dot probe is used to measure the  $V_{\text{meas}}(t)$  at different applied magnetic field. The output  $V_{\text{meas}}(t)$  is integrated and the  $\int V_{\text{meas}}(t) dt$  is plotted with test magnetic field as shown in fig. 5.9.

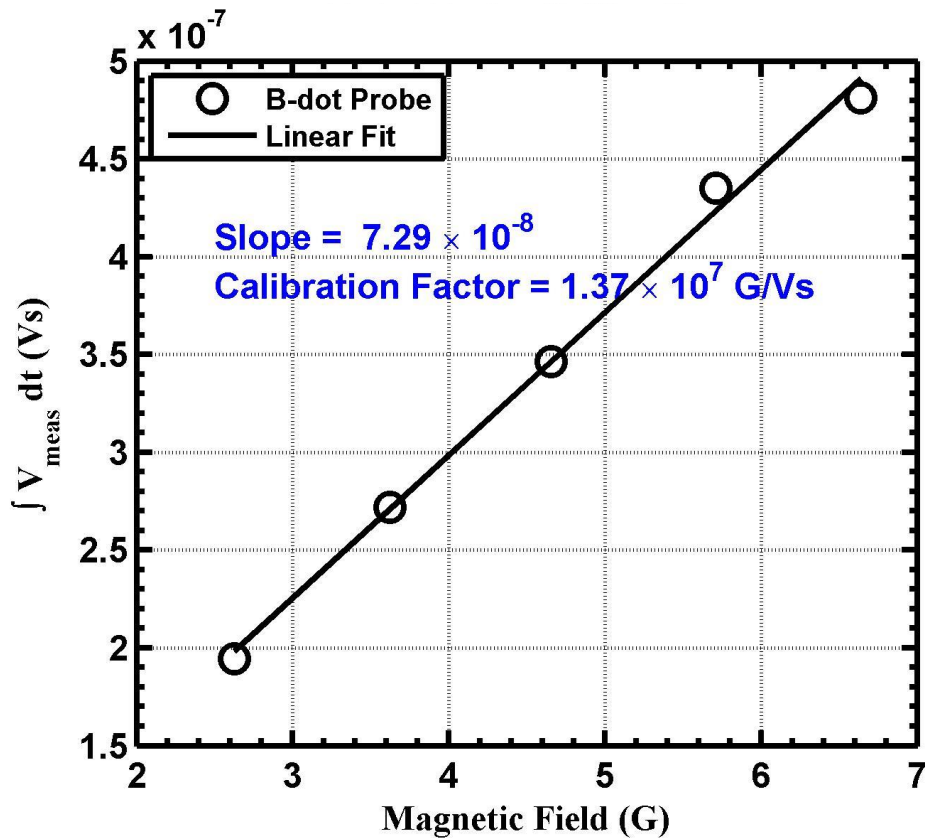


**Fig. 5.9.** Variation of  $\int V_{\text{meas}}(t) dt$  as a function applied magnetic field. Reciprocal of the slope give calibration factor of the B-dot probe.

The calibration factor which is the inverse of slope of the line is found to be  $1.37 \times 10^7$  G/Vs. In order to find the unknown magnetic field produced by the plasma, the output voltage of the B-dot probe is integrated and multiplied by the calibration factor.

---

---

## 5.6 Magnetic field measurement in expanding plasma plume

### 5.6.1 Theory of diamagnetic cavity

The diamagnetism in laser-produced plasma across transverse magnetic field depends on the plasma parameters and applied magnetic field strength. At early stage of the plasma, where the plasma pressure and kinetic pressure is much higher than the magnetic pressure, plasma expansion in this region is considered as expansion in diamagnetic limit. The diamagnetism of plasma plume could be understood as follows [24]. Charge particles in the plasma plume experience the Lorentz force in the presence of magnetic field and therefore gyrate in opposite direction with different radii depending on the charge, mass and velocity of the plume particles. Since the Larmor radius for ions is greater than the plume dimension, the ions can be considered as unmagnetized and therefore, expand radically outward. But the electrons tie to the magnetic field and try to hold the ions back and eventually produce radially inward electric field. The ions on the outer edge are slowed down by the produced radial electric field, but ions inside catch up and thus the plasma get compressed into a thin shell. This results the formation of diamagnetic cavity or magnetic bubble. As the electrons are magnetized,  $E \times B$  drift is created azimuthally relative to the ions which gives rise to a current. This current (known as diamagnetic current) generates a magnetic field opposite to the applied magnetic field. So the applied magnetic field is displaced by the induced magnetic field due to this diamagnetic current in the plasma. We have observed the diamagnetic cavity experimentally from the fast imaging of plasma plume in presence of external magnetic field as shown in Fig. 5.10. The theoretical study suggests that the magnetic field produced by plasma plume in presence of external magnetic field is diamagnetic in nature which means the induced magnetic field is produced in a direction opposite to applied external magnetic field and its magnitude is equal to applied magnetic field. The magnetic lines will expelled

by the plasma plume. To show the diamagnetism of plume, we have measured the induced magnetic field.

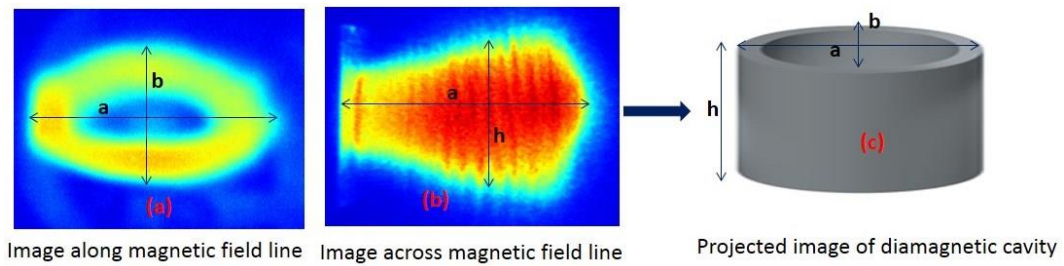


**Fig. 5.10.** ICCD camera image of expanding plasma plume at 0.13 T and 400 ns in a plane (a) perpendicular and (b) parallel to external magnetic field. (c) Schematic of diamagnetic cavity.

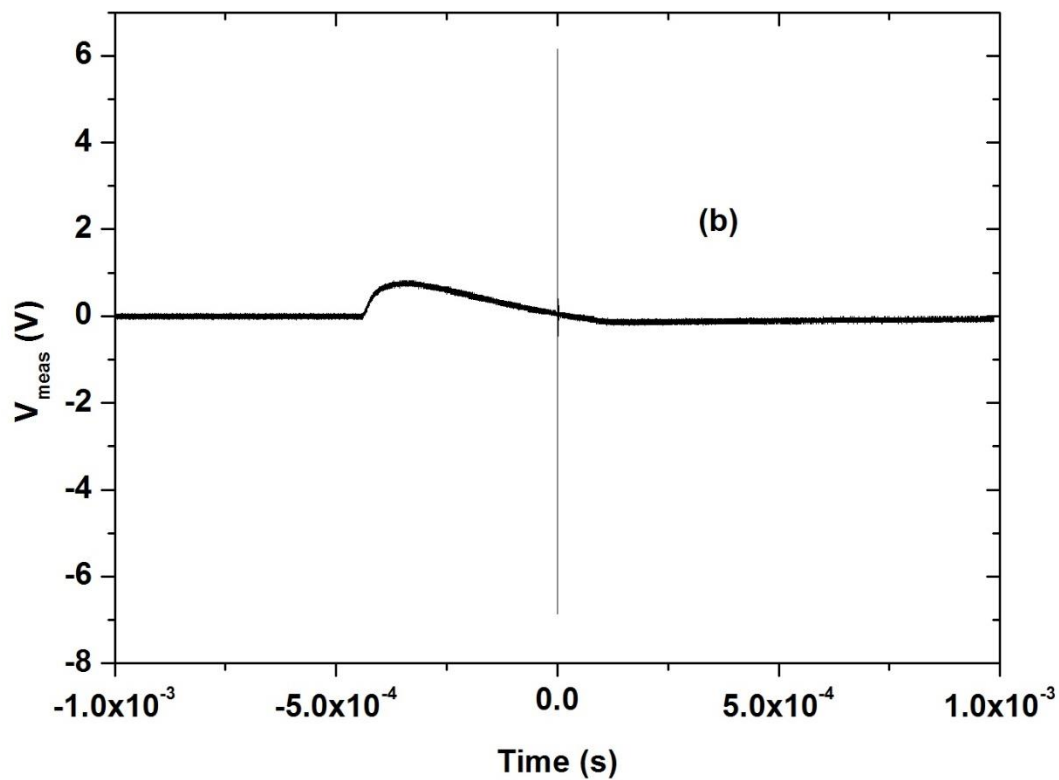
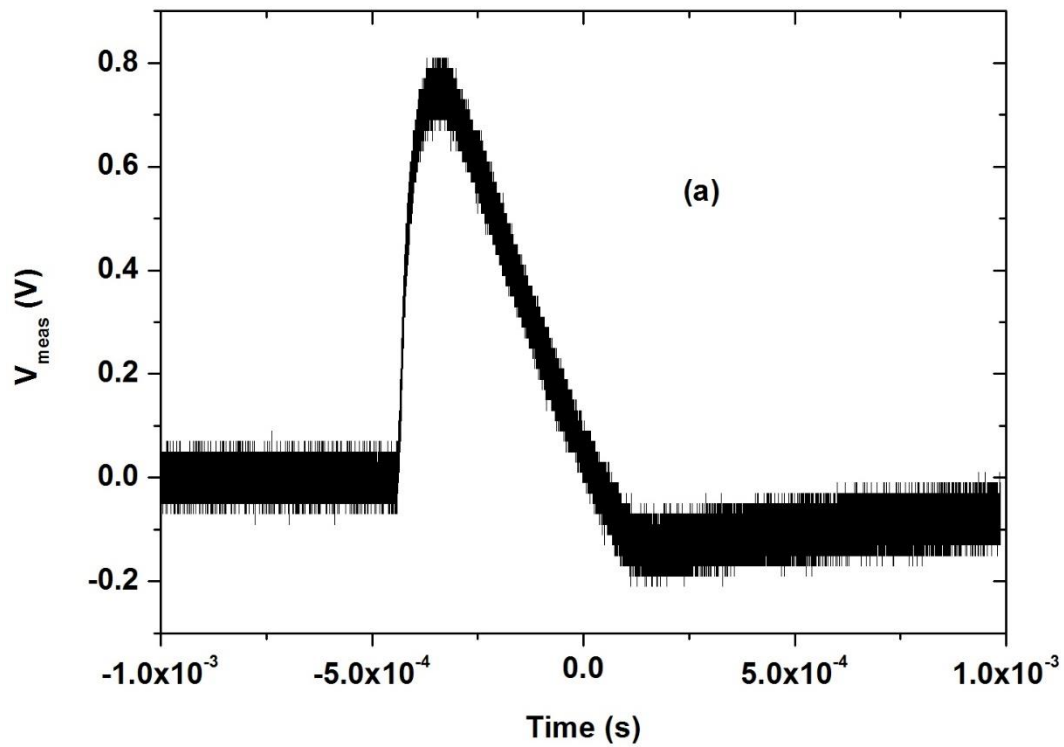
### 5.6.2 Experimental scheme

Detailed description of the experimental setup has been presented in chapter 4 [86]. Only a brief summary, which is important for the present study, is presented here. The plasma plume is created in vacuum chamber having a base pressure less than  $10^{-6}$  Torr using a 1064 nm, 8 ns pulsed Nd:YAG laser. The pulse energy and spot size of the laser beam are set to 150 mJ and 1 mm in diameter at the target, respectively, which can produce the laser fluence  $19.1 \text{ J/cm}^2$  at the target surface. 0.13-0.57 T transverse magnetic field is produced by a Helmholtz coil along with the indigenously developed pulse power supply. The designed B-dot probe is placed at the expected diamagnetic cavity, which can measure the resultant magnetic field ( $\Delta B_{\text{plasma}}$ ) in this region.

### 5.6.3 Results and analysis

Initially, we have applied 0.13 T external magnetic field and the induced voltage is shown in Fig. 5.11a. The laser fired on the aluminium target and plasma generated and the induced magnetic field profile of plasma plume recorded as shown in Fig. 5.11b. From the Fig. 5.11b, it is observed, an additional high frequency signal (Fig. 5.11c) ride over the previously existing magnetic field profile at the zero crossing (where the magnetic field is maximum and the flat top of magnetic field is present). This is the

expected high frequency induced magnetic field signal which is may be responsible for diamagnetism of the laser produced plasma.



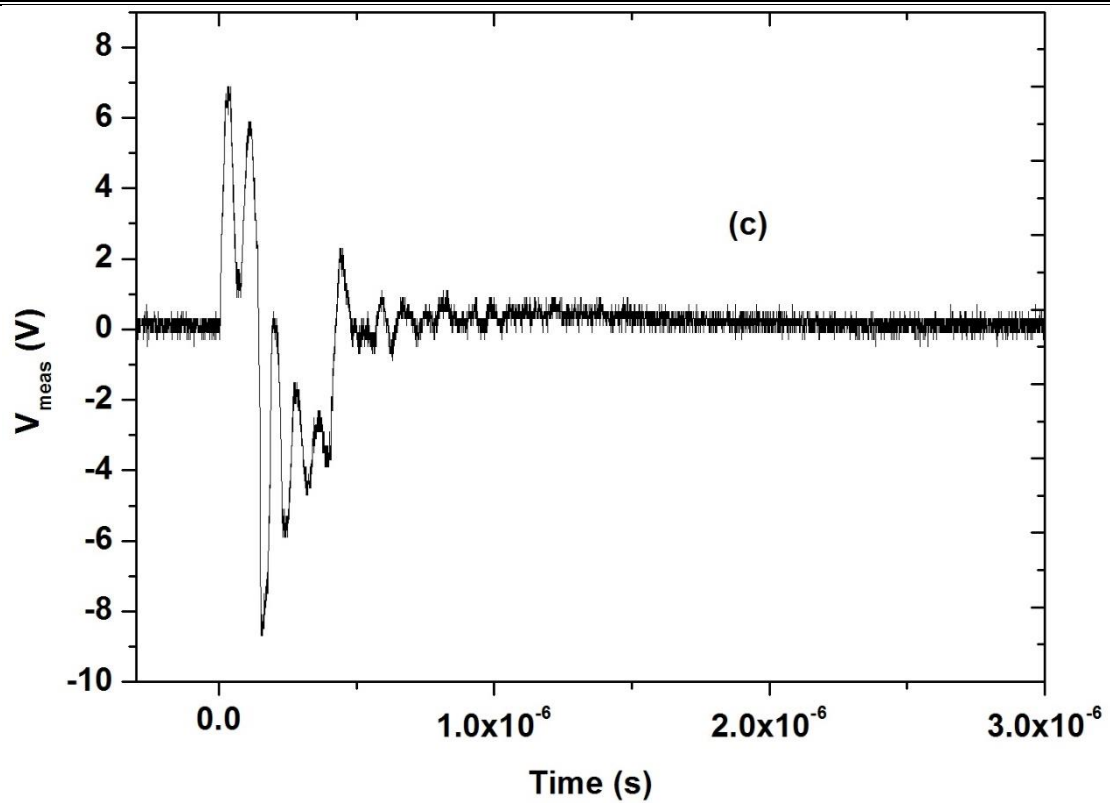


**Fig. 5.11.** Time profile of (a) 0.13 T external magnetic field, (b) induced magnetic field and (c) magnified portion of induced field.

Further, to verify the diamagnetism, the induced voltage profiles of plasma plume are recorded by varying applied magnetic field from 0.13 T to 0.57 T (Fig. 5.12a) and these voltage signals are integrated using the numerical integrator to obtain corresponding magnetic field profile. The high frequency magnetic field signals are shown in Fig. 5.12b.

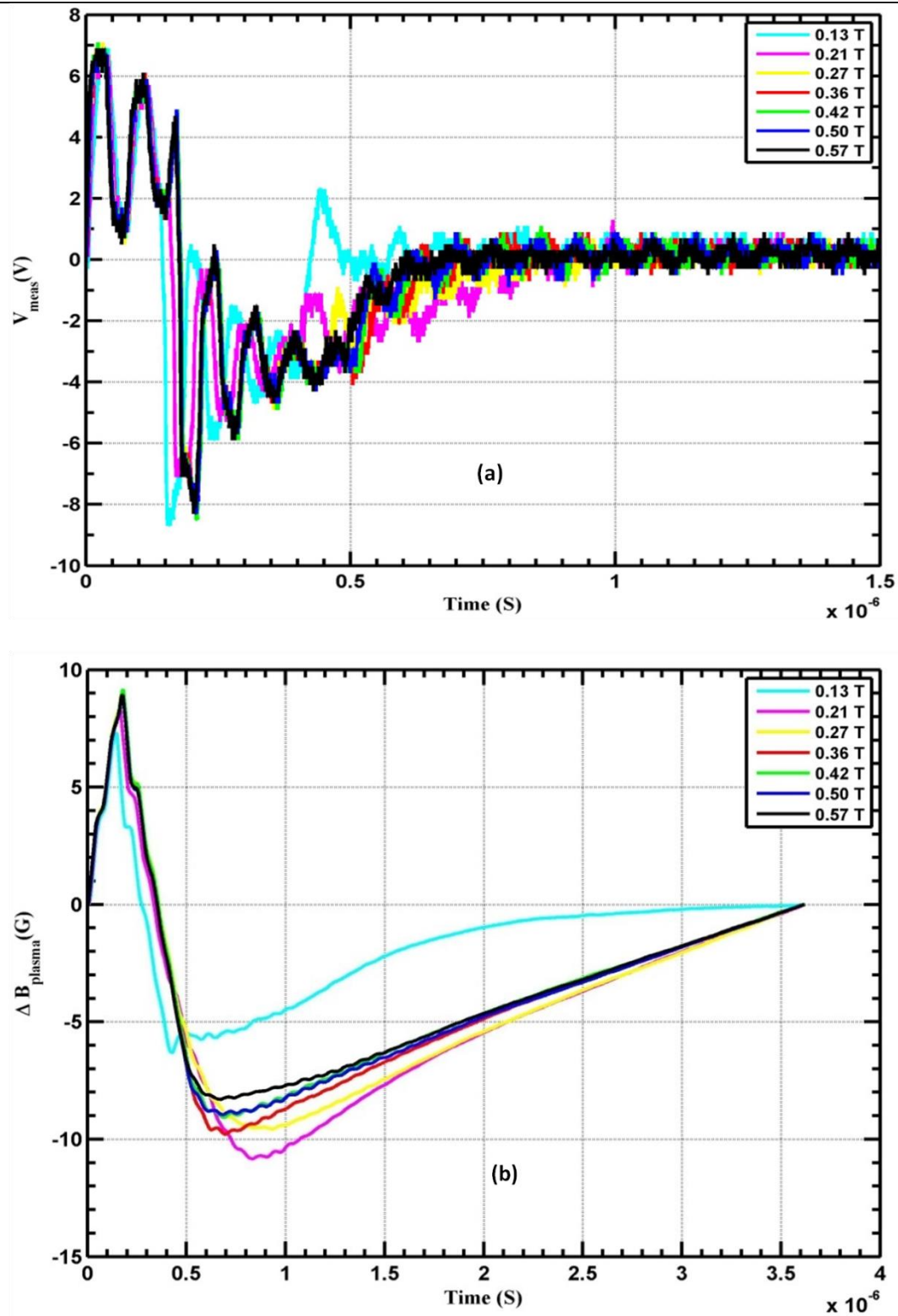


**Fig. 5.12.** Time profile of (a) induced voltage as measured by B-dot and (b) magnetic field obtained by integrating voltage signals in the applied magnetic field range 0.13-0.57 T.

From Fig. 5.12b, the variation of maximum induced magnetic field (diamagnetic field) with applied external magnetic fields is shown in Fig. 5.13. So the maximum induced magnetic field is in the range of 7-9 G (error  $\pm 5\%$ ) (i.e. 0.5-0.1 % of applied magnetic field) and these values can be considered as negligible with respect to applied magnetic field values. In conclusion, for any applied magnetic field, the plasma produces almost same amount of magnetic field in opposite direction and hence the net induced magnetic field measured by B-dot probe is negligible ( $\Delta B_{\text{plasma}} = 7-9\text{ G}$ ). Here, the direction of the gyration of charged particle of is always such that the magnetic field generated by plasma is always opposite to the externally applied magnetic field and hence, plasma tends to reduce the magnetic field, and it becomes diamagnetic. So in laser-produced plasma perfect diamagnetism is verified.

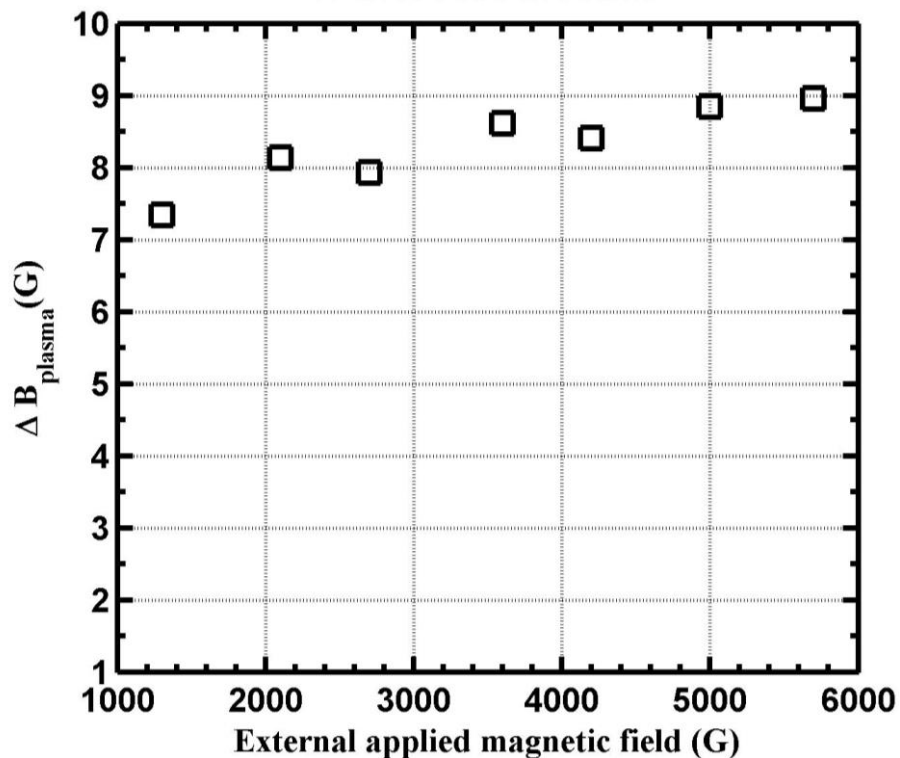


**Fig. 5.13.** The variation of induced magnetic field measured by B-dot probe with different applied external magnetic fields.

---

---

## 5.7 Summary and conclusion

A three-axis, high frequency B-dot is successfully designed, fabricated and calibrated. We have developed a new procedure to calibrate the B-dot probe. Response of the probe is obtained by using both Helmholtz coil and circular inductor. We have ensured that response of the probe up to 10 MHz for measurement of diamagnetism in the range of 200 to 1000 ns. Further, the high frequency probe is calibrated 1.27 MHz using a circular inductor of 22 mm radius, made by 10 turns of 0.8 mm thick copper wire. The designed B-dot probe is placed at the expected diamagnetic cavity (position is inferred from ICCD camera imaging diagnostics) which measured the resultant magnetic field ( $\Delta B_{\text{plasma}}$ ) in the region. The  $\Delta B_{\text{plasma}}$  is measured during expansion of plasma plume for applied magnetic field range of 0.13 - 0.57 T. The observed  $\Delta B_{\text{plasma}}$  is found to be in the range 7-9 G which indicates clearly the reversal of magnetic field direction to the applied magnetic field. For the first time with the designed B-dot probe, we could demonstrate occurrence of diamagnetism of plasma plume during its expansion in external magnetic field.

## Chapter 6

---

# Material dependent diamagnetic cavitation of laser-produced plasma

The diamagnetism is a fundamental entity of laser-produced plasma in the transverse magnetic field. The whole plasma dynamics is effectively controlled by its evolution and dismissal mechanism. In this chapter, we have studied the material dependence of diamagnetism in expanding laser plasma across transverse magnetic field using various atomic number targets starting from low to high values viz., carbon ( $Z = 6$ ), aluminium ( $Z = 13$ ), nickel ( $Z = 28$ ) and tungsten ( $Z = 74$ ). By comparing the plume images of different  $Z$ -materials in identical experimental condition, we have observed that plume geometrical shape, velocity, striation pattern and more importantly formation and shape of the diamagnetic cavity and its evolution are highly dependent on the target material (atomic number). Peculiar behaviour of carbon plasma that is Y-shaped bifurcation of plume in presence of magnetic field are observed, which is strikingly different in comparison to the result observed with other target material. We have also discussed the limitation of established theoretical model to explain the  $Z$ -dependence diamagnetism of laser plasma. We have highlighted some important observations which remain unexplained with existing theoretical model. In this context, we have suggested some important points which are necessary to modify, especially in the expression of bubble radius and magnetic diffusion time.



---

---

## 6.1 Introduction

The diamagnetic cavity always plays an important role on plasma dynamics. The interaction of plasma plume of different materials with external magnetic field is crucial in to understand processes like conversion of kinetic energy into plasma thermal energy, plume confinement, ion acceleration/deceleration, emission enhancement/decrease and plasma instabilities [31, 33-38]. A detail literature survey is given in section 1.8. Though many works have been done to understand plasma plume - magnetic field interaction, parametric study of the formation and evolution of diamagnetic cavity in laser-produced plasma has not been observed to the best of our knowledge.

The diamagnetism in laser-produced plasma across transverse magnetic field depends on the plasma parameters and applied magnetic field strength. At early stage of the plasma, where the plasma pressure and kinetic pressure is much higher than the magnetic pressure, plasma expansion in this region is considered as expansion in diamagnetic limit. The diamagnetism of plasma plume could be understood as follows [25]. Charge particles in the plasma plume experience the Lorentz force in the presence of magnetic field and therefore gyrate in opposite direction with different radii depending on the charge, mass and velocity of the plume particles. Since the Larmor radius for ions is greater than the plume dimension, the ions can be considered as unmagnetized and therefore, expand radically outward. But the electrons tie to the magnetic field and try to hold the ions back and eventually produce radially inward electric field. The ions on the outer edge are slowed down by the produced radial electric field, but ions inside catch up and thus the plasma get compressed into a thin shell. This results the formation of diamagnetic cavity or magnetic bubble. As the electrons are magnetized,  $E \times B$  drift is created azimuthally relative to the ions which gives rise to a current. This current (known as diamagnetic current) generates a

---

---

magnetic field opposite to the applied magnetic field. So the applied magnetic field is displaced by the induced magnetic field due to this diamagnetic current in the plasma and with this the plasma plume also experiences the decelerating force. This diamagnetic cavity exists up to the magnetic diffusion time and then its collapse starts. The material dependence of diamagnetism, which is an interesting problem, is largely ignored in the reported work. Therefore, it needs crucial studies for its z-dependence investigation.

In view of above, we have studied the dynamics and structural behaviour of plasma plume generated by different atomic number ( $Z$ ) targets in the presence of transverse magnetic field. Carbon ( $Z = 6$ ), aluminium ( $Z = 13$ ), nickel ( $Z = 28$ ) and tungsten ( $Z = 74$ ) are considered for this study. By comparing the plume images of different  $Z$ -materials in identical experimental conditions, we have studied  $Z$ -dependence of plume geometrical shape, velocity, striation pattern and more importantly formation and shape of the diamagnetic cavity and its evolution. We have also thoroughly analysed the expression of bubble radius and magnetic diffusion time to explain the observed diamagnetism in laser-produced plasma.

## **6.2 Experimental scheme**

Detailed description of the experimental setup has been described in the Chapter 4 [86]. Only a brief summary, which are important for this Chapter are presented here. The plasma plumes of different target materials are created in vacuum chamber having a base pressure less than  $10^{-6}$  Torr using a 1064 nm, 8 ns pulsed Nd:YAG laser. The pulse energy and spot size of the laser beam are set to 150 mJ and 1 mm in diameter at the target, respectively, which can produce the laser fluence  $19.1 \text{ J/cm}^2$  at the target surface. Transverse magnetic field in the range 0.13-0.57 T is produced by a Helmholtz coil along with the indigenously developed pulse power supply. The targets like carbon, aluminium, nickel and tungsten are mounted on a movable target

---

holder through a vacuum compatible feed-through and placed in between the Helmholtz coil. Time-resolved images of visible expanding plasma plume are recorded using two internally synchronized ICCD cameras (4 Picos, Stanford Computer Optics). The details of camera specification and synchronization mechanism are given in Chapter 1 and 4 respectively.

## **6.3 Results and discussion**

To understand the processes like thermalization, diamagnetism, confinement,  $E \times B$  drift etc. during the plume expansion in magnetic field, time-resolved fast imaging of visible expanding plume is carried out using two internally synchronized ICCD cameras. As our major focus is on the material dependence of diamagnetism in plasma, so we have used various atomic number targets starting from low to high like carbon ( $Z = 6$ ), aluminium ( $Z = 13$ ), nickel ( $Z = 28$ ) and tungsten ( $Z = 74$ ) to generate plasma and their temporal evolution of plume are studied by capturing images of visible expanding plasma plume.

### **6.3.1 Time-resolved fast imaging of tungsten plasma**

The sequence of images of the tungsten plasma plume along and across the magnetic field lines (denoted as X-imaging and Y-imaging respectively) are captured in the absence of magnetic field as shown in Fig 6.1. These images are recorded at different time delays, varying from 50 ns to 2000 ns. Each image represents the spectrally integrated emission intensity in the range 350-750 nm, emitted from plume species. In the absence of magnetic field, plume expansion is mainly governed by the initial pressure gradient inside the plume, and is treated as adiabatic expansion [5]. Due to large pressure gradient in axial direction, plume has an early ellipsoidal shape. Ellipsoidal shape of plume is confirmed by two projection of images where both X-imaging and Y-imaging data are nearly identical. The expansion velocity of tungsten plasma plume is  $\sim 1.86 \times 10^4$  m/s. With time, emission intensity was reduced

considerably and at  $t > 2000$  ns, emission intensity is beyond the detection limit of the ICCD. This is because electron temperature and density reduces rapidly with time and hence the probability of excitation of plume species is also reduced.

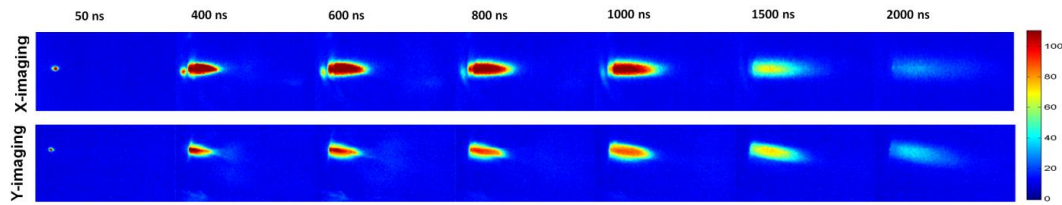


**Fig. 6.1.** The sequence of images of the expanding tungsten plasma plume without magnetic field at different delay times.

By introduction of external magnetic field brings a significant change of expanding tungsten plasma plume dynamics which is clearly visible in Fig. 6.2 and 6.3. Fig. 6.2 and Fig. 6.3 show the sequence of images of the expanding tungsten plasma plume at different delay times, varying from 300 ns to 3000 ns at two different magnetic field, 0.13 T and 0.50 T respectively. Significant enhancement of emission intensity and emissive lifetime of expanding tungsten plasma plume has been observed in comparison to the field-free case.

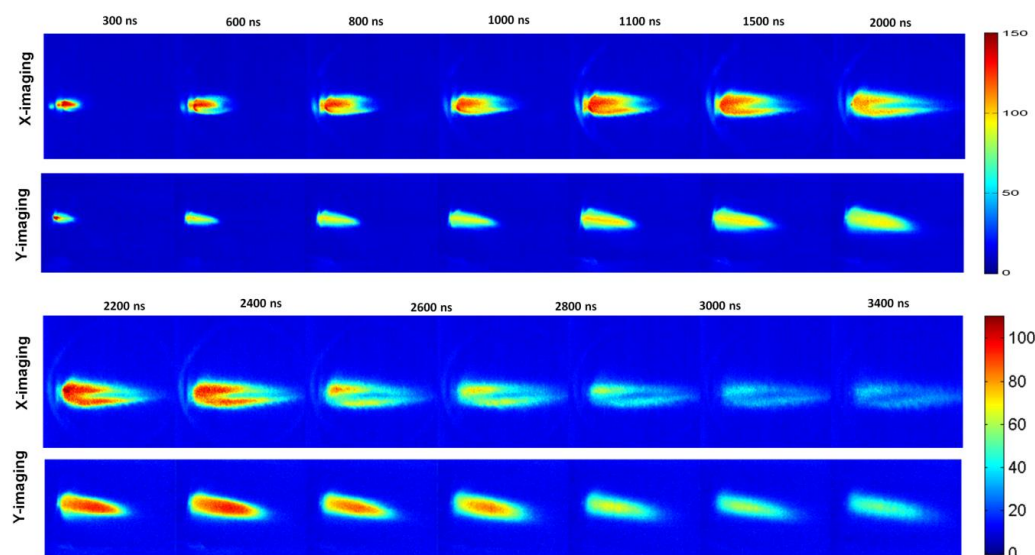


**Fig. 6.2.** The sequence of images of the expanding tungsten plasma plume at 0.13 T transverse magnetic field at different delay times.

A well-defined elliptical cavity (diamagnetic cavity) is observed in the images of expanding plasma plume in a plane perpendicular to the external magnetic field (X-imaging) at the comparatively low magnetic field (0.13 T) as shown in Fig. 6.2. Here the cavity sustains for a longer period of time i.e. up to 3000 ns.

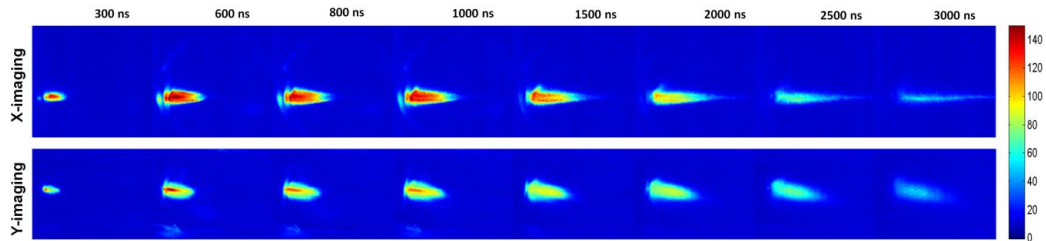


**Fig. 6.3.** The sequence of images of the expanding tungsten plasma plume at 0.50 T transverse magnetic field at different delay times.

In case of higher magnetic field (0.50 T), the ellipticity of cavity structure is increases in comparison to low magnetic field and. In this case cavity like structure is collapse at  $\sim 2000$  ns and form a well-defined line-structure with further increase of time delay  $> 2500$  ns as shown in X-imaging of Fig. 6.3. On the other hand, the striation-like structure is found in the images in a plane parallel to the applied magnetic field (Y-imaging of Fig. 6.2 & 6.3). Due to compression, the striation-like structures overlap on each other and not as clear in the case of aluminium plasma (see, Chapter 4). The possible physics of diamagnetic cavity and magnetic striation-like structure is already discussed in Chapter 4.

### 6.3.2 Time-resolved fast imaging of nickel plasma

Again, the sequence of images of the nickel plasma plume along and across the magnetic field lines are captured in the absence of magnetic field as shown in Fig 6.4. These images are recorded at different time delays, varying from 50 ns to 1500 ns. In the absence of magnetic field, plume expansion is mainly governed by the initial pressure gradient inside the plume and is treated as adiabatic expansion [5]. Due to large pressure gradient in the axial direction, the plume has an early ellipsoidal shape. Ellipsoidal shape of the plume is confirmed by two projection of images where

both X-imaging and Y-imaging data are nearly identical. The expansion velocity of nickel plasma plume is  $\sim 5.6 \times 10^4$  m/s. With time, emission intensity was reduced considerably and at  $t > 1500$  ns, the emission intensity is beyond the detection limit of the ICCD.

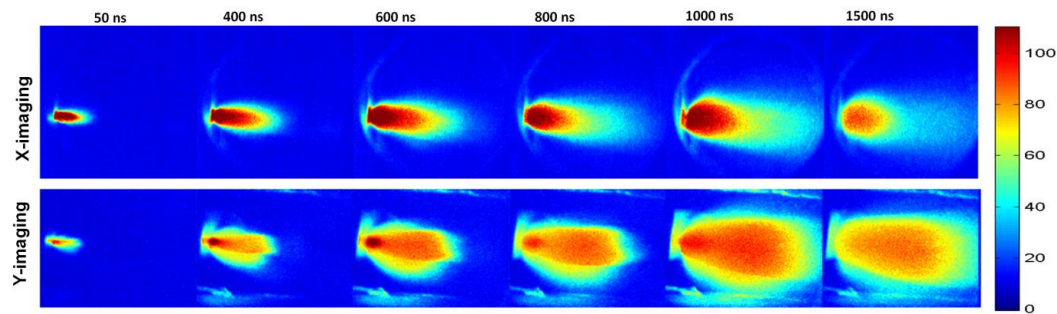


**Fig. 6.4.** The sequence of images of the expanding nickel plasma plume without magnetic field at different delay times.

The effect of external magnetic field causes a significant change of expanding nickel plasma plume dynamics which is very clear from Fig. 6.5 and 6.6. Fig. 6.5 and Fig. 6.6 show the sequence of images of the expanding nickel plasma plume at different delay times, varying from 200 ns to 2000 ns at 0.13 T and 0.50 T applied magnetic field respectively.

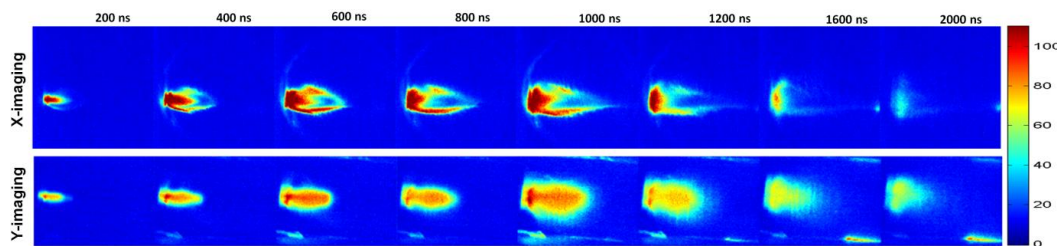


**Fig. 6.5.** The sequence of images of the expanding nickel plasma plume at 0.13 T transverse magnetic field at different delay times.

Again, a well-defined elliptical cavity (diamagnetic cavity) is observed in the images of expanding plasma plume in X-imaging at 0.13 T applied magnetic field as shown in Fig. 6.5. Here the cavity sustains for up to  $\sim 1000$  ns and then starts to collapse.

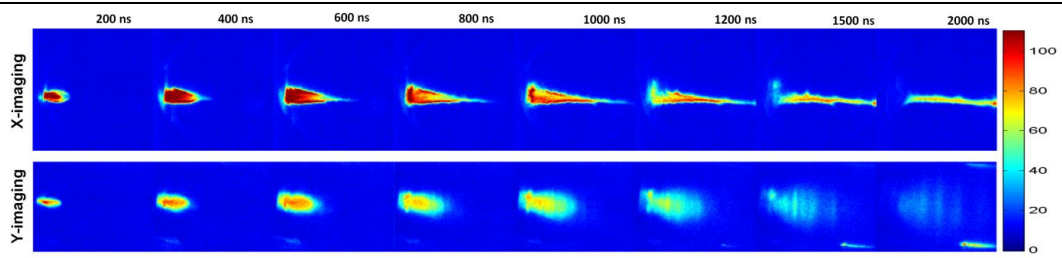


**Fig. 6.6.** The sequence of images of the expanding nickel plasma plume at 0.50 T transverse magnetic field at different delay times.

But in case of 0.50 T, the cavity starts to collapse from  $\sim 600$  ns and form a cone-like structure and subsequently form line-structure as shown in X-imaging of Fig. 6.6. On the other hand, striation-like structures are found in Y-imaging of Fig. 6.6 at later period of expansion. From 1500 ns the striation-like structures are clearly visible. The possible physics of diamagnetic cavity and magnetic striation-like structure is given in Chapter 4.

### 6.3.3 Time-resolved fast imaging of aluminium plasma

The effect of applied magnetic field on the plasma dynamics is discussed in detailed in Chapter 4. In brief, the expanding aluminium plume takes an ellipsoidal shape during its expansion in the absence of external magnetic field. The expansion velocity of aluminium plasma plume is  $\sim 8.4 \times 10^4$  m/s. Again, the existence of diamagnetic cavity is observed at lower magnetic field and lower delay time; whereas striation-like structures are observed at comparatively higher magnetic field and higher delay time.

### 6.3.4 Time-resolved fast imaging of carbon plasma

In order to see the effect of magnetic field on low-Z carbon plasma, the sequence of images of the carbon plasma plume for both the projection (that is X-imaging and Y-Imaging) are captured in the absence of magnetic field are shown in Fig 6.7. These images are recorded at different time delays, varying from 200 ns to 1600 ns. As in the case of above, in the absence of magnetic field, plume expansion is

mainly governed by the initial pressure gradient inside the plume, and is treated as adiabatic expansion [5]. In this case also plume has an ellipsoidal shape which is confirmed by two projection of images where both X-imaging and Y-imaging data are nearly identical. The expansion velocity of carbon plasma plume is  $\sim 1.4 \times 10^4$  m/s. With time, emission intensity was reduced considerably and at  $t > 1600$  ns, emission intensity is beyond the detection limit of the ICCD.

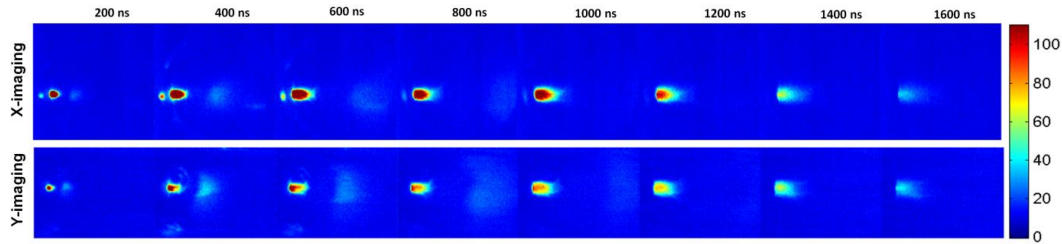


**Fig. 6.7.** The sequence of images of the expanding carbon plasma plume without magnetic field at different delay times.

Surprisingly in case of carbon we have not observed the important earlier expansion dynamics entities like diamagnetic cavity and magnetic striation-like structures by applying the external magnetic field. A well-defined almost symmetrical Y-shaped bifurcation of plasma plume in a plane perpendicular to the magnetic field (X-imaging) is observed in as shown in Fig. 6.8. In contrast to the other material, striation like structure along the magnetic field lines is not observed in case of carbon rather the plume splitting along the expansion axis are clearly visible in Y-imaging of Fig. 6.8 at 0.13 T external transverse magnetic field.

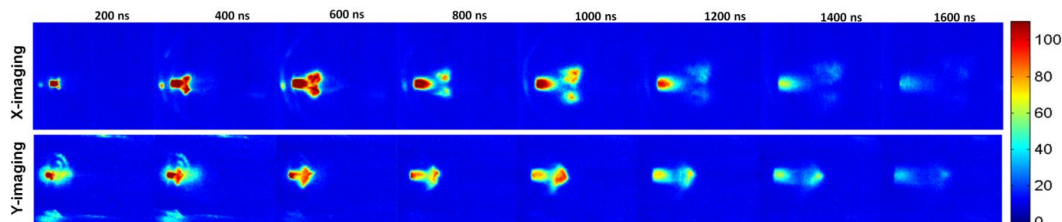


**Fig. 6.8.** The sequence of images of the expanding carbon plasma plume at 0.13 T transverse magnetic field at different delay times.

Interestingly, increase of the magnetic field strength up to 0.50 T doesn't bring remarkable changes in the observed plume structure like the earlier cases. Only the little increase of emission intensity and a change of angle of bending of plume front (tip of Y-shaped bifurcation) are observed (X-imaging of Fig. 6.9) with increase of magnetic field.

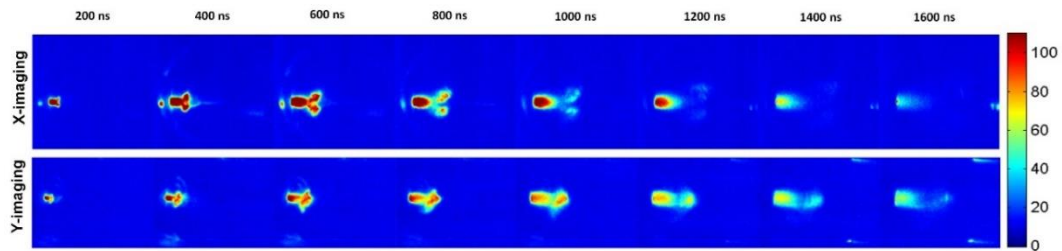


**Fig. 6.9.** The sequence of images of the expanding carbon plasma plume at 0.50 T transverse magnetic field at different delay times.

For the best of our knowledge, Y-shaped bifurcation in carbon plasma in presence of transverse magnetic field is not reported till now. There is no theoretical study and simulation work available to explain observed dynamics and geometrical shape of the carbon plasma. The possible mechanism can be as follows. The splitting of plume into a neutral dominant (toward the target) and charge species dominant (plume front) part is observed [88] (Y-imaging of Fig. 6.8). As the charge species dominate part (plume front) in the influence of external magnetic field will be polarized into electron dominant and ionic dominant part forming a Y-shape bifurcation as observed in X-imaging of Fig. 6.8. The increase the magnetic field affect the strength of polarization which may reflected in observe change in bending of the Y-shaped plume with increase of magnetic field (X-imaging of Fig. 6.9). At this stage, more convincing explanation of the observation is still missing and detailed investigation in this regard is in progress.

### 6.3.5 Comparative study of plasma plumes

Our major focus is to study the material dependence plume features like plume geometrical shape, velocity, striation pattern and more importantly formation and shape of the diamagnetic cavity and its evolution. For the comparative study, the X-imaging and Y-imaging of the expanding carbon, aluminium, nickel and tungsten plasma at 400 ns and 1200 ns delay time in presence of 0.13 T and 0.50 T magnetic field are shown in Fig. 6.10 and Fig. 6.11 respectively.

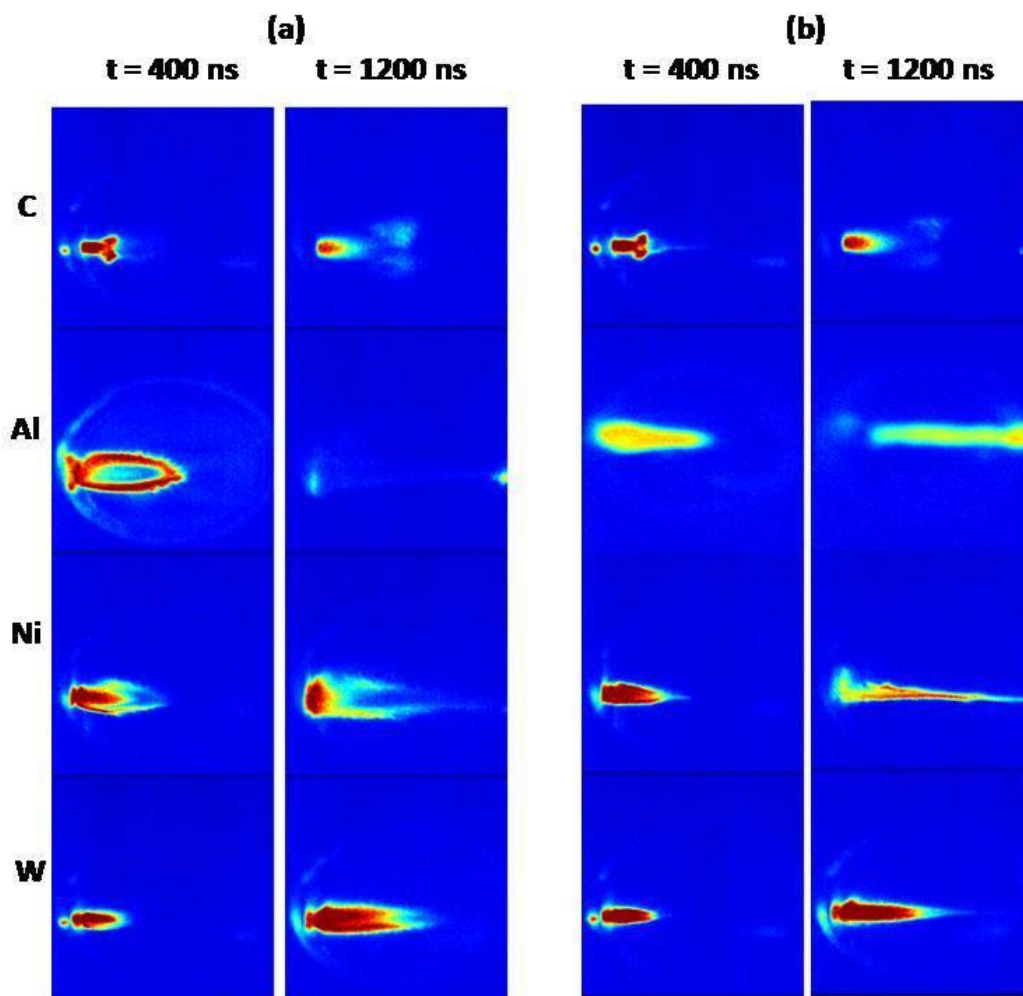


**Fig. 6.10.** The X-imaging of expanding carbon, aluminium, nickel and tungsten plasma at 400 ns and 1200 ns delay time in presence of (a) 0.13 T and (b) 0.50 T transverse magnetic field.

The expansion velocity of expanding carbon, aluminium, nickel and tungsten plasma plume in the absence of external magnetic field are  $1.4 \times 10^4$ ,  $8.4 \times 10^4$ ,  $5.6$

$\times 10^4$  and  $1.86 \times 10^4$  m/s respectively. Except for carbon, the expanding plume velocity decreases with the increase of Z-number and atomic mass. So the all metallic target shows the expected trends in their expansion velocities. The cavity exists for a longer time, but its width is smaller for high Z-materials (e.g. tungsten) as compared to low Z-materials (e.g. aluminium) at the low magnetic field (Fig. 6.10). Again, the numbers of magnetic striation are more but their separations are smaller in high Z-materials as compare to low Z-materials (e.g. aluminium) at the high magnetic field (Fig. 6.11).

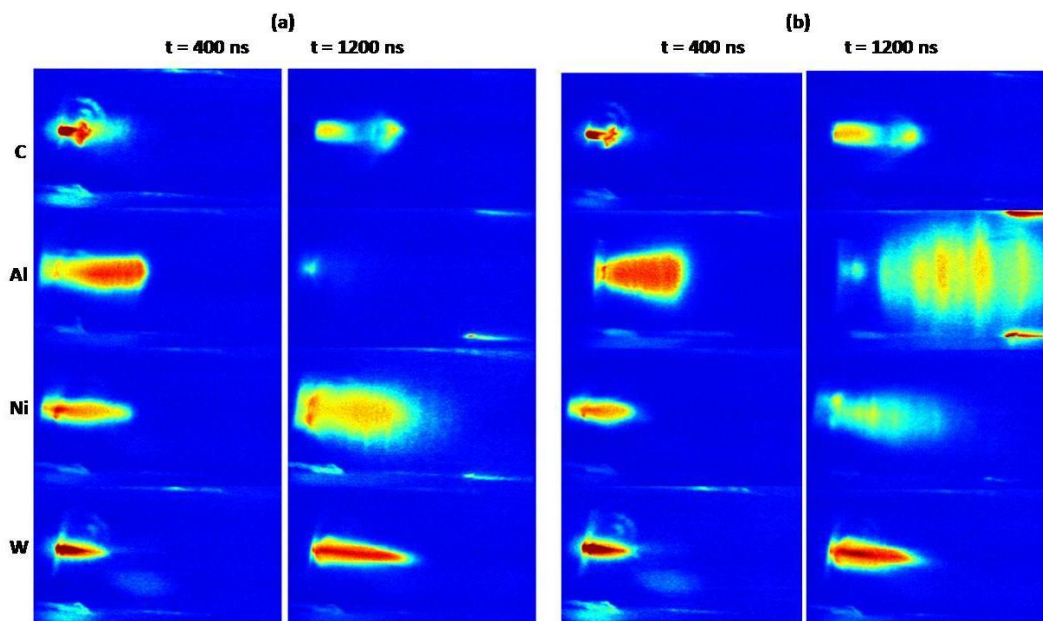


**Fig. 6.11.** The Y-imaging of expanding carbon, aluminium, nickel and tungsten plasma at 400 ns and 1200 ns delay time in presence of (a) 0.13 T and (b) 0.50 T transverse magnetic field.

In this Chapter, our major focus is on the material dependence of diamagnetism in laser-produced plasma. From the above experimental observation, we have found that diamagnetism of laser plasma depends on the nature target material used for plasma formation. From the earlier study, the expansion of laser plasma plume in the magnetic field can be summarized as the plume expands slowly due to magnetic field confinement up to magnetic field diffusion time and then accelerate due to  $E \times B$  drift [71]. Therefore the magnetic field diffusion i.e. the time

after which the diamagnetic cavity starts to collapse is the key predicting parameter for plume dynamics in the magnetic field. Here we have observed that magnetic field diffusion time ( $t_d$ ) is a material dependent. The effect of the material dependence of  $t_d$  can be understood as follows.

The expression of confinement radius (bubble radius) [29, 30] and classical magnetic field diffusion time [28] are,

$$R_b = \left( \frac{3\mu_0 E_{lpp}}{\pi B^2} \right)^{1/3} \quad (6.1)$$

$$t_d = \mu_0 \sigma R_b^2 \quad (6.2)$$

where  $R_b$  is the confinement radius (bubble radius),  $\mu_0$  is the magnetic permeability in free space,  $E_{lpp}$  is the kinetic energy of laser-produced plasma,  $B$  is the applied magnetic field,  $\sigma$  ( $= 1/\eta$ ) is the plasma conductivity and  $\eta$  ( $= 5.2 \times 10^{-5} Z \ln\Lambda T_{ev}^{-3/2}$ ) is the plasma resistivity. So the confinement radius depends on the kinetic energy of laser plasma and the applied magnetic field and the plasma conductivity depending on the electron temperature. Hence, basically magnetic field diffusion time depends on three parameters namely kinetic energy of laser plasma, applied magnetic field and the electron temperature. Here it should be noted that electron temperature is weakly dependent on the metallic target-to-target ( $\sim 1.5-2$  eV) [28, 86] for laser-produced plasma. Therefore, for a fixed magnetic field and laser energy (with the general approximation that 50% of laser energy is utilized for plasma formation), classical cavity radius and magnetic diffusion time are independent of target materials, which contradict the present experimental observation. So, detailed theoretical modeling and supporting simulation are required to explain the present observations as these observed results couldn't explain with the help of the present theory.

Few important points can be highlighted here which will be useful to modify the expression for bubble radius and magnetic diffusion time. As the bubble radius is

---

derived using the energy equation, so the energy equation can be modified by considering the plasma motion and consequently, the magnetic diffusion time can be modified and the expression of the modified energy equation is,

$$\left(\frac{4\pi}{3}R_b^2\right)\left(\frac{B^2}{2\mu_0} + \frac{mnv^2}{2}\right) = E_{lpp} \quad (6.3)$$

Again, we need to find the aspect ratio (from the asymmetric structure of plasma plume) to calculate the exact  $t_d$  for different materials.

## 6.4 Summary and conclusion

In summary, the plume features such as plume geometrical shape, velocity, striation pattern and more importantly formation and shape of the diamagnetic cavity and its evolution are studied using different target materials (carbon, aluminium, nickel and tungsten). The formation and dynamics of the diamagnetic cavity and striation-like structures are highly dependent on the target material. We have observed the expansion velocities of plasmas of metallic target decrease with the increase of  $Z$ -number. The diamagnetic cavity exists for a longer time, and its width is smaller for high  $Z$ -materials (e.g. tungsten) as compared to the low  $Z$ -materials (e.g. aluminium). As the time evolved, the cavity changed to jet/cone-like structure which in turn changes to the slab-like structure at an earlier time in case of low  $Z$ -material, this means the magnetic diffusion time is less for low  $Z$ -materials as compared to high  $Z$ -materials. Also, the number of magnetic striations is more and closely spaced in high  $Z$ -materials in comparison to low  $Z$ -materials where the striation is broader and well-separated. On the other hand, it is observed that, the carbon plasma shows a dramatic behaviour in the presence of magnetic field. For the first time, we have observed the plume splitting and Y-shaped almost symmetrical bifurcation in expanding carbon plume instead of well-defined cavity structure and striation-like structure in the presence of the magnetic field. We have also discussed the dependence of magnetic

diffusion time on the plasma parameters in the applied magnetic field and the limitation of presently established theory used to explain the diamagnetism of laser plasma. We have highlighted some important observations which should be explained by using theory and required to be supported by simulation studies as these observed results couldn't explain with the help of the present theory. In addition, we have also suggested some important points (modification of energy equation by considering plasma motion and estimating aspect ratio from the asymmetric structure of plasma plume) which will be useful to modify the expression for bubble radius and magnetic diffusion time.

## Chapter 7

---

### **Conclusion and future scope**

The major outcomes of the thesis research work those are discussed in the previous chapters have been summarized in this chapter. Few important possible future scope of this thesis research work has also been provided.



---

---

## 7.1 Conclusion

Systematic experimental investigations have been performed to study the 1D & 2D dynamical and geometrical behaviors of laser-produced plasmas across the transverse magnetic field. Time-resolved emission spectroscopy, fast imaging and indigenously developed a three-axis, high-frequency B-dot probe have been used to characterize the expanding plasma plume. Both permanent bar magnets and Helmholtz coils are utilized to produce uniform magnetic field to study expansion of plasma plume. Majority of previous experiments have been performed with permanent bar magnet where plume imaging along the magnetic field lines is not possible because of experimental constraints. But the plume structure in magnetic field is highly asymmetrical and therefore complete geometrical information cannot be extracted from plume images projected across the magnetic field direction only. This problem was resolved by developing a special designed Helmtotz coil configuration which not only produces different uniform magnetic fields but also allows the fast imaging of expanding plasma plume along and across the applied external magnetic field.

Distinct features of axial and radial expansion of the plume across the fix transverse magnetic field have been observed in vacuum as well as in argon environment which are significantly different from the reported results for similar experiments. It has been found that expanding plume experiences resistive force and approaches the stagnation limit. The stagnation limit is agreeing well with the estimated field diffusion time and confinement radius of the plasma plume. Stagnation condition is maintained for some time and there-after plume begins to expand with uniform velocity. The above behaviour is explained on the basis of plume expansion in evolving diamagnetism of the plume and expansion in non-diamagnetic regimes where the magnetic field diffuse into the plasma plume and plume experiences the  $E \times B$  drift. Also, the hidden structured profile of the plasma plume in transverse

---

magnetic field (which is not visible in plume images) is extracted by the singular-value decomposition (SVD) of the image data matrix. Interestingly, in presence of both magnetic field and ambient gas, plume expands with uniform intensity distribution in a large area (extended up to separation between the bar magnets). This is the important finding which can be utilized in large area film deposition.

Different phases of plasma expansion, e.g., formation of diamagnetic cavity and its dependence of the delay time and field strength, disappearance of diamagnetism, and  $E \times B$  drift of the plasma plume are experimentally demonstrated for the first time by with indigenously designed setup, based on Helmholtz coil and mutually synchronized two gated ICCD cameras. Time and field strength dependence of diamagnetism of laser-produced plasma, that is formation and evolution of the diamagnetic cavity, cavity collapse and  $E \times B$  drift of bulk plasma is thoroughly investigated. Observes plasma structure such as elliptical cylinder followed by jet and finally, slab-like structure in different phases of expansion is correlated with time-varying plasma parameters and field diffusion into the plasma plume. Based on the projections of plume images in two perpendicular planes, the three dimensional structure of the plasma plume is modelled as an elliptical cylinder-like structure. The expression for bubble radius of diamagnetic cavity and magnetic diffusion time is modified to explain the observed diamagnetic cavity and its evolution. The striation-like structures along the magnetic field line is observed which is dominant at comparatively higher delay times and higher magnetic fields. The existence of plasma instability which is responsible for striation like structure is also discussed.

A high frequency, three-axis B-dot probe has been indigenously designed, constructed, optimized and calibrated for confirming the diamagnetism of laser produced plasma. Different approach have been utilized to test the frequency response up to 10 MHz and to calibrate the probe for measuring the time varying the magnetic

---

field of the range 200-1000 ns (cavitation life time). The estimated resultant magnetic field for different applied was found to be  $\sim 7-10$  G, which confirm the induced diamagnetic field in the cavity region.

Further material dependence of plume expansion across the magnetic field, produced by low and high atomic number targets (carbon, aluminium, nickel and tungsten) is thoroughly studied. It has been observed that formation and structure of diamagnetic cavity and its temporal evolution and dismissal are highly dependent on the target material. The unconventional behavior of carbon plasma that is, instead of formation of the diamagnetic cavity, a Y-shaped symmetrical bifurcation in presence of magnetic field is also discussed. For high Z-materials, it has been observed that the diamagnetic cavity exists for a longer time, and its width is smaller as compared to the low Z-materials. As the time evolved, the cavity changed to jet/cone-like structure which in turn changes to the slab-like structure at an earlier time for low Z-material. Also, the number of magnetic striations is more and closely spaced in high Z-materials in comparison to low Z-materials where the striation is broader and well-separated. we have also highlighted some important points which are necessary to modify for convincing explanation of the present observations.

## **7.2 Future scope**

The present investigation shows that formation of diamagnetic cavity and formation of striation-like structures is time-varying phenomenon and also highly dependent on magnetic field strength. The observed time-varying geometrical features are not completely explored. Therefore, the present work provides the tremendous scope for theoretical work and simulation in this area [89].

Further, this work can be extended as planning similar study in presence of variable axial magnetic field. The complete dynamical and geometrical behaviour of the plasma plume in transverse and axial magnetic field is highly useful in various

---

practical applications, like beam diagnostics for tokamak plasma, improve the sensitivity of laser-induced breakdown spectroscopy (LIBS) [33, 39], targeted and wide area pulsed laser deposition [90], manipulation of shape and size of plasma plume etc. It has been observed that plasma is confined in small volume in presence of magnetic field in comparison to field free case. The confined plasma increases the collision frequencies between the plume species which leads to an increase in the number of atoms in high-energy states and hence, enhanced emission intensity. The enhance emission intensity can be utilised to improve the sensitivity of laser-induced breakdown spectroscopy (LIBS). Also, Laser plasma expansion in magnetic field, especially in case of barium plasma [91] is highly useful in space applications for the study of ionospheric plasmas, to trace the atmospheric plasmas and laboratory simulation of artificial releases in space. Further, uniform intensity distribution in a large volume and almost flat expansion of the plume in presence of magnetic field in specific condition can be utilized in large area film deposition.

# References

---

1. F. F. Chen, "Introduction to Plasma Physics and Controlled Fusion Volume 1: Plasma Physics" (Springer, US, 1984).
2. E. J. Hemsworth, "Laser-induced plasmas: Theory and application" (Nova Science Publishers, Inc., New York, 2010).
3. Ed. C. Phipps, "Laser ablation and its applications" (Springer-Verlag, Berlin-Heidelberg, 2006).
4. S. Amoroso, R. Bruzzese, N. Spinelli and R. Velotta, "Characterization of laser-ablation plasmas". *J. Phys. B: At., Mol. and Opt. Phys.* **32**, R131 (1999).
5. R. K. Singh and J. Narayan, "Pulsed-laser evaporation technique for deposition of thin films: Physics and theoretical model", *Phys. Rev. B* **41**, 8843 (1990).
6. A. Bogaerts, Z. Chen, R. Gijbels and A. Vertes, "Laser ablation for analytical sampling: what can we learn from modeling?", *Spectrochim. Acta B* **58**, 1867 (2003).
7. A. Bogaerts and Z. Chen, "Effect of laser parameters on laser ablation and laser-induced plasma formation: A numerical modeling investigation", *Spectrochim. Acta B* **60**, 1280 (2005).
8. J. Lindl., "Development of the indirect-drive approach to inertial confinement fusion and the target physics basis for ignition and gain", *Phys. Plasmas* **2**, 3933(1995).
9. M. F. Becker, J. R. Brock, H. Cai, D. E. Henneke, J. W. Keto, J. Lee, W. T. Nichols and H. D. Glicksman., "Metal nanoparticles generated by laser ablation", *Nanostruct. Mater.* **10**, 853 (1998).
10. R. P. Drake, J. J. Carroll III, T. B. Smith and P. Keiter, "Laser experiments to simulate supernova remnants", *Phys. Plasmas* **7**, 2142 (2000).
11. J. D. Lindl, "Inertial Confinement Fusion", (Springer, New York, 1998).

12. E. M. Campbell, J. T. Hunt, E. S. Bliss, D. R. Speck, and R. P. Drake., “Nova experimental facility”, *Rev. Sci. Instrum.* **57**, 2101 (1986).
13. H. Motz, “The Physics of Laser Fusion” (London, Academic Press, 1979).
14. K. Nishikawa and M. Wakatani., “Plasma Physics: Basic Theory with Fusion Applications” (Berlin: Springer-Verlag, 2nd. ed., 1994).
15. R.W. Eason., “Pulsed Laser Deposition of Thin Films: Applications- Led Growth of Functional Materials” (Wiley, New York, 2006).
16. P. R. Willmott and J. R. Huber., “Pulsed laser vaporization and deposition”, *Rev. Mod. Phys.* **72**, 315 (2000).
17. D. B. Chrisey and G. K. Hubler, “Pulsed Laser Deposition of Thin Films” (Wiley, New York, 1994).
18. S. Bollanti, F. Bonfigli, E. Burattini, P. Di Lazzaro, F. Flora, A. Grilli, T. Letardi, N. Lisi, A. Marinai, L. Mezi, D. Murra and C. Zheng., “High-efficiency clean EUV plasma source at 10-30 nm, driven by a long-pulse-width excimer laser”, *Appl. Phys. B* **76**, 277 (2003).
19. A. Kaldos, H.J. Pieper, E. Wolf and M. Krause, “Laser machining in die making - a modern rapid tooling process”, *J. Mater. Process. Tech.* **155-156**, 1815 (2004).
20. Ya. B. Zel’dovich and Yu. P. Raizer, “Physics of shock waves and high-temperature hydrodynamics phenomena” (Dover Publications, New York, 2002).
21. J. P. Singh and S. N. Thakur, “Laser-Induced Breakdown Spectroscopy” (Elsevier publications, UK, 2007).
22. D. B. Geohegan, “Fast intensified-ccd photography of YBa<sub>2</sub>Cu<sub>3</sub>O<sub>7-x</sub> laser ablation in vacuum and ambient oxygen”. *Appl. Phys. Lett.* **60**, 2732 (1992).
23. D. B. Geohegan, “Physics and diagnostics of laser ablation plume propagation for high-T, superconductor film growth”, *Thin solid Films*, 220, 138 (1992).

24. S. George, A. Kumar, R. K. Singh and V. P. N. Nampoore, "Effect of ambient gas on the expansion dynamics of plasma plume formed by laser blow off of thin film", *Appl. Phys. A* **98**, 901 (2010).
25. D. Winske, "Development of flute modes on expanding plasma clouds", *Phys. Fluids B* **1**, 1900 (1989).
26. W. H. Bostick, "Experimental Study of Ionized Matter Projected across a Magnetic Field", *Phys. Rev.* **104**, 292 (1956).
27. G. Schmidt, "Plasma motion across magnetic fields", *Phys. Fluids* **3**, 961 (1960).
28. S. S. Harilal, M. S. Tillack, B. O'Shay, C. V. Bindhu, and F. Najmabadi, "Confinement and dynamics of laser-produced plasma expanding across a transverse magnetic field", *Phys. Rev. E* **69**, 026413 (2004).
29. G. Dimonte and L. Wiley, "Structure of an exploding laser-produced plasma", *Phys. Rev. Lett.* **67**, 1755 (1991).
30. M. VanZeeland and W. Gekelman, "Laser-plasma diamagnetism in the presence of an ambient magnetized plasma", *Phys. Plasmas* **11**, 320 (2004).
31. T. A. Peyser, C. K. Manka, B. H. Ripin, G. Ganguli, "Electron-ion hybrid instability in laser-produced plasma expansions across magnetic fields", *Phys. Fluids B* **4**, 2448 (1992).
32. S. George, A. Kumar, R. K. Singh and V. P. N. Nampoore, "Fast imaging of laser-blow-off plume: Lateral confinement in ambient environment", *Appl. Phys. Lett.* **94**, 141501 (2009).
33. Y. Li, C. Hu, H. Zhang, Z. Jiang and Z. Li, "Optical emission enhancement of laser-produced copper plasma under a steady magnetic field" *Appl. Opt.* **48**, B105 (2009).
34. C. Ducruet, N. Kornilov, C. De Julián Fernández and D. Givord, "Laser generated plasmas characterized under magnetic field", *Appl. Phys. Lett.* **88**, 044102 (2006).

35. A. Neogi and R. K. Thareja, "Laser-produced carbon plasma expanding in vacuum, low pressure ambient gas and nonuniform magnetic field", *Phys. Plasmas* **6**, 365 (1999).
36. A. Kumar, H. C. Joshi, V. Prahlad and R. K. Singh, "Effect of magnetic field on laser-blow-off plasma plume: Structured temporal emission profile" *Phys. Lett. A* **374**, 2555 (2010).
37. H. C. Joshi, A. Kumar, R. K. Singh and V. Prahlad, "Effect of a transverse magnetic field on the plume emission in laser-produced plasma: An atomic analysis", *Spectrochim. Acta, Part B, At. Spectrosc.* **65**, 415 (2010).
38. L. Torrisi, D. Margarone, S. Gammino and L. Ando, "Ion energy increase in laser-generated plasma expanding through axial magnetic field trap", *Laser Part. Beams* **25**, 453 (2007).
39. X. K. Shen, Y. F. Lu, T. Gebre, H. Ling and Y. X. Han, "Optical emission in magnetically confined laser-induced breakdown spectroscopy", *J. Appl. Phys.* **100**, 053303 (2006).
40. J. D. Haverkamp, M. A. Bourham, S. Du and J. Narayan, "Plasma plume dynamics in magnetically assisted pulsed laser deposition", *J. Phys. D, Appl. Phys.* **42**, 025201 (2008).
41. T. García, E. de Posada, M. Villagrán, J. L. Sánchez, P. Bartolo-Pérez and J.L. Pe'na, "Effects of an external magnetic field in pulsed laser deposition", *Appl. Surf. Sci.* **255**, 2200 (2008).
42. M. Takichi and T. Kobayashi, "Manipulation of Laser Ablation Plume by Magnetic Field Application", *Jpn. J. Appl. Phys.* **38**, 3642 (1999).
43. S.S. Harilal, B. O'Shay and M.S. Tillack, "Debris mitigation in a laser-produced tin plume using a magnetic field", *J. Appl. Phys.* **98**, 036102 (2005).

- 
44. D. N. Patel, Pramod K. Pandey and Raj K. Thareja, "Brass plasmoid in external magnetic field at different air pressures", *Phys. Plasmas* **20**, 103503 (2013).
  45. D. K. Bhadra, "Expansion of a Resistive Plasmoid in a Magnetic Field", *Phys. Fluids* **11**, 234 (1968).
  46. R. G. Tuckfield and F. Schwirzke., "Dynamics of laser created plasma expanding in a magnetic field", *Plasma Phys.* **11**, 11 (1969).
  47. A. N. Mostovych, B. H. Ripin and J. A. Stamper, "Laser produced plasma jets: Collimation and instability in strong transverse magnetic fields", *Phys. Rev. Lett.* **62**, 2837 (1989).
  48. B.A. Bryunetkin, U.Sh. Begimkulov, V. M. Dyakin, G.A. Koldashov, S. N. Priyatkin, A. Yu. Repin, E. L. StupitskiT, and A. Ya. Faenov., "Laser plasma expansion in a magnetic field", *Sov. J. Quantum Electron.* **22**, 223 (1992).
  49. B. H. Ripin, E. A. McLean, C. K. Manka, C. Pawley, J. A. Stamper, T. A. Peyser, A. N. Mostovych, J. Grun, A. B. Hassam and J. Huba., "Large-Larmor-radius interchange instability", *Phys. Rev. Lett.* **59**, 2299 (1987).
  50. H. Ripin, J. D. Huba, E. A. McLean, C. K. Manka, T. Peyser, H. R. Burris, and J. Grun, "Sub-Alfvénic plasma expansion", *Phys. Fluids B* **5**, 3491 (1993).
  51. P. K. Pandey and R. K. Thareja, "Rotating copper plasmoid in external magnetic field", *Phys. Plasmas* **20**, 022117 (2013).
  52. J. D. Huba, A. B. Hassam, and D. Winske, "Stability of sub-Alfvénic plasma expansions", *Phys. Fluids B: Plasma Phys.* **2**, 1676 (1990).
  53. S. S. Harilal, B. O'shay, M. Tao and M. Tillack, "Ion debris mitigation from tin plasma using ambient gas, magnetic field and combined effects", *Appl. Phys. B* **86**, 547 (2007).

54. S. S. Harilal, B. O'Shay, M. S. Tillack, C. V. Bindhu and F. Najmabadi, "Fast photography of a laser generated plasma expanding across a transverse magnetic field", IEEE Trans. Plasma Sci. **33**, 474 (2005).
55. R. Qindeel, N. B. Bidin and Y. Mat daud., "Dynamics expansion of laser produced plasma with different materials in magnetic field", J. Phys.: Conf. Ser. **142**, 012069 (2008).
56. M. S. Rafique, M. Khaleeq-UR-Rahman, I. Riaz, R. Jalil and N. Farid., "External magnetic field effect on plume images and X-ray emission from a nanosecond laser produced plasma", Laser and Part. Beams **26**, 217 (2008).
57. Instruction manual, Continuum laser ([www.continuum.com](http://www.continuum.com)).
58. M. S. Raju, R. K. Singh, P. Gopinath and A. Kumar, "Influence of magnetic field on laser-produced barium plasmas: Spectral and dynamic behaviour of neutral and ionic species", J. Appl. Phys. **116**, 153301 (2014).
59. Instruction Manual, Stanford Computer Optics ICCD 4 Picos (<http://www.stanfordcomputeroptics.com>).
60. Instruction Manual, Acton Advanced Spectrograph SP2500A (<http://www.princetoninstruments.com>).
61. R. C. Issac, K. V. Pillai, S. S. Harilal, G. K. Varier, C. V. Bindhu, P. Gopinath, P. Radhakrishnan, V. P. N. Nampoori and C. P. G. Vallabhan., "Dynamics of laser produced silver plasma under film deposition conditions studied using optical emission spectroscopy", Appl. Surf. Sci. **125**, 227 (1998).
62. R. K. Singh, Ajai Kumar, V. Prahlad and H. C. Joshi., "Generation of fast neutrals in a laser-blow-off of LiF-C film: A formation mechanism", Appl. Phys. Lett. **92**, 171502 (2008).

63. S. Amoroso, R. Bruzzese, N. Spinelli, R. Velotta, M. Vitiello and X. Wang, “Dynamics of laser-ablated MgB<sub>2</sub> plasma expanding in argon probed by optical emission spectroscopy”, *Phys. Rev. B* **67**, 224503 (2003).
64. S. S. Harilal, Riju C. Issac, C. V. Bindhu, V. P. N. Nampoori and C. P. G. Vallabhan., “Emission characteristics and dynamics of C<sub>2</sub> from laser produced graphite plasma”, *J. Appl. Phys.* **81**, 3637 (1997).
65. D. A. Cremers and L. J. Radziemski, “Handbook of laser induced breakdown spectroscopy” (John Wiley & Sons Ltd, 2006).
66. H. R. Griem, *Plasma Spectroscopy* (McGraw-Hill, New York, 1997).
67. H. R. Griem, *Spectral Line Broadening by Plasma* (Academic Press, New York, 1974).
68. E. T. Everson et al., “Design, construction, and calibration of a three-axis, high-frequency magnetic probe (B-dot probe) as a diagnostic for exploding plasmas”, *Rev. Sci. Instrum.* **80** (11), 113505 (2009).
69. F. F. Chen and J. P. Chang, “Lecture Notes on Principles of Plasma Processing” (Springer, 2003).
70. A. Kumar, V. Chaudhari, K. Patel, S. George, S. Sunil, R. K. Singh and R. Singh, “An experimental setup to study the expansion dynamics of laser blow-off plasma plume in variable transverse magnetic field”, *Rev. Sci. Instrum.* **80**, 033503 (2009).
71. N. Behera, R. K. Singh and A. Kumar, “Confinement and re-expansion of laser induced plasma in transverse magnetic field: Dynamical behaviour and geometrical aspect of expanding plume”, *Phys. Lett. A* **379**, 2215 (2015).
72. S. Okada, K. Sato and T. Sekiguchi, *Jpn. J. Appl. Phys.* **20**, 157 (1981).
73. Yu. P. Zakharov, V.M. Antonov, E. L. Boyarintsev, A.V. Melekhov, V.G. Posukh, I. F. Shaikhislamov and V. V. Pickalov, *Plasma Phys. Rep.* **32**, 183 (2006).

- 
74. A. Collette and W. Gekelman, "Structure of an exploding laser-produced plasma", *Phys. Plasmas* **18**, 055705 (2011).
  75. J. E. Borovsky, "Limits on the cross-field propagation of streams of cold plasma", *Phys. Fluids* **30**, 2518 (1987).
  76. S. S. Harilal, B. O'Shay, Y. Tao and M.S. Tillack, "Ambient gas effects on the dynamics of laser-produced tin plume expansion", *J. Appl. Phys.* **99**, 083303 (2006).
  77. C. Plechaty, R. Presura, S. Stein, D. Martinez, S. Neff, V. Ivanov and Y. Stepanenko, "Penetration of a laser-produced plasma across an applied magnetic field", *High Energy Density Physics* **6**, 258 (2010).
  78. A. Kumar, R. K. Singh, V. Prahlad and H. C. Joshi, "Comparative study of laser produced Li plasma plumes from thin film and solid target", *J. Appl. Phys.* **104**, 093302 (2008).
  79. J. C. S. Kools, "Monte Carlo simulations of the transport of laser-ablated atoms in a diluted gas", *J. Appl. Phys.* **74**, 6401 (1993).
  80. G. Strang, "Introduction to Linear Algebra" (Wellesley-Cambridge, 1998).
  81. B. Chaudhury, P. K. Chattopadhyay, D. Raju, and S. Chaturvedi, "Transient Analysis of Creeping Wave Modes Using 3-D FDTD Simulation and SVD Method", *IEEE Trans. Antennas Propag.*, **57**, 754 (2009).
  82. D. Raju, A. Kumar and R. K. Singh, "Study of Laser-Blow-Off Plume Dynamics Using Singular Value Decomposition Technique", *IEEE Trans. Plasma Sci.* **39**, 630 (2011).
  83. J. D. Huba, *NRL Plasma Formulary* (Naval Research Laboratory, Washington, D.C., 2002).

- 
84. N. Behera, R. K. Singh and A. Kumar, “Dynamics and structural behaviour of laser induced plasma in transverse magnetic field”, Proceedings of the DAE-BRNS National Laser Symposium **23**, CP- 07-15 (2014).
85. N. Behera, R. K. Singh and A. Kumar, “Singular Value Decomposition of Laser Produced Plasma in Transverse Magnetic field”, Proceedings of the DAE-BRNS National Laser Symposium **25**, CP-7.20 (2016).
86. N. Behera, R. K. Singh, V. Chaudhari and A. Kumar, “Two directional fast imaging of plasma plume in variable magnetic field: Structure and dynamics of the plume in diamagnetic and non-diamagnetic limits”, Phys. Plasmas **24**, 033511 (2017).
87. N. Behera, R. K. Singh and A. Kumar, “Diffusion of external magnetic field into laser-produced plasma plume”, in *Frontiers in Optics / Laser Science*, OSA Technical Digest (Optical Society of America, 2018), paper JW3A.37.
88. N. M. Bulgakova, A. V. Bulgakov and O. F. Bobrenok, “Double layer effects in laser-ablation plasma plumes”, Phys. Rev. E **62**, 5624 (2000).
89. B. G. Patel, A. Das, P. Kaw, R. Singh and A. Kumar, “Numerical modeling of plasma plume evolution against ambient background gas in laser blow off experiments”, Phys. Plasmas **19**, 073105 (2012).
90. N. Wakiya, T. Kawaguchi, N. Sakamoto, H. Das, K. Shinozaki, H. Suzuki, “Progress and impact of magnetic field application during pulsed laser deposition (PLD) on ceramic thin films”, *Special Articles: The 71st CerSJ Awards for Academic Achievements in Ceramic Science and Technology: Review* **125**, 856 (2017).
91. R. Lüst, “Barium cloud experiments in the upper atmosphere” in Bleeker J.A.M., Geiss J., Huber M.C.E. (eds), “The Century of Space Science” (Springer, Dordrecht, 2001).

